DISSERTATION

Coupled Cluster Theory Applied To Zero-Dimensional Systems

zur Erlangung des akademischen Grades

Doktor der technischen Wissenschaften

eingereicht von

Faruk Salihbegović

Matrikelnummer 1028643

ausgeführt am Institut für Theoretische Physik
der Fakultät für Physik der Technischen Universität Wien

Betreuer: Univ.-Prof. Dr. Andreas Grüneis

Wien, _____ _____

(Unterschrift Verfasser/in) (Unterschrift Betreuer/in)

Declaration of Authorship

Hiermit erkläre ich, dass ich diese Arbeit selbständig verfasst habe, dass ich die venting Quellen und Hilfsmittel vollständig angegeben habe und dass ich die Stellen der Arbeit - einschließlich Tabellen, Karten und Abbildungen -, die anderen Werken oder dem Internet im Wortlaut oder dem Sinn nach entnommen sind, auf jeden Fall unter Angabe der Quelle als Entlehnung kenntlich gemacht habe.

Unterschrift: _____

Datum: _____

Abstract

Low-dimensional systems are at the heart of nanotechnology research, as, their unique physical properties make them promising candidates for a wide range of applications. Examples of low-dimensional systems include quantum dots, quantum wells, nanowires, nanotubes, point defects and graphene, among others. The focus of this work is on the two-dimensional parabolic quantum dot and silicon self-interstitial point defects. In quantum chemistry and condensed matter physics, the equations of quantum mechanics are applied to study the properties of physical systems. This approach allows for the calculation of properties such as energy levels, electronic band structures, optical spectra and chemical reactivity. The most popular method is density functional theory (DFT) due to its good tradeoff between computational cost and accuracy. However, its general applicability is often hindered by uncontrollable approximations used for the construction of the exchange-correlation functional. The methods of computational quantum chemistry constitute a hierarchy that allows to systematically improve the description of quantum many-body effects with increasing computational cost.

In this work a wide range of ab initio many-body methods is used, including density functional theory, Hartree-Fock theory, Møller–Plesset perturbation theory and coupled cluster theory. These methods are applied to calculate the ground and excited states energies of the two-dimensional parabolic quantum dot and to calculate the formation energies of the silicon self-interstitial point defects. The quantum dot is modeled as a two-dimensional quantum harmonic oscillator and the Coulomb integrals are calculated using a semi analytic solution that allows to integrate over the Coulomb kernel's singularity in discretized real space in any number of dimensions. The ground state energy of the quantum dot is calculated with coupled cluster singles and doubles theory (CCSD) while for the excited states energy the equation of motion formalism of coupled cluster singles and doubles theory (EOM-CCSD) is used. The ground and excited state energies are calculated with varying number of electrons in the quantum dot and varying correlation strengths tuned through the harmonic potential parameter. The resulting CCSD ground and excited state energies are compared to values available from the literature with which we are in excellent agreement. Further, the formation energies of the silicon self interstitials are calculated using a periodic supercell approach, at the level of CCSD theory including a perturbative estimate for the triples amplitudes (CCSD(T)). The basis set incompleteness error (BSIE) and the finite size incompleteness error (FSIE) are

taken into account with extrapolation schemes tailored to periodic coupled cluster theory using a plane wave basis set. Our converged CCSD(T) formation energies are compared to quantum Monte Carlo (QMC) data from the literature and partly to experiment, with which we are in good agreement.

Zusammenfassung

Niedrigdimensionale Systeme stehen im Zentrum der Nanotechnologieforschung, da ihre einzigartigen physikalischen Eigenschaften sie zu vielversprechenden Kandidaten für eine Vielzahl von Anwendungen machen. Beispiele für niedrigdimensionale Systeme sind Quantenpunkte, Quantenbrunnen, Nanodrähte, Nanoröhren, Punktdefekte, Quantenfraktalnetzwerke und Graphen, unter anderem. Der Fokus dieser Arbeit liegt auf dem zweidimensionalen parabolischen Quantenpunkt und den Silizium-eigenpunktdefekten. In der Quantenchemie und kondensierten Materiephysik werden die Gleichungen der Quantenmechanik angewendet, um die Eigenschaften physikalischer Systeme zu untersuchen. Dieser Ansatz ermöglicht die Berechnung von Eigenschaften wie Energieniveaus, elektronischen Bandstrukturen, optischen Spektren und chemische Reaktivität. Die beliebteste Methode ist die Dichtefunktionaltheorie (DFT) aufgrund ihres guten Kompromisses zwischen Rechenkosten und Genauigkeit. Allerdings wird ihre allgemeine Anwendbarkeit oft durch unkontrollierbare Approximationen behindert, die für die Konstruktion der Austausch-Korrelationsfunktion verwendet werden. Die Methoden der Quantenchemie bilden eine Hierarchie, die es ermöglicht, die Beschreibung der Effekte von Quantenvielteilchensystemen mit steigendem Rechenaufwand systematisch zu verbessern.

In dieser Arbeit wird eine breite Palette von ab initio Vielteilchenmethoden verwendet, einschließlich Dichtefunktionaltheorie, Hartree-Fock-Theorie, Møller-Plesset-Störungstheorie und Coupled Cluster theorie. Diese Methoden werden angewendet, um die Grundzustands- und angeregten Zustandsenergien des zweidimensionalen parabolischen Quantenpunkts zu berechnen und die Bildungsenergien der Silizium-eigenpunktdefekte zu ermitteln. Der Quantenpunkt wird als zweidimensionaler Quantenharmonischer Oszillator modelliert, und die erforderlichen Coulomb-Integrale werden mithilfe einer halbanalytischen Lösung berechnet, die es ermöglicht, über die Singularität des Coulomb-Kernels im diskretisierten reellen Raum in beliebig vielen Dimensionen zu integrieren. Die Energie des Grundzustands des Quantenpunkts wird mit Coupled Cluster singles and doubles theorie (CCSD) berechnet, während für die Energie der angeregten Zustände der Bewegungsgleichungsformalismus der Coupled Cluster Singles Doubles theorie (EOM-CCSD) verwendet wird. Die Grundzustands- und angeregten Zustandsenergien werden unter

Variation der Anzahl von Elektronen im Quantenpunkt und unter Variation der Korrelationsstärken berechnet, die durch den harmonischen Potentialparameter eingestellt werden. Die resultierenden CCSD-Grundzustands- und angeregten Zustandsenergien werden mit Werten verglichen, die in der Literatur verfügbar sind, mit denen wir eine ausgezeichnete Übereinstimmung haben. Darüber hinaus werden die Bildungsenergien der Silizium-eigenpunktdefekt mit einem periodischen superzellen Ansatz auf dem niveau der CCSD-Theorie unter Berücksichtigung einer perturbativen Schätzung der Tripelamplituden (CCSD(T)) berechnet. Der Fehler aufgrund unvollständiger Basissätze (Basis Set Incompleteness Error, BSIE) und der Fehler aufgrund endlicher Größe (Finite Size Incompleteness Error, FSIE) werden mithilfe von Extrapolationsschemata berücksichtigt, die auf die periodische Coupled Cluster theorie unter Verwendung einer ebenen Wellenbasis abgestimmt sind. Unsere konvergierten CCSD(T)-Bildungsenergien werden mit Quanten-Monte-Carlo-Daten (QMC) aus der Literatur und teilweise mit Experimenten verglichen, mit denen wir gute Übereinstimmung erzielen.

Acknowledgements

I am sincerely grateful to my supervisor, Andreas Grüneis, for his constant guidance and unwithering support. I also thank my colleagues and friends for the insightful and fun discussions that were had along the way, especially Alejandro Gallo whose strong opinions invited me to delve deeper into many exciting topics, and last but not least, I thank my family for their unwavering encouragement. This achievement wouldn't have been possible without all of you. Thank you.

Contents

List of Figures

List of Tables

Abbreviations

DFT	**D**ensity **F**unctional **T**heory
QMC	**Q**uantum **M**onte **C**arlo
BSE	**B**ethe-**S**alpeter **E**quation
HF	**H**artree **F**ock
CI	**C**onfiguration **I**nteraction
FCI	**F**ull **C**onfiguration **I**nteraction
MP	**M**øller–**P**lesset perturbation theory
MP2	second-order **M**øller–**P**lesset perturbation theory
CC	**C**oupled **C**luster
CCSD	**C**oupled **C**luster **S**ingles and **D**oubles
EOM	**E**quation **o**f **M**otion
CCSD(T)	**C**oupled **C**luster **S**ingles **D**oubles and perturbative **T**riples
XC	e**X**change-**C**orrelation
LDA	**L**ocal **D**ensity **A**pproximation
GGA	**G**eneralized **G**radient **A**pproximation
PBE	**P**erdew–**B**urke–**E**rnzerhof
HSE	**H**eyd–**S**cuseria–**E**rnzerhof
RPA	**R**andom **P**hase **A**pproximation
DIIS	**D**irect **I**nversion in the **I**terative **S**ubspace
PAW	**P**rojector **A**ugmented **W**ave
NO	**N**atural **O**rbital
FNO	**F**rozen **N**atural **O**rbital
CBS	**C**omplete **B**asis **S**et
BSIE	**B**asis **S**et **I**ncompleteness **E**rror
FPC	**F**ocal-**P**oint **C**orrection

FSIE	**F**inite **S**ize **I**ncompleteness **E**rror
HOMO	**H**ighest **O**ccupied **M**olecular **O**rbital
LUMO	**L**owest **U**noccupied **M**olecular **O**rbital
GTO	**G**aussian **T**ype **O**rbital
STO	**S**later **T**ype **O**rbital
QD	**Q**uantum **D**ot

Dedicated to my family...

Chapter 1

Introduction

Low-dimensional systems are at the heart of nanotechnology research, as, their unique physical properties make them promising candidates for a wide range of applications. In these systems, the confinement of electrons, excitons and phonons leads to a quantization of energy levels and enhancements of the interaction between the different constituents. This results in phenomena such as quantum confinement, tunable band gaps, and strong light-matter interactions, which can be harnessed for many different applications in electronics, optics, energy conversion, and sensing technology. Examples of low-dimensional systems include quantum dots, quantum wells, nanowires, nanotubes, point defects and graphene, among others.

In order to deepen our understanding of these systems, one has to model them by applying many-body methods. This approach allows for the calculation of properties such as energy levels, electronic band structures, optical spectra and chemical reactivity, typically done by freezing the nuclei and solving the electronic part of the Schrödinger equation approximately. An important goal of electronic structure theory is the ab initio description of a system, allowing for accurate predictions of its electronic and optoelectronic properties. The most popular method is DFT due to its good trade off between computational cost and accuracy. Although DFT is in principle exact and therefore an ab initio theory, in order for it to be applied to a specific system one has to know a-priori which exchange correlation functional performs well for the given system. For this purpose, an experimental or high level wavefunction based theory reference is needed. Note that the validation of certain exchange correlation functionals in DFT with the use of more accurate methods is an ongoing research in the field of quantum chemistry. In many cases experimental references are hard to come by and the typical high level wavefucntion based reference theory is either QMC or CCSD(T). This makes these two methods an invaluable benchmark tool in the toolkit of condensed matter physics and

computational quantum chemistry. With the steady advancements in computational power and the help of super computers, electronic structure theory nowadays is routinely applied to compute and predict structures, spectroscopic parameters, as well as reaction barriers for moderate-sized systems and with more computation power in the future electronic structure theory will continue to extend its scope.

This work aims at both applying coupled cluster (CC) theory to calculate the ground and excited state energies of the quantum dot in different regimes of correlation and the formation energies of the silicon self-interstitials in order to model them, as well as evaluating the performance of CC theory itself. By performing these calculations, we will gain insights into the accuracy of CC theory on different types of low dimensional systems and expand our understanding of the strengths and limitations of the method for future investigations of other important systems.

In the upcoming chapters a ground up description of the theory, methods and tools necessary to perform these calculations is presented. Further, there are two standalone chapters specifically on the quantum dot and the silicon self-interstitials containing all details on what has been achieved in this thesis.

Chapter 2

Interacting Electrons in an Atom

The first principles (ab initio) modeling of microscopic systems is an important goal of condensed matter physics and computational quantum chemistry. In quantum mechanics, particle dynamics are understood in terms of a wave-equation, the Schrödinger equation, which was proposed in 1926 [1]. The Schrödinger equation allowed solving hydrogen and hydrogen-like atoms analytically by reformulating it to an eigenvalue problem. From the solution, the three principal quantum numbers emerged, giving rise to an ab initio understanding of atomic orbitals. Nonetheless, another quantum number needed to be introduced in order for the Schrödinger equation to fit observation, the spin quantum number, which has been done empirically by Pauli in 1925 [2]. Note that spin is only a simulacrum, it has nothing to do with spinning particles. Pauli called the fourth quantum number a "Classically Non-Describable Two-Valuedness". Later spin emerged from the Clifford algebra within the Dirac equation, which was derived by incorporating special relativity into a linearized, Lorentz invariant, Schrödinger equation [3].

In general, atomic orbitals are ubiquitous for understanding the electronic configuration of the elements and their chemical bonding, reactivity and spectroscopy. The atomic orbital plays a central role in modeling point like structures and molecular orbitals. In the upcoming section the atomic orbitals will be presented and used to estimate at which point a relativistic treatment of the particles is necessary, in order to motivate the Schrödinger equation.

2.1 Hydrogen-like Atom

A hydrogen atom consists of one positively charged proton and a single negatively charged electron bound to the nucleus by the coulomb force. A hydrogen-like atom

differs from hydrogen only by the charge and mass of the nucleus, it is an atom with only one electron for example, He^{+} or Li^{++}. Since the charge of the nucleon is only a constant in the Schrödinger equation, one can solve it for all charges in one go.

2.1.1 The Hamiltonian and its Solutions

The full Hamiltonian of a hydrogenic atom with nucleon charge Ze and mass m_N is

$$-\frac{\hbar^2}{2m_N}\nabla_N^2\psi - \frac{\hbar^2}{2m_e}\nabla_e^2\psi - \frac{Ze^2}{4\pi\epsilon_0|\vec{r}_N - \vec{r}_e|}\psi = E\psi(\vec{r}_e, \vec{r}_N). \tag{2.1}$$

It contains, in order, the kinetic energy of the nucleus, the kinetic energy of the electron, and the Coulomb attraction between them. The wavefunction depends on the coordinates of both the nucleus and the electron. The center of mass and relative movement of the constituents can be separated with the center of mass coordinate transformation,

$$\vec{R} = \frac{m_N\vec{r}_N + m_e\vec{r}_e}{M}, \tag{2.2}$$

$$M = m_N + m_e, \tag{2.3}$$

$$\vec{r} = \vec{r}_N - \vec{r}_e, \tag{2.4}$$

$$\mu = \frac{m_N m_e}{m_N + m_e}, \tag{2.5}$$

$$\psi(\vec{r}_e, \vec{r}_N) = \psi(\vec{R}, \vec{r}). \tag{2.6}$$

Resulting in the separable equation

$$-\frac{\hbar^2}{2M}\nabla_{\vec{R}}^2\psi - \frac{\hbar^2}{2\mu}\nabla_{\vec{r}}^2\psi - \frac{Ze^2}{4\pi\epsilon_0 r}\psi = E\psi(\vec{R}, \vec{r}). \tag{2.7}$$

Separating the variables

$$\psi(\vec{R}, \vec{r}) = \psi(\vec{R})\psi(\vec{r}), \tag{2.8}$$

yields the equation

$$-\frac{\hbar^2}{2M}\nabla_{\vec{R}}^2\psi = E_M\psi(\vec{R}), \tag{2.9}$$

for the center of mass movement and

$$\left(-\frac{\hbar^2}{2\mu}\nabla_{\vec{r}}^2 - \frac{Ze^2}{4\pi\epsilon_0 r}\right)\psi = E_r\psi(\vec{r}), \tag{2.10}$$

for the relative movement of the electron and nucleus, with

$$E = E_M + E_r. \tag{2.11}$$

Both can be solved analytically. The center of mass equation represents a free particle and its solutions are the plane waves

$$\psi(\vec{R}) = e^{i\vec{k}\vec{R}}, \tag{2.12}$$

and every linear combination of them. Equation 2.10 describes the hydrogenic atom in its inertial frame and can be further separated into radial and angular parts with the well known solutions

$$\psi(\vec{r}) = \psi(r, \theta, \phi) = R_{nl}(r) Y_{lm}(\theta, \phi), \tag{2.13}$$

$$R_{nl}(r) = \sqrt{\left(\frac{2Z}{na_\mu}\right)^3 \frac{(n-l-1)!}{2n(n+l)!}} e^{-Zr/na_\mu} \left(\frac{2Zr}{na_\mu}\right)^l L_{n-l-1}^{2l+1}\left(\frac{2Zr}{na_\mu}\right), \tag{2.14}$$

$$E_n = -\left(\frac{Z^2\hbar^2}{2\mu a_\mu^2}\right)\frac{1}{n^2}, \tag{2.15}$$

where $Y_{lm}(\theta, \phi)$ are the spherical harmonics, $L_{n-l-1}^{(2l+1)}$ are the generalized Laguerre polynomials and

$$a_\mu = \frac{4\pi\epsilon_0\hbar^2}{\mu e^2}. \tag{2.16}$$

The quantum numbers n, l and m can take the values

$$n = 1, 2, 3, 4, ... \tag{2.17}$$

$$l = 0, 1, 2, ..., n-1 \tag{2.18}$$

$$m = -l, -l+1, ..., 0, ..., l-1, l \tag{2.19}$$

2.2 Relativistic Limit

For the sake of argumentation we now use a semi-classical picture of the electron as a particle. With the wavefunction from equation 2.13, one can calculate the expectation value of the momentum operator for an arbitrary atomic orbital, to see if the electron reaches momenta that require relativistic treatment. The expectation value for the speed of an electron in an atomic orbital with quantum number n around a nucleus with charge Ze is

$$v = \frac{\alpha c Z}{n}, \tag{2.20}$$

with

$$\alpha = \frac{e^2}{4\pi\epsilon_0\hbar c}. \tag{2.21}$$

This amounts approximately to 0.73% of the speed of light for an electron in a hydrogen atom ($Z = 1$) in the ground state, $n = 1$. With increasing charge Z, the speed increases

linearly, meaning that the innermost electrons have to be treated with relativistic corrections, while for the inner electrons of the heaviest elements Schrödinger theory cannot be used. With more electrons around the nucleus, the outer electrons, that already have lower speed due to their distance to the nucleus ($n > 1$), see a screened charge, further lowering their speed. Which means that the outermost electrons of heavier atoms can be treated non-relativistically. These electrons account for the chemical bonding and reactivity properties of atoms. Further, in materials they account for the electrical, optical and thermal properties. Note that the orbitals of these outer electrons will be and are influenced by the relativistic inner orbitals through the aufbau principle.

The relativistic and non-relativistic momenta of a classical particle are

$$p_{rel} = mc\sqrt{\frac{v^2}{c^2 - v^2}}, \tag{2.22}$$

$$p = mv. \tag{2.23}$$

From figure 2.1 we can see that at 10% of the speed of light, both the relativistic

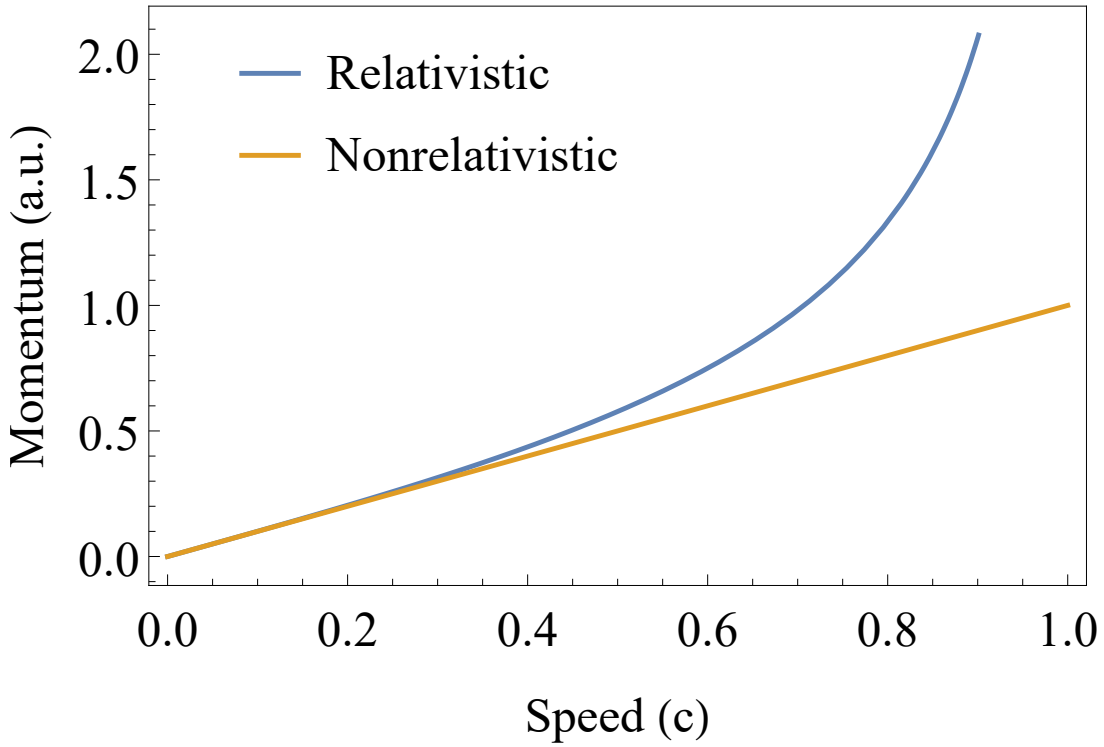

FIGURE 2.1: The relativistic and non-relativistic momentum of a point like particle as a function of the speed of light. Expressed in terms of Hartree atomic units.

and non-relativistic momenta are starting to disagree, with $p_{rel} = 1.005p$. This speed corresponds to the speed of the innermost electron in a silicon atom, the heaviest atom treated in this thesis.

The full relativistic treatment of the hydrogen atom would include, besides, a correction for the kinetic energy term, delocalisation effects due to the Compton wavelength of the electron and spin-orbit coupling due to the electron spin interacting with the magnetic field that is seen by its motion through the electric field of the nucleus [4].

2.3 Adding more Electrons

By adding more electrons to the Hamiltonian of the hydrogenic atom, a new term needs to be accounted for, the electron-electron Coulomb repulsion. This is the main source of headache in the field of electronic structure theory. The Hamiltonian of n electrons orbiting a nucleus with charge Ze and mass m_N is

$$-\frac{\hbar^2}{2m_N}\nabla_N^2\psi + \sum_i^n -\frac{\hbar^2}{2m_e}\nabla_i^2\psi + \sum_i^n -\frac{Ze^2}{4\pi\epsilon_0 r_{iN}}\psi + \sum_{i<j}^n \frac{e^2}{4\pi\epsilon_0 r_{ij}}\psi = E\psi(\vec{r}_1, ..., \vec{r}_n; \vec{r}_N). \tag{2.24}$$

This equation can no longer be solved analytically, nonetheless we can uncover necessary symmetries of the wavefunction by requiring that electrons are fundamentally indistinguishable. Assume we have a solution to equation 2.24

$$\psi(\vec{r}_1, ..., \vec{r}_n; \vec{r}_N). \tag{2.25}$$

Switching two electrons a and b in the wavefunction would still have to represent the same particle probability distribution

$$|\psi(\vec{r}_1, ..., \vec{r}_a, ..., \vec{r}_b, ..., \vec{r}_n; \vec{r}_N)|^2 = |\psi(\vec{r}_1, ..., \vec{r}_b, ..., \vec{r}_a, ..., \vec{r}_n; \vec{r}_N)|^2, \tag{2.26}$$

otherwise, the electrons could be distinguished through the wavefunction. This is only the case if the wavefunction is either symmetrical or antisimmetrical with respect to permutations in electron arguments,

$$\psi(\vec{r}_1, ..., \vec{r}_a, ..., \vec{r}_b, ..., \vec{r}_n; \vec{r}_N) = \pm\psi(\vec{r}_1, ..., \vec{r}_b, ..., \vec{r}_a, ..., \vec{r}_n; \vec{r}_N). \tag{2.27}$$

2.3.1 Spin Statistics

Experimental observation of the helium spectrum and many other atomic spectra has shown an interesting result: The whole wavefunction of an atom is always antisymmetrical with respect to permutations between two arbitrary electrons. Further, it is known through many experiments that the electron has an intrinsic quantized magnetic

moment. Due to these and many other experimental results, the Pauli principle was postulated [2], stating that a quantum state with unique quantum numbers (n, l, m_l, m_s) can only be occupied by a single electron. Where m_s is the spin magnetic quantum number that can take the values $\pm\frac{1}{2}$ in units of $\hbar$. Later theoretical examinations lead to the spin-statistics theorem [5] that states that the Pauli exclusion principle is true for all particles with half integer spins and they obey the Fermi-Dirac statistics. These particles are called fermions and include protons, electrons and neutrons. On the other hand, particles with integer spin are called bosons and their overall wavefuction is symmetric. They obey the Bose-Einstein statistic and include photons and phonons, amongst many others.

The spin quantum number σ is added to the electronic coordinates of an electron $\vec{r} = (x, y, z)$ to form the spin-orbital

$$\mathbf{r} = (\vec{r}, \sigma) = (x, y, z, \sigma), \tag{2.28}$$

which uniquely defines the state of a single electron.

Chapter 3

Interacting Electrons in Solids

Depending on the types of bonding between the constituent particles and their macroscopic properties solids can be classified into many categories. The most important distinction for this thesis is between crystalline solids and amorphous solids, with the primary interest of this work being in crystalline solids. Crystalline solids are characterized by a highly ordered and repetitive arrangement of atoms or molecules. They have a long ranged positional order (fernordnung) forming well-defined crystal structures. The main idea is to solve the Schrödinger equation in the unit cell, and recover the properties of the whole with appropriate periodic boundary conditions that incorporate the symmetries of the crystal. This is easier said than done.

In the next chapter, a short presentation of the mathematics of crystal structure will be shown, leading to the Schrödinger equation with periodic boundary conditions and Bloch's theorem. From there the many-body Hamiltonian of an arbitrary crystal will be presented together with the Born-Oppenheimer approximation, leading to the electronic structure Hamiltonian, which is the starting point of wavefunction based electronic structure theory.

3.1 Fernordnung

In a solid crystal, the atoms form a well-defined periodic arrangement known as the crystal structure. The crystal structure is characterized by its unit cell and the symmetry of the crystal structure is constrained by the requirement that the unit cell stacks perfectly with no gaps in all directions. In general, one can define an atom to sit at the zero point in the coordinate system and define a vector that points to an arbitrary neighbor atom

$$\vec{T}(m_1, m_2, m_3) = m_1\vec{a} + m_2\vec{b} + m_3\vec{c}. \tag{3.1}$$

Where $\vec{a}$, $\vec{b}$ and $\vec{c}$ are vectors pointing to the nearest neighboring atom (lattice vectors) and m_1, m_2 and m_3 are integers. The vector $\vec{T}$ is called the translation vector, and it contains the periodicity of the system. Many crystals don't have a single atom sitting on the grid, rather they have a group of atoms. It's enough to define the position of these atoms in the unit cell, and together with the vector $\vec{T}$ the crystal structure is uniquely defined. Further, it is expedient for the analysis of experimental data of crystal structures to define the reciprocal lattice vectors

$$\vec{a}^* = 2\pi \frac{\vec{b} \times \vec{c}}{\vec{a} \cdot (\vec{b} \times \vec{c})}, \tag{3.2}$$

$$\vec{b}^* = 2\pi \frac{\vec{c} \times \vec{a}}{\vec{b} \cdot (\vec{c} \times \vec{a})}, \tag{3.3}$$

$$\vec{c}^* = 2\pi \frac{\vec{a} \times \vec{b}}{\vec{c} \cdot (\vec{a} \times \vec{b})}. \tag{3.4}$$

The dimension of the reciprocal lattice vectors is one over length, already hinting that they are useful for describing the $\vec{k}$ vector. These vectors are defining a reciprocal lattice

$$\vec{G} = \vec{a}^* h + \vec{b}^* k + \vec{c}^* l, \tag{3.5}$$

with h,k and l being integers. The unit cell of the reciprocal lattice is called the Brillouin zone, and it is not the parallelepiped spanned by the vectors $\vec{a}^*$, $\vec{b}^*$ and $\vec{c}^*$. Rather, it is the polyhedron restricted by the planes that go through the middle of the vectors and are orthogonal to them.

Solving the Schrödinger equation inside the unit cell with periodic boundary conditions recovers the wavefunction of the whole crystal.

3.1.1 Bloch's Theorem

When we have electrons moving in a periodic potential, as it is the case for an electron moving in the potential of the ions of a crystal, it is expected that the wavefunction will also have periodicity. Bloch's theorem states that solutions to the Schrödinger equation in a periodic potential take the form of a plane wave modulated with a periodic function [4]

$$\psi_{\vec{k}}(\vec{r}) = u_{\vec{k}}(\vec{r}) e^{i\vec{k}\vec{r}}. \tag{3.6}$$

Where u has the same periodicity as the crystal and $\vec{k}$ is the crystal momentum vector. Usually these eingenstates are written as $\psi_{n\vec{k}}$ where n is a natural number called the band index and $\vec{k}$ is continuous. This wavefunction ansatz serves as a suitable basis for

electrons in crystals and the continuity of $\vec{k}$ gives rise to the band structure $\epsilon_n(\vec{k})$

$$\hat{H}\psi_{n\vec{k}} = \epsilon_n(\vec{k})\psi_{n\vec{k}}. \tag{3.7}$$

The quantum state in a solid is uniquely defined by $\psi_{n\vec{k}}$, but due to the periodicity of the crystal $\psi_{n\vec{k}} = \psi_{n(\vec{k}+\vec{K})}$, where $\vec{K}$ is an arbitrary reciprocal lattice vector. This means that the quantum state can be described exclusively in the Brillouin zone without loss of generality and the other quantum states outside the Brillouin zone are included through the periodicity.

3.2 The Many-Body Hamiltonian

The full Hamiltonian of interacting nuclei and interacting electrons including all terms is

$$\hat{\mathcal{H}} = \hat{T}_{\text{el}} + \hat{T}_{\text{nuc}} + V_{\text{el–nuc}} + V_{\text{el–el}} + V_{\text{nuc–nuc}}. \tag{3.8}$$

with

$$\hat{T}_{\text{el}} = \sum_i -\frac{\hbar^2}{2m_e}\nabla_i^2, \tag{3.9}$$

$$\hat{T}_{\text{nuc}} = \sum_N -\frac{\hbar^2}{2M}\nabla_N^2, \tag{3.10}$$

$$V_{\text{el–nuc}} = \sum_{iN} -\frac{Ze^2}{4\pi\epsilon_0 r_{iN}}, \tag{3.11}$$

$$V_{\text{el–el}} = \sum_{i<j}^{n} \frac{e^2}{4\pi\epsilon_0 r_{ij}}, \tag{3.12}$$

$$V_{\text{nuc–nuc}} = \sum_{M<N} \frac{Z^2e^2}{4\pi\epsilon_0 r_{MN}}. \tag{3.13}$$

In principle, the only task left, is to solve the Schrödinger equation

$$\hat{\mathcal{H}}\Psi_n(\vec{r}_1, ..., \vec{r}_n; \vec{R}_1, ..., \vec{R}_N) = E_n\Psi_n(\vec{r}_1, ..., \vec{r}_n; \vec{R}_1, ..., \vec{R}_N). \tag{3.14}$$

3.2.1 Born-Oppenheimer Approximation

Equation 3.14 has the curse of dimensionality and can only be solved exactly for up to two electrons. One has to find approximations in order to simplify the equation, without affecting the accuracy of the quantitative description we are looking for. The Born-Oppenheimer approximation allows to decouple the motion of the electrons and

the nuclei. This approximation is justified because the nuclei are four to five orders of magnitude heavier than the electron, meaning that the characteristic timescales also differ by the same amount. This means that any change in the position of the nuclei may be described as instantaneous from the perspective of the electrons. The zeroth-order Born-Oppenheimer approximation [6], also called the clamped-nuclei approximation, treats the nuclei as points that are fixed at the lattice sites. This approximation reduces the $V_{\text{nuc–nuc}}$ term to a simple constant and ignores the $\hat{T}_{\text{nuc}}$ term. Which leaves us with the non-relativistic electronic structure Hamiltonian in Hartree atomic units as

$$\hat{\mathcal{H}}_{\text{e}} = -\frac{1}{2}\sum_{i}\nabla_i^2 - \sum_{iN}\frac{Z}{|\vec{R}_N - \vec{r}_i|} + \frac{1}{2}\sum_{i\neq j}\frac{1}{|\vec{r}_i - \vec{r}_j|}. \tag{3.15}$$

With the $\vec{R}_N$ being well-defined constants describing the position of the nuclei. The resulting time independent Schrödinger equation

$$\hat{\mathcal{H}}_{\text{e}}(\mathbf{r})\Psi_n(\mathbf{r}) = E_n\Psi_n(\mathbf{r}), \tag{3.16}$$

is the main equation to solve in electronic structure theory. With $\mathbf{r} = \vec{r}_1, ..., \vec{r}_n$.

Chapter 4

Ab Initio Many-Body Methods

Ab initio many-body methods attempt to solve the electronic Schrödinger equation (equ 3.16) given the position of the nuclei and the number of electrons in order to yield useful information about the properties of the studied system from first principles. The computational ability to run these calculations has allowed theoreticians to bridge a wide knowledge gap [7]. Ab initio many-body methods can be classified as wavefunction based methods and non wavefunction based methods.

The most popular method is DFT, which is not wavefunction based. Further, the simplest wavefunction based electronic structure calculation method is the Hartree-Fock (HF) method. There is an array of methods trying to improve on the HF results, these are generally called post-Hartree-Fock methods and include Møller–Plesset perturbation theory (MP), configuration interaction (CI) and coupled cluster (CC). Another promising wavefunction based method is quantum Monte Carlo (QMC). The term encompasses a large family of computational methods, which all rely on repeated random sampling to solve the multidimensional integrals that arise in the different formulations of QMC. Although for most calculations these theories are based on a single-reference, they can be made to be multi-reference by generalization of the ansatz, but this work's focus is on single-reference theories only. Further, the techniques of machine learning have opened up new ways of accelerating calculations and exploring chemical space, that can be incorporated in the existing methods in many ways [7].

4.1 Density Functional Theory

DFT [8] is the most popular approach for electronic structure calculations of solids and large molecules due to its good trade off between accuracy and computational cost. The

basic idea of DFT is not to find the many-electron wavefunction, but rather the electronic density $n(\mathbf{r})$. This is made possible by two theorems by Hohenberg and Kohn [9]. The first theorem states that the non-relativistic ground state electron density $n(\mathbf{r})$ is uniquely defined by the potential $V_{ext}(\mathbf{r})$. The second theorem states that variations of the ground state electron density $n(\mathbf{r})$ can only lead to an increase in energy. Meaning that the ground state is unique and can be reached with a systematic variation of the electron density as a minimum. The theorems are mathematically proven and can be expanded to work for degenerate systems and time-dependent densities [10]. They allow writing the energy as a functional of the electron density

$$E[n(\mathbf{r})] = \int V_{ext}(\mathbf{r})n(\mathbf{r})\mathrm{d}\mathrm{r} + F[n(\mathbf{r})]. \tag{4.1}$$

where $V_{ext}(\mathbf{r})$ is the potential of the nuclei the electrons are moving through and $F[n(\mathbf{r})]$ is a system independent functional that includes the kinetic energy of the electrons and their Coulomb repulsion. The Coulomb repulsion between the electrons is the main culprit in making the Schrödinger equation practically unsolvable. The Hohenberg-Kohn theorem was further developed by Kohn and Sham to produce Kohn-Sham DFT [11]. In this framework, the problem of interacting electrons in a static potential is reduced to non-interacting electrons moving in an effective potential, where the effective potential includes the static potential of the nuclei and the effects of the Coulomb interactions of the electrons. Having non-interacting electrons allows us to write the electron density in terms of sums of orbitals

$$n(\mathbf{r}) = \sum_{i}^{N} |\psi_i(\mathbf{r})|^2. \tag{4.2}$$

where the index i runs over all occupied orbitals $\psi_i(\mathbf{r})$. This allows to write the total energy of a system expressed as a functional of the charge density in atomic units

$$E[n(\mathbf{r})] = -\frac{1}{2}\sum_i \int \psi_i^*(\mathbf{r})\nabla^2\psi_i(\mathbf{r})\mathrm{d}\mathbf{r} + \int V_{ext}(\mathbf{r})n(\mathbf{r})\mathrm{d}\mathbf{r} + \frac{1}{2}\int\int \frac{n(\mathbf{r})n(\mathbf{r}')}{|\mathbf{r}-\mathbf{r}'|}\mathrm{d}\mathbf{r}\mathrm{d}\mathbf{r}' + E_{xc}[n(\mathbf{r})]. \tag{4.3}$$

The first term is the kinetic energy $T[n(\mathbf{r})]$ of the non-interacting electrons occupying one-body orbitals $\psi_i(\mathbf{r})$, the second term is the interaction of the charge density with the static potential of the nuclei, the third term, is the Hartree energy $E_H[n(\mathbf{r})]$, representing the classical energy it would take to hold the shape of the charge density against its own Coulomb repulsion and the last term is the so-called exchange correlation (XC) energy, which represents the remaining error to the energy functional and is defined as

$$E_{xc}[n(\mathbf{r})] = F[n(\mathbf{r})] - T[n(\mathbf{r})] - E_H[n(\mathbf{r})]. \tag{4.4}$$

Minimization of the energy functional from equation 4.3 leads to a set of self-consistent equations, the Kohn-Sham equations [11]

$$\left(-\frac{1}{2}\nabla_i^2 + V_N(\mathbf{r}) + V_H(\mathbf{r}) + V_{xc}(\mathbf{r})\right)\psi_i(\mathbf{r}) = \epsilon_i\psi_i(\mathbf{r}). \tag{4.5}$$

where V_N is the nuclear electrostatic potential, V_H is the Hartree potential

$$V_H(\mathbf{r}) = \int \frac{n(\mathbf{r}')}{|\mathbf{r}-\mathbf{r}'|}\mathrm{d}\mathbf{r}' \ , \tag{4.6}$$

and $V_{xc}(\mathbf{r})$ the so-called XC potential

$$V_{xc}(\mathbf{r}) = \frac{\delta E_{xc}[n(\mathbf{r})]}{\delta n(\mathbf{r})} \ . \tag{4.7}$$

The presented approach is in principle exact, but the general exchange correlation energy is unknown and has to be approximated. This is the starting point of XC approximations with increasing complexity, that constitute a hierarchy of density functional approximation theories (DFA).

4.1.1 Exchange Correlation Approximation Hierarchy

The different types of exchange correlation functionals with increasing accuracy are presented in figure 4.1 called the Jacobs ladder [12].

The simplest approximation to the XC functional and first on the Jacobs ladder, is called Local Density Approximation (LDA)

$$E_{xc}[n(\mathbf{r})] = \int \epsilon_{xc}(n(\mathbf{r}))n(\mathbf{r})\mathrm{d}\mathbf{r}, \tag{4.8}$$

where the $\epsilon_{xc}(n(\mathbf{r}))$ is the XC correlation energy density of the uniform electron gas (UEG) with the density $n(\mathbf{r})$. The exchange part of the UEG is well known, the first accurate description of the correlation part has been achieved with QMC [14]. LDA gives accurate predictions of equilibrium geometries of solids and molecules, as well as bond lengths [15]. However, it fails for the accurate description of band gaps and reaction energies. One way to improve upon LDA is to include the gradient of the charge density

$$E_{xc}[n(\mathbf{r})] = \int \epsilon_{xc}(n(\mathbf{r}), \nabla n(\mathbf{r}))n(\mathbf{r})\mathrm{d}\mathbf{r} \ , \tag{4.9}$$

where ϵ_{xc} is typically expanded into a set of parameterized non-linear functions. This is called a general gradient approximation (GGA). The most widely-used GGA functional in solid state calculations is PBE [16]. To improve further, one can include the kinetic

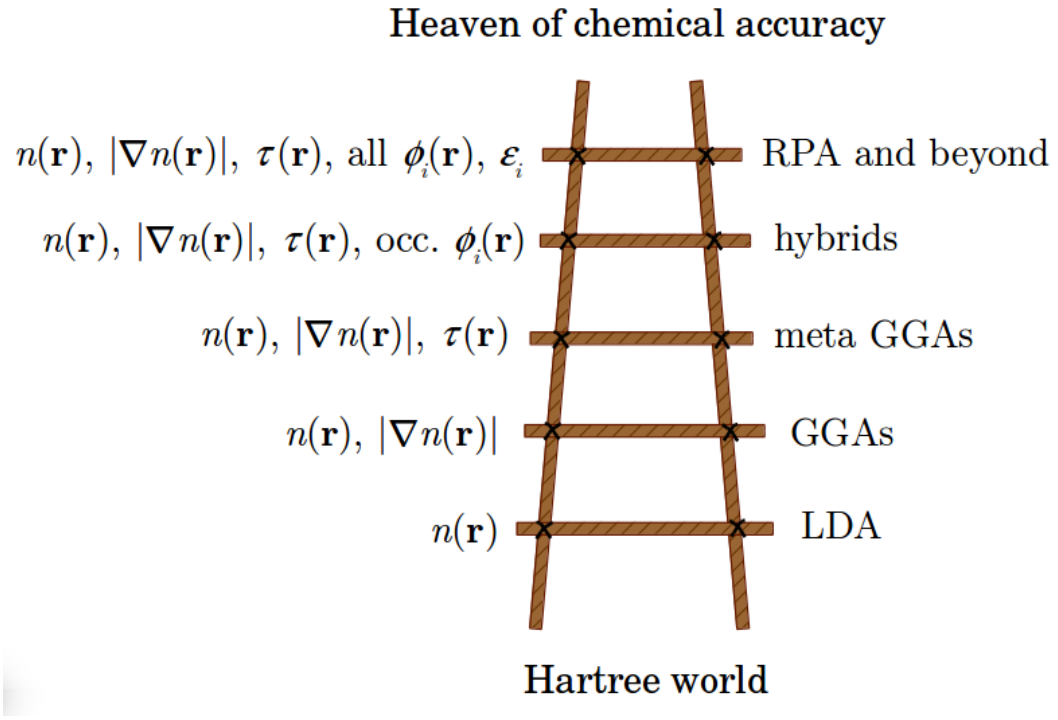

FIGURE 4.1: Jacob's ladder of approximations to the XC functional from Ref. [13].

energy density $\tau(\mathbf{r})$ to the XC functional, referred to as meta-GGA [17]. At this point, the XC correlation functional is still semi-local in the Kohn-Sham calculation, meaning that it can still be expressed as an integral over three-dimensional space with ingredients that are available at each point $\mathbf{r}$. The next step in improving the XC functional approximation is adding the fully non-local exact exchange energy from HF. This is typically done with a weighting parameter α, the resulting XC functional is called a hybrid functional [18].

$$E_{\mathrm{XC}}^{\mathrm{Hybrid}} = E_{\mathrm{XC}}^{\mathrm{GGA}} + \alpha(E_{\mathrm{X}}^{\mathrm{exact}} - E_{\mathrm{X}}^{\mathrm{GGA}}) \,, \tag{4.10}$$

At this point, all the occupied orbitals are included in the XC functional, including the exchange energy. Further improvement can be achieved by including the unoccupied orbitals. This can be done with random phase approximation [19, 20] (RPA) or by means of perturbation theory on top of the Kohn-Sham orbitals as it is done by double hybrid approximations [21].

4.2 Hartree Fock Theory

Hartree-Fock theory [22–24] is a wavefunction based method build on the Hartree product ansatz

$$\psi(x_1, x_2, ..., x_n) = \psi(x_1)\psi(x_2)....\psi(x_n). \tag{4.11}$$

This ansatz would lead to the analytically exact solution in the case of non-interacting electrons. However, as we have seen in chapter 2.3.1, the many-electron wavefunction is always antisymmetric with respect to permutations of two electron arguments. We can construct an antisymmetric linear combination of Hartree products with the Slater determinant

$$\Psi(\mathbf{x}_1, \mathbf{x}_2, \ldots, \mathbf{x}_N) = \frac{1}{\sqrt{N!}} \begin{vmatrix} \psi_1(\mathbf{x}_1) & \psi_1(\mathbf{x}_2) & \ldots & \psi_1(\mathbf{x}_N) \\ \psi_2(\mathbf{x}_1) & \psi_2(\mathbf{x}_2) & \ldots & \psi_2(\mathbf{x}_N) \\ \vdots & \vdots & \vdots & \vdots \\ \psi_N(\mathbf{x}_1) & \psi_N(\mathbf{x}_2) & \ldots & \psi_N(\mathbf{x}_N) \end{vmatrix} . \tag{4.12}$$

Where the $\mathbf{x}$ is includes the spatial and spin coordinates of the electron. In HF theory, we are trying to solve the general electronic structure Hamiltonian 3.15 by employing the variational principle to self-consistently optimize the one electron orbitals in the Slater determinant, in order to get an upper bound to the ground state energy, implying an mean field theory. Note that the exact exchange is taken into account through the antisymmetry of the Slater determinant. Also the orbitals $\psi_n(\mathbf{x}_n)$ are orthonormal.

By using the Slater-Condon rules (see appendix A) and the Slater determinant as the wavefunction ansatz, the variational HF energy takes the form

$$E_{\mathrm{HF}} = \langle \Psi | \hat{\mathcal{H}} | \Psi \rangle = \sum_{i}^{\mathrm{occ.}} \langle \psi_i | \hat{h} | \psi_i \rangle + \frac{1}{2} \sum_{i,j}^{\mathrm{occ.}} \left(\langle \psi_i \psi_j | \psi_i \psi_j \rangle - \langle \psi_i \psi_j | \psi_j \psi_i \rangle \right) , \tag{4.13}$$

with the one-body integral $\langle \psi_i | \hat{h} | \psi_i \rangle$ defined as

$$\langle \psi_i | \hat{h} | \psi_i \rangle = -\frac{1}{2} \langle \psi_i | \nabla^2 | \psi_i \rangle + \langle \psi_i | V_{\mathrm{N}}(\mathbf{r}) | \psi_i \rangle , \tag{4.14}$$

and $V_{\mathrm{N}}(\mathbf{r})$ being the nuclear potential . The first two-electron integral describes the classical electrostatic Coulomb interaction between two charge densities

$$\langle \psi_i \psi_j | \psi_i \psi_j \rangle = \int \int \psi_i^*(\mathbf{x}) \psi_j^*(\mathbf{x}') \frac{1}{|\mathbf{r} - \mathbf{r}'|} \psi_i(\mathbf{x}) \psi_j(\mathbf{x}') \mathrm{d}\mathbf{x} \mathrm{d}\mathbf{x}' . \tag{4.15}$$

The second two-electron integral has no classical counterpart

$$\langle \psi_i \psi_j | \psi_j \psi_i \rangle = \int \int \psi_i^*(\mathbf{x}) \psi_j^*(\mathbf{x}') \frac{1}{|\mathbf{r} - \mathbf{r}'|} \psi_j(\mathbf{x}') \psi_i(\mathbf{x}) \mathrm{d}\mathbf{x} \mathrm{d}\mathbf{x}' . \tag{4.16}$$

It arises out of the antisymmetry of the wavefunction ansatz and is referred to as the exchange integral.

Using the method of Lagrange multipliers with the constraint that the one-electron orbitals are orthonormal $\langle\psi_i|\psi_j\rangle = \delta_{ij}$ we get the self-consistent HF equations [25]

$$\hat{h}(\mathbf{r})\psi_i(\mathbf{x}) + \sum_j \left(\int \psi_j^*(\mathbf{x}') \frac{1}{|\mathbf{r}-\mathbf{r}'|} \psi_j(\mathbf{x}') \mathrm{d}\mathbf{x}' \right) \psi_i(\mathbf{x}) \\ - \sum_j \left(\int \psi_j^*(\mathbf{x}') \frac{1}{|\mathbf{r}-\mathbf{r}'|} \psi_i(\mathbf{x}') \mathrm{d}\mathbf{x}' \right) \psi_j(\mathbf{x}) = \epsilon_i \psi_i(\mathbf{x}) \ , \tag{4.17}$$

where ϵ_i are eigenenergies of the one-electron orbitals ψ_i. This equation is often written in the form

$$\left(\hat{h}(\mathbf{r}) + \sum_j \left[\hat{J}_j - \hat{K}_j \right] \right) \psi_i(\mathbf{x}) = \epsilon_i \psi_i(\mathbf{x}). \tag{4.18}$$

With $\hat{J}_j$ being the Coulomb operator, and the $\hat{K}_j$ the exchange operator. Further, the Fock operator is defined as

$$\hat{f} = \hat{h}(\mathbf{r}) + \sum_j \left[\hat{J}_j - \hat{K}_j \right] \ , \tag{4.19}$$

making it possible to write the HF equations in the compact form

$$\hat{f}\psi_i = \epsilon_i \psi_i \ . \tag{4.20}$$

The presented HF theory has no assumptions regarding the spin part of the spin-orbitals. When each spatial orbital is occupied twice, with one spin-up and one spin-down electron the theory is called closed shell or restricted. Carrying out the spin integration explicitly in equation 4.13 gives the prefactors two, four and two for the three constituents resulting in

$$E_{\mathrm{HF}} = 2\sum_i^{\mathrm{occ.}} \langle\psi_i|\hat{h}|\psi_i\rangle + \sum_{i,j}^{\mathrm{occ.}} \left(2\langle\psi_i\psi_j|\psi_i\psi_j\rangle - \langle\psi_i\psi_j|\psi_j\psi_i\rangle \right) \ , \tag{4.21}$$

where the summation over i and j is now covering only the spatial part of the spin-orbitals.

The correlation energy is defined as

$$E_{\mathrm{corr}} = E_{\mathrm{exact}} - E_{\mathrm{HF}}. \tag{4.22}$$

The correlation energy is often just a small contribution to the overall energy, but it usually contributes significantly to energy differences that are of great importance in determining chemical properties. By definition correlation energy is the part of the non-relativistic energy that is missing in HF theory, thus more sophisticated theories have to be used, commonly referred to as post-Hartree-Fock theory.

4.2.1 Introducing a Basis Set: Roothaan Equations

In all computer implementations of HF theory, the one-electron orbitals $\psi_i(\mathbf{x})$ are represented in terms of a basis set with basis functions χ_μ and coefficients $C_{\mu i}$

$$\psi_i(\mathbf{r}) = \sum_{\mu=1}^{N_\mathrm{b}} \chi_\mu(\mathbf{r}) C_{\mu i}. \tag{4.23}$$

The basis set can be composed of atomic orbitals, which is the usual choice for atoms and molecules. Several choices of atomic orbitals can be used, the most used are Slater-type orbitals (STO), Gaussian-type orbitals (GTO) and even numerical orbitals [26]. Out of the three, GTO's are most often used because they allow an efficient implementation of post-Hartree-Fock methods. In periodic systems, a plane wave basis set represent a convenient choice [26]. They are often used in combination with an 'effective core potential' or pseudopotential [27], such that the plane waves are only used to describe the valence charge density.

By using a complete orthonormal basis set, every orbital can be represented uniquely and exactly. In principle, one needs an infinite amount of functions to do that. Thus, a truncated basis set is used in practice, introducing the basis set incompleteness error (BSIE). Inserting the basis set representation of the orbitals 4.26 into the Fock eigenstate equation 4.20 leads to the Roothaan equations [25]

$$\hat{f} \sum_{\mu=1}^{N_\mathrm{b}} \chi_\mu(\mathbf{r}) C_{\mu i} = \epsilon_i \sum_{\mu=1}^{N_\mathrm{b}} \chi_\mu(\mathbf{r}) C_{\mu i}. \tag{4.24}$$

By multiplying from the left with $\chi^*_\nu(\mathbf{r})$ and integrating over $\mathbf{r}$ the Roothaan equations can be written in the compact form

$$\sum_\nu F_{\mu\nu} C_{\nu i} = \epsilon_i C_{\mu i} \ , \tag{4.25}$$

where $F_{\mu\nu}$ is the Fock matrix in an orthonormal basis set

$$F_{\mu\nu} = \langle \chi_\mu | \hat{f} | \chi_\nu \rangle \ . \tag{4.26}$$

4.3 Post Hartree-Fock

In HF theory the many-electron wavefunction is represented as a single Slater determinant constructed from orbitals that are variationally optimized by minimizing the

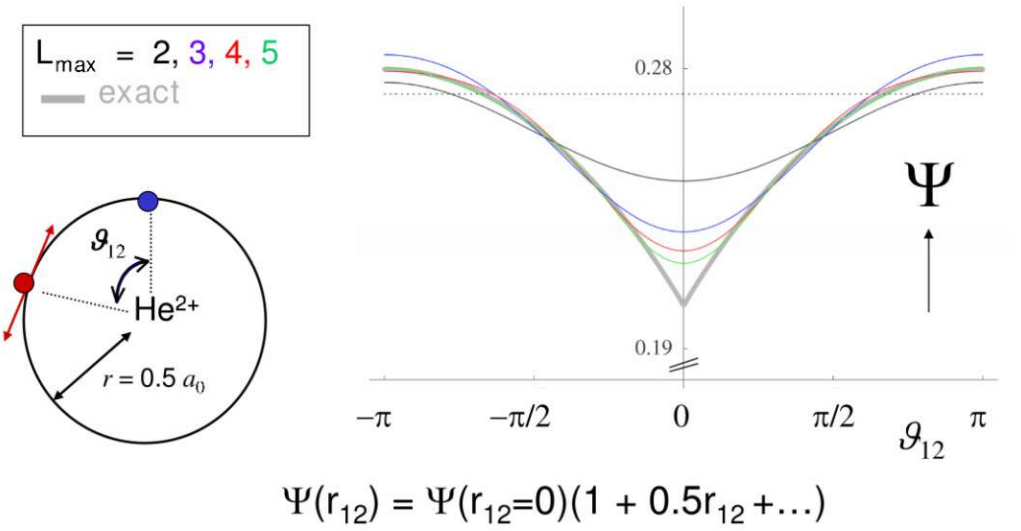

FIGURE 4.2: Two-electron wavefunction of the He atom as a function of the angle θ_{12} for a fixed radial distance. Figure taken from Ref [30]

energy. In post Hartree-Fock theory the many-electron wavefunction is expanded as a linear combination of Slater determinants, constructed from the unoccupied HF one-electron orbitals. This gives rise to a specific convergence problem with basis set size at the so called electron-electron cusp.

4.3.0.1 Electron-Electron Cusp

The electron-electron cusp arises from the fact that in the limit of the interelectronic distance going to zero, the Coulomb repulsion between the electrons diverges [28, 29]. In order for the energy to remain finite, the singularity has to be canceled out by an opposite singularity in the kinetic energy, creating a discontinuity in the first derivative of the wavefunction and a cusp in the wavefunction. Such a cusp can be approximated using a finite basis set but only in the limit of $N_\mathrm{b} \to \infty$ will the discontinuity mathematically be there. This results in slow convergence of chemical properties with increasing basis set size as shown in figure 4.2 for the helium atom.

Every post HF theory has this electron-electron cusp convergence issue and in practice tricks have to be used to model the cusp in order to speed up the convergence of the electronic structure calculations.

4.3.1 Configuration Interaction

In Configuration interaction, the wavefunction is represented as a linear combination of excited Slater determinants [25]. An excited Slater determinant is obtained by replacing an occupied orbital ψ_i in the HF determinant 4.12 with a virtual orbital ψ_a as shown in equation 4.27 and 4.28.

$$\Psi(\mathbf{x}_1,\ldots,\mathbf{x}_N) = \frac{1}{\sqrt{N!}} \begin{vmatrix} \psi_1(\mathbf{x}_1) & \psi_1(\mathbf{x}_2) & \ldots & \psi_1(\mathbf{x}_N) \\ \psi_2(\mathbf{x}_1) & \psi_2(\mathbf{x}_2) & \ldots & \psi_2(\mathbf{x}_N) \\ \vdots & \vdots & \vdots & \vdots \\ \psi_i(\mathbf{x}_1) & \psi_i(\mathbf{x}_2) & \ldots & \psi_i(\mathbf{x}_N) \\ \vdots & \vdots & \vdots & \vdots \\ \psi_N(\mathbf{x}_1) & \psi_N(\mathbf{x}_2) & \ldots & \psi_N(\mathbf{x}_N) \end{vmatrix}, \tag{4.27}$$

$$\Psi_i^a(\mathbf{x}_1,\ldots,\mathbf{x}_N) = \frac{1}{\sqrt{N!}} \begin{vmatrix} \psi_1(\mathbf{x}_1) & \psi_1(\mathbf{x}_2) & \ldots & \psi_1(\mathbf{x}_N) \\ \psi_2(\mathbf{x}_1) & \psi_2(\mathbf{x}_2) & \ldots & \psi_2(\mathbf{x}_N) \\ \vdots & \vdots & \vdots & \vdots \\ \psi_a(\mathbf{x}_1) & \psi_a(\mathbf{x}_2) & \ldots & \psi_a(\mathbf{x}_N) \\ \vdots & \vdots & \vdots & \vdots \\ \psi_N(\mathbf{x}_1) & \psi_N(\mathbf{x}_2) & \ldots & \psi_N(\mathbf{x}_N) \end{vmatrix}. \tag{4.28}$$

By substituting one, two or three orbitals one obtains singly, doubly and triply excited determinants. The occupied orbitals are typically denoted by the indexes $i, j \ldots$ and the virtual orbitals with $a, b, \ldots$. Note that due to the antisymmetric mixing of orbitals, it doesn't matter which electron is excited. The many-electron wavefunction is expanded in the basis of Slater determinants as

$$\Psi_{\mathrm{CI}} = \sum_I c_I \Phi_I \ . \tag{4.29}$$

Where I is the set of all indices describing excited Slater determinants up to N-th order and Φ_I is the corresponding Slater determinant. With the one-particle orbitals being orthonormal and complete ($\langle\phi_i|\phi_j\rangle = \delta_{ij}$) all possible Slater determinants are also orthonormal and complete ($\langle\Phi_I|\Phi_J\rangle = \delta_{IJ}$). The expansion coefficients c_I can be obtained variationally minimizing the energy expectation value

$$E_{\mathrm{CI}} = \frac{\langle\Psi_{\mathrm{CI}}|\hat{\mathcal{H}}|\Psi_{\mathrm{CI}}\rangle}{\langle\Psi_{\mathrm{CI}}|\Psi_{\mathrm{CI}}\rangle} \ . \tag{4.30}$$

which leads to an eigenvalue equation [25]

$$\langle \Phi_I | \hat{\mathcal{H}} - E_{\mathrm{CI}} | \Psi_{\mathrm{CI}} \rangle = \sum_J \left[\langle \Phi_I | \hat{\mathcal{H}} | \Phi_J \rangle - \lambda c_J \delta_{IJ} \right] = 0 \ , \tag{4.31}$$

that can be rewritten in compact form

$$\mathbf{Hc} = \mathbf{Ec}, \tag{4.32}$$

where **H** is the Hamiltonian matrix in the Slater determinant basis, **c** is the vector containing the coefficients, and **E** is a diagonal matrix with the energy expectation values of the ground and excited states. When all possible excitations are included in the CI expansion, this is referred to as the the full CI (FCI) expansion. FCI is often called exact diagonalization, as it represents the exact solution within the employed basis set. In practice not all excitations can be included, one has to cut the determinant space at some level of excitation. This gives rise to a hierarchy of CI theory, CIS, CISD, CISDT and so on, where the suffixes S, D and T mean singly, doubly and triply excited Slater determinants are included in the CI expansion.

A major issue of the truncated CI methods, is that they are not size consistent. Meaning that the sum of energies of independently computed parts of a system is not equal to the energy of the total system, even if the parts are not interacting. Note that the FCI method is size consistent. For example, let's consider two Helium atoms separated by an infinite distance described by CISD theory. A single atom has two electrons, and CISD is equivalent to FCI in this case. The energy of two infinitely separated helium atoms should be equivalent to two times the energy of the single helium atom, since they are not interacting. This is not the case with CISD, since the product of both atoms being doubly excited is now a quadruple excitation in the two atom (four electron) system and is not included in the expansion of the wavefunction. This problem is solved by the exponential ansatz in CC theory, which will be shown later.

4.3.2 Møller–Plesset Perturbation Theory

Perturbation theory in quantum mechanics refers to an approximation scheme. The basic idea is to split the Hamiltonian into an unperturbed part, to which solutions are already known, and an ideally small perturbation. By introducing the perturbation to the known Hamiltonian, we break down the problem into two parts: a solvable unperturbed system and a small perturbation that causes deviations from these exact known solutions.

$$\hat{H} = \hat{H}^{(0)} + \lambda \hat{V}, \tag{4.33}$$

The wavefunction and corresponding energies are expanded in a series in terms of λ, that converges faster when the λ is small. Note that one can derive a system dependent convergence criterion as a function of λ, that has to be fulfilled in order for the perturbation expansion to converge at all. In quantum mechanics, this is generally called Rayleigh-Schödinger perturbation theory [31] (see appendix B). Note that the convergence can be oscillating. In the case of the unperturbed Hamiltonian being the self-consistent HF ground state this is called Møller–Plesset (MP) perturbation theory [32]. The Hamiltonian is written as

$$\hat{\mathcal{H}} = \hat{\mathcal{H}}^{(0)} + \hat{\mathcal{V}}, \tag{4.34}$$

$$\hat{\mathcal{H}}^{(0)} = \sum_{i}^{\text{occ.}} \hat{f}(i) \ , \tag{4.35}$$

$$\hat{\mathcal{V}} = \hat{\mathcal{H}} - \hat{\mathcal{H}}^{(0)} \ . \tag{4.36}$$

Where the unperturbed Hamiltonian is the sum of all Fock operators defined in equation 4.19 and $\hat{\mathcal{H}}$ is the exact electronic Hamiltonian. The HF Slater determinant $\Psi^{(0)}$, consisting of canonical HF orbitals (eigenstates of the Fock operators), is the solution to the unperturbed Hamiltonian

$$\hat{\mathcal{H}}^{(0)}\Psi^{(0)} = E^{(0)}\Psi^{(0)} \ . \tag{4.37}$$

Where $E^{(0)}$ is the zeroth-order energy and is the sum of the eigenenergies of the canonical HF orbitals

$$E^{(0)} = \sum_{i}^{\text{occ.}} \epsilon_i \ . \tag{4.38}$$

The first order energy correction to the zeroth-order Hamiltonian yields the HF energy

$$\langle\Psi^{(0)}|\hat{\mathcal{H}}^{(0)}|\Psi^{(0)}\rangle + \langle\Psi^{(0)}|\hat{\mathcal{V}}|\Psi^{(0)}\rangle = E^{(0)} + E^{(1)} = E_{\text{HF}} \tag{4.39}$$

In order to improve on the HF ground state with MP theory, we have to go at least to the second order energy

$$E^{(2)} = \langle\Psi^{(1)}|\hat{\mathcal{V}}|\Psi^{(0)}\rangle = \langle\Psi^{(1)}|\hat{\mathcal{H}} - \hat{\mathcal{H}}^{(0)}|\Psi^{(0)}\rangle \ . \tag{4.40}$$

The equations above depends on the first order wavefunction $\Psi^{(1)}$, which can be written in the basis of excited Slater determinants

$$\Psi^{(1)} = \sum_{i}^{\text{occ.}}\sum_{a}^{\text{vir.}} t_i^a \Phi_i^a + \sum_{i<j}^{\text{occ.}}\sum_{a<b}^{\text{vir.}} t_{ij}^{ab}\Phi_{ij}^{ab} + \dots . \tag{4.41}$$

Using this wavefunction ansatz with Rayleigh-Schrödinger perturbation theory (see appendix B) and projecting onto the excited Slater determinants $\langle\Phi_i^a|, \langle\Phi_{ij}^{ab}|, \dots$, yields

the following equations

$$\begin{aligned}
&\sum_{k}^{\text{occ.}}\sum_{c}^{\text{vir.}}\langle\Phi_i^a|\hat{\mathcal{H}}^{(0)}-E^{(0)}|\Phi_k^c\rangle t_k^c+\langle\Phi_i^a|\hat{\mathcal{H}}|\Phi\rangle=0\\
&\sum_{k>l}^{\text{occ.}}\sum_{c>d}^{\text{vir.}}\langle\Phi_{ij}^{ab}|\hat{\mathcal{H}}^{(0)}-E^{(0)}|\Phi_{kl}^{cd}\rangle t_{kl}^{cd}+\langle\Phi_{ij}^{ab}|\hat{\mathcal{H}}|\Phi\rangle=0\\
&\vdots
\end{aligned} \tag{4.42}$$

Slater determinants that are built from canonical HF orbitals are eigenstates of $\hat{\mathcal{H}}^{(0)}$, so that the first term on the left-hand side of equation 4.42 yields

$$\begin{aligned}
&\sum_{k}^{\text{occ.}}\sum_{c}^{\text{vir.}}\langle\Phi_i^a|\hat{\mathcal{H}}^{(0)}-E^{(0)}|\Phi_k^c\rangle t_k^c=(\epsilon_a-\epsilon_i)t_i^a\\
&\sum_{k>l}^{\text{occ.}}\sum_{c>d}^{\text{vir.}}\langle\Phi_{ij}^{ab}|\hat{\mathcal{H}}^{(0)}-E^{(0)}|\Phi_{kl}^{cd}\rangle t_{kl}^{cd}=(\epsilon_a+\epsilon_b-\epsilon_i-\epsilon_j)t_{ij}^{ab}\ .
\end{aligned} \tag{4.43}$$

We thus arrive at the following result for the amplitudes

$$\begin{aligned}
t_i^a&=-\frac{\langle\Phi_i^a|\hat{\mathcal{H}}|\Phi\rangle}{(\epsilon_a-\epsilon_i)}\\
t_{ij}^{ab}&=-\frac{\langle\Phi_{ij}^{ab}|\hat{\mathcal{H}}|\Phi\rangle}{(\epsilon_a+\epsilon_b-\epsilon_i-\epsilon_j)}\ .
\end{aligned} \tag{4.44}$$

Due to the Slater-Condon rules (see appendix A) for two-electron operators, Slater determinants with more than double excitations yield zero amplitudes. Further, singly excited amplitudes also vanish due to the Brillouin condition for canonical HF orbitals $\langle\Phi_i^a|\hat{\mathcal{H}}|\Phi\rangle=\hat{f}_i^a=0$.

Consequently, we have arrived at the result that only double excitations contribute to the first-order wavefunction and the second-order energy in Møller–Plesset perturbation theory. The first-order wavefunction is therefore

$$\Psi^{(1)}=\sum_{i<j}^{\text{occ.}}\sum_{a<b}^{\text{vir.}}t_{ij}^{ab}\Phi_{ij}^{ab}\ , \tag{4.45}$$

where the amplitudes are

$$t_{ij}^{ab}=-\frac{\langle\psi_i\psi_j|\psi_a\psi_b\rangle-\langle\psi_j\psi_i|\psi_a\psi_b\rangle}{\epsilon_a+\epsilon_b-\epsilon_i-\epsilon_j}\ . \tag{4.46}$$

The second order energy is thus

$$E^{(2)} = \langle \Psi^{(1)} | \hat{\mathcal{H}} | \Psi^{(0)} \rangle = \sum_{i<j}^{\text{occ.}} \sum_{a<b}^{\text{vir.}} t_{ij}^{ab} \langle \Phi_{ij}^{ab} | \hat{\mathcal{H}} | \Phi \rangle$$
$$= -\sum_{i<j}^{\text{occ.}} \sum_{a<b}^{\text{vir.}} \frac{\Big[\langle \psi_i \psi_j | \psi_a \psi_b \rangle - \langle \psi_j \psi_i | \psi_a \psi_b \rangle \Big]^2}{\epsilon_a + \epsilon_b - \epsilon_i - \epsilon_j} \,. \tag{4.47}$$

Where $\langle \psi_i \psi_j | \psi_a \psi_b \rangle$ is the physicist notation for the Coulomb integral defined in equation 4.15. A closed shell expression in terms of spatial orbitals can be derived by assuming that every orbital is occupied twice with a spin-up and spin-down electron. Spin integration yields

$$E^{(2)} = -\sum_{i,j}^{\text{occ.}} \sum_{a,b}^{\text{vir.}} \frac{\langle \phi_i \phi_j | \phi_a \phi_b \rangle \Big[2 \langle \phi_i \phi_j | \phi_a \phi_b \rangle - \langle \phi_j \phi_i | \phi_a \phi_b \rangle \Big]}{\epsilon_a + \epsilon_b - \epsilon_i - \epsilon_j} \,, \tag{4.48}$$

where the indices i, j, a, and b, run over the spatial orbitals ϕ. The total MP2 energy takes the form

$$E_{\text{MP2}} = E^{(0)} + E^{(1)} + E^{(2)} = E_{\text{HF}} + E^{(2)} \,. \tag{4.49}$$

MP2 theory is the simplest many-body theory that captures correlation effects. MP2 theory provides a fair compromise between efficiency and accuracy, capturing non-local Van der Waals (vdW) interactions. However, if the HOMO-LUMO gap or band gap in periodic systems is small, MP2 theory gives less reliable results. Higher-order perturbation expansions are also straight forward, however, they are rarely used due to their computational cost.

4.3.3 Coupled Cluster Theory

Møller–Plesset perturbation theory offers a finite-order approximation to the electronic correlation, coupled-cluster (CC) theory [33] on the other hand provides a framework of infinite-order approximations. By trying to correlate the spin-orbitals of electrons using a correlation function, as described in [33], an exponential excitation ansatz emerges naturally. Coupled cluster theory can be seen as a size consistent expansion of correlation space, no matter the order of the excitation space cut off.

In the CC method, the wavefunction is written using the exponential ansatz

$$|\Psi_{\text{CC}}\rangle = \exp(\hat{T}) |0\rangle \,, \tag{4.50}$$

where the cluster operator $\hat{T}$ is defined as

$$\hat{T} = \hat{T}_1 + \hat{T}_2 + \hat{T}_3 + \dots \ . \tag{4.51}$$

The excitation operators can be written in terms of second quantisation

$$\begin{aligned}
\hat{T}_1 &= \sum_i \sum_a t_i^a \hat{a}_a^\dagger \hat{a}_i \\
\hat{T}_2 &= \frac{1}{4} \sum_{ij} \sum_{ab} t_{ij}^{ab} \hat{a}_a^\dagger \hat{a}_b^\dagger \hat{a}_j \hat{a}_i \\
\hat{T}_3 &= \frac{1}{36} \sum_{ijk} \sum_{abc} t_{ijk}^{abc} \hat{a}_a^\dagger \hat{a}_b^\dagger \hat{a}_c^\dagger \hat{a}_k \hat{a}_j \hat{a}_i \\
&\vdots
\end{aligned} \tag{4.52}$$

Them acting on the reference Slater determinant creates excited Slater determinants with coefficients $t_i^a, t_{ij}^{ab}, t_{ijk}^{abc}, \dots$. The reference Slater determinant is typically the HF Slater determinant.

The exponential of the cluster operator is given by the expansion

$$\exp\left(\hat{T}\right) = 1 + \hat{T} + \frac{1}{2!}\hat{T}\hat{T} + \frac{1}{3!}\hat{T}\hat{T}\hat{T} + \cdots \equiv \sum_0^\infty \frac{1}{n!}\hat{T}^n \ . \tag{4.53}$$

For an N-electron system, the cluster operator $\hat{T}$ contains up to N-fold excitations and is exact. In practice, the cluster operator $\hat{T}$ is truncated at some number of excitations, yielding a hierarchy of CC theories termed CCS, CCSD, CCSDT, etc., where the suffixes S, D and T, stand for singles, doubles and triples excitations included. Due to the cut-off happening in the argument of the exponential instead in the wavefunction expansion itself, all combinations of excited Slater determinants (up to the order of the cut-off) are included in the wavefunction and thus the theory is guaranteed to be size consistent.

First we will take a look at CCSD theory. The cluster operator is now truncated after $\hat{T}_2$ and the wavefunction ansatz reads

$$\hat{T} = \hat{T}_1 + \hat{T}_2, \tag{4.54}$$

$$|\Psi_{\mathrm{CCSD}}\rangle = \exp\left(\hat{T}_1 + \hat{T}_2\right)|0\rangle = \left(1 + \hat{T}_1 + \hat{T}_2 + \frac{1}{2!}\hat{T}_1^2 + \hat{T}_1\hat{T}_2 + \frac{1}{3!}\hat{T}_1^3 + \frac{1}{4!}\hat{T}_1^4 + \frac{1}{2!}\hat{T}_2^2 + \dots\right)|0\rangle \ . \tag{4.55}$$

Where $|0\rangle$ is the HF reference wavefunction. In order to compute the CC energy and the t_i^a and t_{ij}^{ab} amplitudes, we plug the CCSD wavefunction $|\Psi_{\mathrm{CCSD}}\rangle$ into the Schrödinger

equation and project onto the HF, singly and doubly excited Slater determinants

$$\langle 0|\big(\hat{\mathcal{H}} - E_{\mathrm{CCSD}}\big)|\Psi_{\mathrm{CCSD}}\rangle = 0 \tag{4.56}$$
$$\langle \Phi_i^a|\big(\hat{\mathcal{H}} - E_{\mathrm{CCSD}}\big)|\Psi_{\mathrm{CCSD}}\rangle = 0 \tag{4.57}$$
$$\langle \Phi_{ij}^{ab}|\big(\hat{\mathcal{H}} - E_{\mathrm{CCSD}}\big)|\Psi_{\mathrm{CCSD}}\rangle = 0\ . \tag{4.58}$$

Note that from now on we are talking about closed shell CCSD with intermediate normalization $\langle 0|\Psi_{\mathrm{CCSD}}\rangle = 0$. From equation 4.56 the CCSD correlation energy is obtained

$$\begin{aligned} E_{\mathrm{corr}} = E_{\mathrm{CCSD}} - E_{\mathrm{HF}} &= \langle 0|\big(\hat{\mathcal{H}} - E_{\mathrm{CCSD}}\big)|\Psi_{\mathrm{CCSD}}\rangle = \langle 0|\hat{\mathcal{H}}\big(\frac{1}{2}\hat{T}_1^2 + \hat{T}_2\big)|0\rangle \\ &= \sum_{i,j}^{\text{occ.}}\sum_{a,b}^{\text{vir.}}\big(\frac{1}{2}t_i^a t_j^b + t_{ij}^{ab}\big)\Big[2\langle\phi_i\phi_j|\phi_a\phi_b\rangle - \langle\phi_j\phi_i|\phi_a\phi_b\rangle\Big]\ . \end{aligned} \tag{4.59}$$

Note that equation 4.59 is valid for every CC theory, since higher than double excitations have vanishing matrix elements (see appendix A). Also with cannonical HF orbitals the only contributions to the energy comes from doubly excited Slater determinants, namely the double excitation cluster operator $\hat{T}_2$ and twice the single excitation cluster operator $\hat{T}_1^2$. The equations 4.57 and 4.58 lead to a set of non-linear amplitude equations that can be solved iteratively. Typically, these equations are reformulated by multiplying the Schrödinger equation with $e^{-\hat{T}}$ from the left.

$$\begin{aligned} \langle 0|e^{-\hat{T}}\hat{\mathcal{H}}e^{\hat{T}}|0\rangle &= E_{\mathrm{CCSD}} \\ \langle \Phi_i^a|e^{-\hat{T}}\hat{\mathcal{H}}e^{\hat{T}}|0\rangle &= 0 \\ \langle \Phi_{ij}^{ab}|e^{-\hat{T}}\hat{\mathcal{H}}e^{\hat{T}}|0\rangle &= 0\ . \end{aligned} \tag{4.60}$$

This is called the similarity transformation, with $\tilde{\mathcal{H}} = e^{-T}\hat{\mathcal{H}}e^{T}$ being the similarity transformed Hamiltonian. The singles and doubles amplitude equations need to be solved iteratively by optimizing the amplitudes, for this to happen the residuals, as defined below, need to vanish

$$\begin{aligned} r_i^a &= \langle \Phi_i^a|e^{-\hat{T}}\hat{\mathcal{H}}e^{\hat{T}}|0\rangle \\ r_{ij}^{ab} &= \langle \Phi_{ij}^{ab}|e^{-\hat{T}}\hat{\mathcal{H}}e^{\hat{T}}|0\rangle\ . \end{aligned} \tag{4.61}$$

In every iteration, the CCSD amplitudes are updated as following

$$\begin{aligned} r_i^a =& t_i^a - \underbrace{\frac{R_i^a}{\epsilon_a - \epsilon_i}}_{\text{New amplitudes } t_i^a} \\ r_{ij}^{ab} =& t_{ij}^{ab} - \underbrace{\frac{R_{ij}^{ab}}{\epsilon_a + \epsilon_b - \epsilon_i - \epsilon_j}}_{\text{New amplitudes } t_{ij}^{ab}} , \end{aligned} \tag{4.62}$$

where R_i^a and R_{ij}^{ab} are computed using the amplitudes t_i^a and t_{ij}^{ab}. The equations for R_i^a and R_{ij}^{ab} are given below.

After the first iteration, R_{ij}^{ab} are just the two-electron integrals $\langle\phi_i\phi_j|\phi_a\phi_b\rangle$ and the amplitudes are equivalent to MP2 theory. This procedure works well when the MP2 amplitudes are a reasonably good starting point, typically for systems with a large HOMO-LUMO gap or in solid state physics a large band gap. The iterative procedure can be accelerated using the direct inversion in the iterative subspace (DIIS) method [34].

The doubles amplitudes from equations 4.60 involve up to quadruple excitations, since Hamiltonian matrix elements vanish if the Slater determinant differs by more than two orbitals. Analogously, the singles amplitudes involve up to triples excitations. Using the Baker-Campbell-Hausdorf (BHC) expansion

$$e^{-\hat{T}}\hat{\mathcal{H}}e^{\hat{T}} = \hat{\mathcal{H}} + \left[\hat{T},\hat{\mathcal{H}}\right] + \frac{1}{2!}\Big[\left[\hat{\mathcal{H}},\hat{T}\right],\hat{T}\Big] + \frac{1}{3!}\Big[\Big[\left[\hat{\mathcal{H}},\hat{T}\right],\hat{T}\Big],\hat{T}\Big] + \frac{1}{4!}\Big[\Big[\Big[\left[\hat{\mathcal{H}},\hat{T}\right],\hat{T}\Big],\hat{T}\Big],\hat{T}\Big] , \tag{4.63}$$

one can derive the amplitudes equations. Note that this expansion truncates after fourth-order, the reason being that the Hamiltonian contains only up to two-body operators. Deriving the equations is a difficult task, unlike MP2 theory where the amplitudes depend only on one specific Coulomb integral (and its exchange contribution), in CCSD theory all possible two-electron integrals are needed. We present the closed shell expression for the singles and doubles amplitudes from the work of Hirata *et. al* [35]

$$\begin{aligned} R_i^a =& \sum_c \kappa_c^a t_i^c - \sum_k \kappa_i^k t_k^a + \sum_{kc} \kappa_c^k \left(2t_{ki}^{ca} - t_{ik}^{ca}\right) + \sum_{kc} \kappa_c^k t_i^c t_k^a + \sum_{kc} w_{ic}^{ak} t_k^c + \\ & \sum_{kcd} w_{cd}^{ak} t_{ik}^{cd} + \sum_{kcd} w_{cd}^{ak} t_i^c t_k^d - \sum_{klc} w_{ic}^{kl} t_{kl}^{ac} - \sum_{klc} w_{ic}^{kl} t_k^a t_l^c \end{aligned} \tag{4.64}$$

$$
\begin{aligned}
R_{ij}^{ab} =& v_{ij}^{ab} + \sum_{kl} \chi_{ij}^{kl} t_{kl}^{ab} + \sum_{kl} \chi_{ij}^{kl} t_k^a t_l^b + \sum_{cd} \chi_{cd}^{ab} t_{ij}^{cd} + \sum_{cd} \chi_{cd}^{ab} t_i^c t_j^d + P \sum_c \lambda_c^a t_{ij}^{cb} - \\
& P \sum_k \lambda_i^k t_{kj}^{ab} + P \sum_c \big(v_{ic}^{ab} - \sum_k v_{ic}^{kb} t_k^a \big) t_j^c - P \sum_k \big(v_{ij}^{ak} + \sum_c v_{ij}^{ak} t_j^c \big) t_k^b + \\
& P \sum_{kc} \big(2\chi_{ic}^{ak} - \chi_{ci}^{ak} \big) t_{kj}^{cb} - P \sum_{kc} \chi_{ic}^{ak} t_{kj}^{bc} - P \sum_{kc} \chi_{ci}^{bk} t_{kj}^{ac}
\end{aligned} \tag{4.65}
$$

$$
\begin{aligned}
\kappa_i^k &= \sum_{lcd} w_{cd}^{kl} t_{il}^{cd} + \sum_{lcd} w_{cd}^{kl} t_i^c t_l^d \\
\kappa_c^a &= \sum_{kld} w_{cd}^{kl} t_{kl}^{ad} + \sum_{kld} w_{cd}^{kl} t_k^a t_l^d \\
\kappa_c^k &= \sum_{ld} w_{cd}^{kl} t_l^d \\
\lambda_i^k &= \kappa_i^k + \sum_{lc} w_{ic}^{kl} t_l^c \\
\lambda_c^a &= \kappa_c^a + \sum_{kd} w_{cd}^{ak} t_k^d \\
\chi_{ij}^{kl} &= v_{ij}^{kl} + \sum_c v_{ic}^{kl} t_j^c + \sum_c v_{cj}^{kl} t_i^c + \sum_{cd} v_{cd}^{kl} t_{ij}^{cd} + \sum_{cd} v_{cd}^{kl} t_i^c t_j^d \\
\chi_{cd}^{ab} &= v_{cd}^{ab} - \sum_k v_{cd}^{ak} t_k^b - \sum_k v_{cd}^{kb} t_k^a \\
\chi_{ic}^{ak} &= v_{ic}^{ak} - \sum_l v_{ic}^{lk} t_l^a + \sum_d v_{dc}^{ak} t_i^d - \frac{1}{2} \sum_{ld} v_{dc}^{lk} t_{il}^{da} - \sum_{ld} v_{dc}^{lk} t_i^d t_l^a + \frac{1}{2} \sum_{ld} w_{dc}^{lk} t_{il}^{ad} \\
\chi_{ci}^{ak} &= v_{ci}^{ak} - \sum_l v_{ci}^{lk} t_l^a + \sum_d v_{cd}^{ak} t_i^d - \frac{1}{2} \sum_{ld} v_{cd}^{lk} t_{il}^{da} - \frac{1}{2} \sum_{ld} w_{dc}^{lk} t_i^d t_l^a \ ,
\end{aligned} \tag{4.66}
$$

where v_{sr}^{pq} are the two-electron integrals defined by

$$
v_{sr}^{pq} = \langle \phi_p \phi_q | \phi_s \phi_r \rangle, \tag{4.67}
$$

and w_{sr}^{pq} the antisymmetrized two-electron integrals given by

$$
w_{sr}^{pq} = 2\langle \phi_p \phi_q | \phi_s \phi_r \rangle - \langle \phi_p \phi_q | \phi_r \phi_s \rangle \ . \tag{4.68}
$$

P is the permutation operator

$$
P \left\{ \dots \right\}_{ij}^{ab} = \left\{ \dots \right\}_{ij}^{ab} + \left\{ \dots \right\}_{ji}^{ba} \ . \tag{4.69}
$$

The computationally most expensive tensor contraction is $v_{cd}^{ab} t_{ij}^{cd}$, that requires $N_v^4 N_o^2$ operations. Thus, the computational complexity of CCSD theory is of order $\mathcal{O}(N^6)$ where N is a measure of the size of the system. Including higher excitations increases the computational complexity by another N^2. Meaning, CCSDT scales as $\mathcal{O}(N^8)$, CCSDTQ as $\mathcal{O}(N^{10})$, and so on.

4.3.3.1 CCSD(T)

Since CCSD theory already entails a quite expensive calculation, CCSDT can only be done on relatively small systems. Nevertheless, it is desirable to incorporate a greater level of correlation, even if only approximated [36]. One popular scheme to go beyond CCSD theory is to evaluate the triples excitation level in a non-iterative perturbative way [37]. The general idea is to include an estimate of the triples excitation energy correction inspired by MP5 perturbation theory [36]. This is referred to as coupled cluster singles, doubles with perturbative triples theory, CCSD(T). While CCSD contains all the terms that appear in third-order perturbation theory (MP3) and more, CCSDT on the other hand, does not contain all terms from MP4 theory [33, 38]. CCSD(T) contains effects of triple excitations in CC theory in a one-shot sense, including a balanced subset of fifth-order terms from MP5. CCSD(T) scales as $\mathcal{O}(N^7)$ and it achieves chemical accuracy consistently in the description of a large set of molecules compared to other many-body methods [39–41].

4.4 Quantum Monte Carlo

Quantum Monte Carlo refers to a family of methods that all share two common ideas: The quantum properties are written as path integrals and these path integrals are computed with stochastic (Monte Carlo) methods. The starting point of Quantum Monte Carlo [42] is the time-dependent Schrödinger equation with its solution

$$i\hbar\frac{|\Psi(t)\rangle}{\partial t} = \mathcal{H}t|\Psi(t)\rangle \tag{4.70}$$

$$|\Psi(t)\rangle = e^{-i\mathcal{H}t}|\Psi(0)\rangle \tag{4.71}$$

where $\Psi(0)$ is an arbitrary initial state. As far as we are interested in obtaining the time-independent eigensolutions of $\mathcal{H}$ time plays no fundamental role; it can be considered a parameter. Writing the time-dependent wavefunction in the basis of $\mathcal{H}$

$$\mathcal{H}|\phi_n\rangle = E_n|\phi_n\rangle \tag{4.72}$$

$$|\Psi(t)\rangle = \sum_n e^{-itE_n}c_n|\phi_n\rangle \tag{4.73}$$

together with the imaginary time transformation $t \to -it$ yields

$$|\Psi(t)\rangle = \sum_n c_n e^{-tE_n}|\phi_n\rangle, \tag{4.74}$$

where the c_n are the coefficients $\langle\phi_n|\Psi(0)\rangle$. Once the solution to $|\Psi(t)\rangle$ has been obtained, it is possible to extract the low-lying spectrum simply by evolution in imaginary time.

$$|\Psi(t)\rangle \sim |\phi_0\rangle + \mathcal{O}(e^{-t(E_1-E_0)})|\phi_1\rangle. \tag{4.75}$$

The quantity to be computed can be expressed in terms of a time-independent N-body Green's function

$$\Psi(x,t) = \langle x|e^{-t\mathcal{H}}|\Psi(0)\rangle, \tag{4.76}$$

$$\Psi(x,t) = \int dx_0 \langle x|e^{-t\mathcal{H}}|x_0\rangle\Psi(x_0,t=0), \tag{4.77}$$

$$G(x,x_0,t) = \langle x|e^{-t\mathcal{H}}|x_0\rangle. \tag{4.78}$$

In general the Green's function is unknown and has to be computed and approximated. The imaginary time can be divided into N small intervals such that $t = N\tau$. Then the exponential operator is split

$$e^{-t\mathcal{H}} = e^{-\tau\mathcal{H}-\tau\mathcal{H}...-\tau\mathcal{H}} = e^{-\tau\mathcal{H}}e^{-\tau\mathcal{H}}...e^{-\tau\mathcal{H}}. \tag{4.79}$$

By inserting the resolution of the identity between each $e^{-\tau\mathcal{H}}$ in equation 4.78, we get an exact relation for any N

$$G(x,x_0,t) = \int dx_1...dx_{N-1}\Pi_{i=0}^{N-1}G(x_i,x_{i+1},\tau), \tag{4.80}$$

where $x = x_N$. A general short-time approximation to the Green's function is known

$$G_{\text{approx}} = G_0(x,x_0,\tau)e^{-\tau\mathcal{V}(\mathbf{x})}, \tag{4.81}$$

with G_0 being a simple Gaussian known in physics from heat diffusion

$$G_0(x,x_0,\tau) = \frac{1}{\sqrt{2\pi\tau}}e^{-\frac{(x-x_0)^2}{2\tau}} + \mathcal{O}(\tau^2) \tag{4.82}$$

and $\mathcal{V}$ being the Coulomb potential. Combining all these considerations leads us to the main result

$$\phi_0 = \lim_{t\to\infty}\lim_{N\to\infty}\int dx_1...dx_2\Pi_{i=0}^{N-1}G_{\text{approx}}(x_i,x_{i+1},\tau)\Psi_T(x_0,t=0). \tag{4.83}$$

The ground state of the time-independent Schrödinger equation can be expressed as a multidimensional integral of a known function with an arbitrary trial wavefunction Ψ_T. In the limit of infinite infinitesimal timesteps $N\to\infty$ and $\tau\to\frac{t}{N}$, the short time approximation is analytical. In the limit of imaginary time $t\to\infty$ only the ground state remains, as can be seen in equation 4.74. Equation 4.83 is formally written in terms of

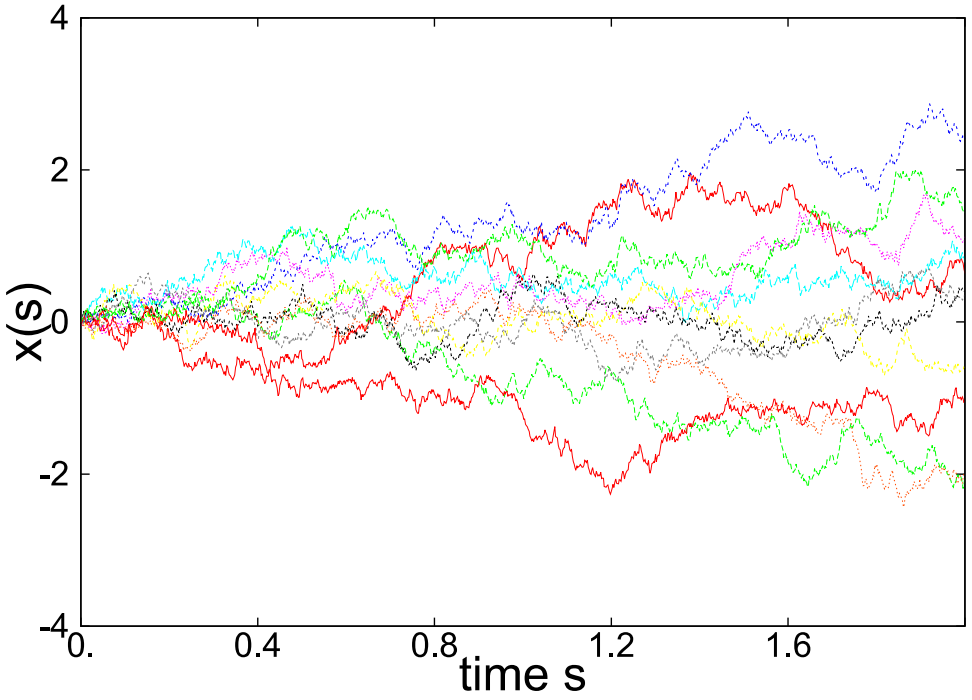

FIGURE 4.3: The time evolution of the Brownian walker. Figure taken from ref. [43].

Feynman path-integrals with

$$\Pi G_0 = e^{-\int_0^t dsT[x(s)]} \tag{4.84}$$

where

$$T = \frac{1}{2}\frac{\partial x(t)^2}{\partial t}, \tag{4.85}$$

and similarly

$$\Pi e^{-\mathcal{V}} = e^{-\int_0^t dsV[x(s)]}, \tag{4.86}$$

yielding the formal expression for the ground state

$$\phi_0(x) = \sum_{\text{paths}} e^{-\int_0^t dsT[x(s)]} e^{-\int_0^t dsV[x(s)]}, \tag{4.87}$$

where the integration over all x_i is substituted for a sum over all possible paths.

The quantity from equation 4.84 is the probability density associated with Brownian trajectories. This puts forward the idea of simulating all possible paths stochastically as Brownian paths. However, the quantity 4.86 varies too wildly as a function of the paths, as shown in figure 4.3. This stems from the fact that the Brownian paths are blind with respect to the Coulomb potential; they visit the configuration space uniformly. One needs a way to guide the Brownian trajectories to regions of importance for the exact wavefunction $\Phi_0(\mathbf{x})$. This can be done using an appropriate trial wavefunction $\Psi_T(\mathbf{x})$.

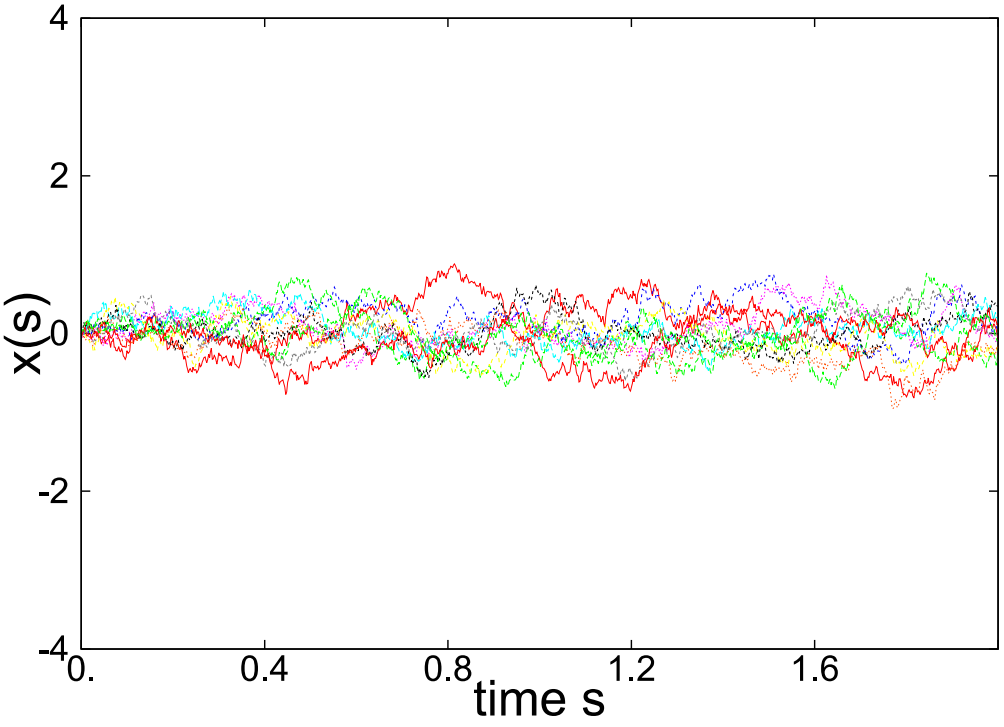

FIGURE 4.4: The time evolution of the drifted Brownian walker with a Gaussian trial wavefunction. Figure taken from ref. [43].

Introducing a new density $f(x,t) = \Psi_T(\mathbf{x})\Psi(x,t)$ and multiplying each side of the time dependent Schrödinger equation by Ψ_T we get

$$\frac{\partial f(\mathbf{x},t)}{\partial t} = -\Psi_T \mathcal{H} \frac{1}{\Psi_T} f(\mathbf{x},t). \tag{4.88}$$

With some simple algebra [42] we arrive at the new equation of evolution

$$\frac{\partial f(\mathbf{x},t)}{\partial t} = \frac{1}{2}\nabla^2 f(\mathbf{x},t) - \nabla[\mathbf{b}(\mathbf{x})] - E_L(\mathbf{x}) f(\mathbf{x},t) \tag{4.89}$$

with the drift vector

$$\mathbf{b}(\mathbf{x}) = \frac{\nabla\Psi_T}{\Psi_T} \tag{4.90}$$

and the local energy

$$E_L(\mathbf{x}) = \frac{\mathcal{H}\Psi_T}{\Psi_T}. \tag{4.91}$$

Now the bare potential $\mathcal{V}(\mathbf{x})$ is replaced with a screened potential E_L and the free diffusion (kinetic energy) is replaced with a drifted diffusion. Further, the statistical fluctuation of E_L vanishes if the trial wavefunction is equal to the ground state $\Psi_T = \Phi_0$. This is referred to as the zero variance property. Figure 4.4 shows the effect a Gaussian trial wavefunction has on the Brownian walkers. Until now, we have tried to find a solution to the Schrödinger equation, disregarding the fact that the wavefunction of a

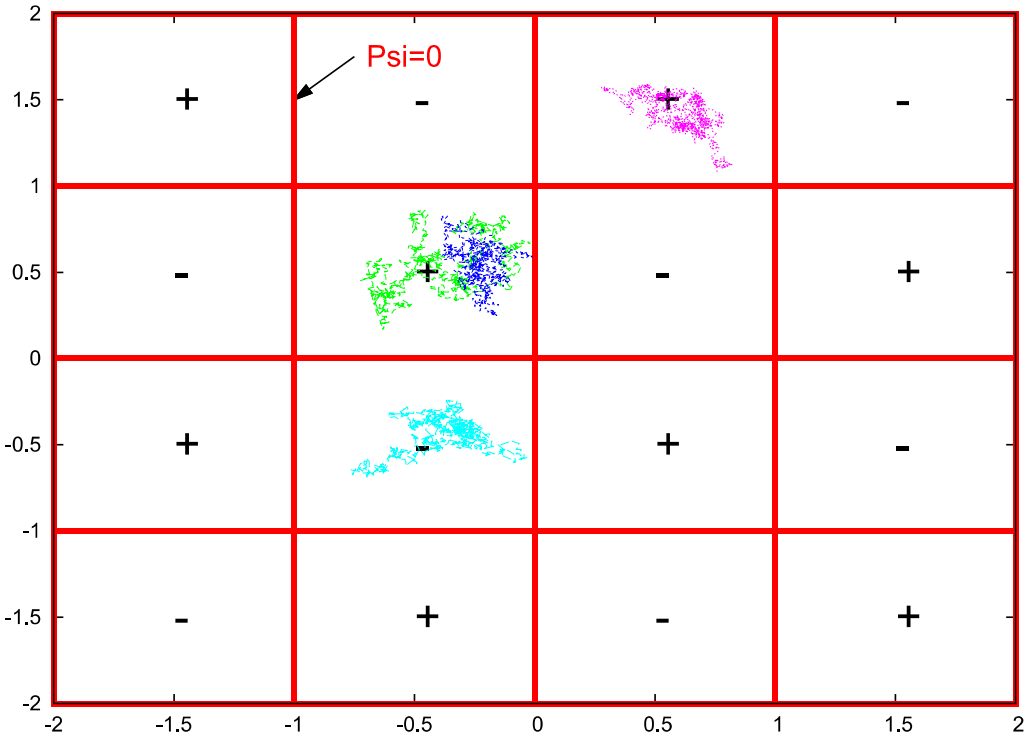

FIGURE 4.5: The time evolution of the drifted Brownian walker within the nodal pockets of the antisymmetric trial wavefunction. Figure taken from ref. [43].

fermionic system has to be antisymmetric. In principle, this can be taken into account by properly antisymmetrizing the trial wavefunction. If Ψ_T is properly antisymmetric:

$$\langle \Psi_T | e^{-t\mathcal{H}} | \mathbf{x}_0 \rangle = \sum_n e^{-E_n t} \langle \phi_n | \Psi_T \rangle \phi_n(\mathbf{x_0}) \tag{4.92}$$

with ϕ_n being either bosonic or fermionic, however

$$\langle \phi_n^{\text{boson}} | \Psi_T \rangle = 0, \tag{4.93}$$

therefore, only the fermionic wavefunction will be left. The problem with this approach comes from the nodes of the antisymmetric trial wavefunction. At these locations, the drift vector 4.90 diverges. Therefore, these nodes represent a repulsive barrier for the drifted Brownian walkers. They will be trapped forever in domains delimited by the nodal structure of the trial wavefunction (nodal pockets) as shown in figure 4.5. For that reason, the Schrödinger equation is solved with the additional constraint that the solution has the same sign as the trial wavefunction, this is referred to as the fixed-node approximation [44]. The problem with this approach is that the nodal surfaces of the trial wavefunction have to coincide with the nodal surfaces of the exact wavefunction, which is in general unknown.

In order to have exact ab initio QMC simulations, one must take a non-vanishing trial wavefunction (bosonic) and add an antisymmetric weight to the averages to project out the fermionic ground state. This leads to widely unstable simulations due to the fluctuations in the sign of the average. This problem is generally referred to as the sign problem [45]. Solving this problem would allow for exact QMC simulations, which would be comparable to finding an exact XC functional in DFT.

The presented approach is shared for variational Monte Carlo (VMC) and diffusion Monte Carlo (DMC). VMC is commonly used in many sorts of quantum problems, while DMC is the most common high-accuracy method for electrons, since it comes close to the exact ground state energy fairly efficiently.

4.5 Calculating Excited States

All previously presented many-body methods in this chapter are routinely used to calculate ground state energies. However, one is generally interested in the excited states as well and most of the many-body methods presented can be extended to include excited state energies. Time-dependent DFT (TDDFT) [10, 46], theories based on the GW approximation [47, 48] and the Bethe-Salpeter equation [49] (BSE) are widely used to calculate excited states in molecules and solids. Further, density matrix renormalization group (DMRG) [50], HF, MP2, CI and excited states extensions of CC theory can also be used to calculate the excited states of a system.

In TDDFT theory, the results depend strongly on the choice of the XC functional. Similarly, in G_0W_0 theory the quasiparticle energies depend strongly on the Kohn-Sham orbital energies. Further, for full GW-BSE calculations, many approximations have to be made, hindering it's range of applicability. DMRG theory is routinely used for low-dimensional systems. CI theory yields excited state energies in addition to the ground state energy naturally, through exact diagonalization. The drawbacks of CI theory have been discussed in section 4.3.1. The equation of motion formalism of CC theory (EOM-CC) can be used to calculate the excited state energies with a similar computational cost to CC ground state calculations.

In this work, EE-EOM-CCSD [51] theory has been used to calculate the excited states of the parabolic two dimensional quantum dot.

4.5.1 Equation of Motion CC Theory

Similar to how excited states are obtained in CI, in CC theory, excited states can be obtained through diagonalization of the similarity transformed Hamiltonian $\tilde{\mathcal{H}}$ in a suitable subspace of the Hilbert space. We use a charge-neutral variant of this methodology, for which the number of electrons is conserved with no spin flip restrictions on the amplitudes. The ansatz for the excited state, with a CCSD groundstate is

$$|\Psi_{\mathrm{EOM}}\rangle = \hat{R}|\Psi_{\mathrm{CCSD}}\rangle = \hat{R}\exp\left(\hat{T}_1 + \hat{T}_2\right)|0\rangle, \tag{4.94}$$

$$\hat{\mathcal{H}}|\Psi_{\mathrm{EOM}}\rangle = E_R|\Psi_{\mathrm{EOM}}\rangle, \tag{4.95}$$

where $\hat{R}$ is the excited cluster operator

$$\hat{R} = r_0 + \sum_i \sum_a r_i^a \hat{a}_a^\dagger \hat{a}_i + \sum_{ij} \sum_{ab} r_{ij}^{ab} \hat{a}_a^\dagger \hat{a}_b^\dagger \hat{a}_i \hat{a}_j + \ldots, \tag{4.96}$$

and E_R is the excitation energy.

It should be noted that EOM-CC theory is an exact procedure, however in practical calculations $\hat{T}$ and $\hat{R}$ have to be truncated to some tractable level of excitation, usually singles and doubles excitation. Nevertheless, EOM-CCSD theory provides an exact treatment of two electron systems.

This formalism is called equation of motion for its resemblance to the equation of motion equation for operators in the Heisenberg picture of quantum mechanics, subtracting

$$\hat{R}\hat{\mathcal{H}}|\Psi_{\mathrm{CCSD}}\rangle = E_{\mathrm{CCSD}}\hat{R}|\Psi_{\mathrm{CCSD}}\rangle \tag{4.97}$$

from equation 4.95 yields,

$$[\hat{\mathcal{H}}, \hat{R}]|\Psi_{\mathrm{CCSD}}\rangle = (E_R - E_{\mathrm{CCSD}})|\Psi_{\mathrm{CCSD}}\rangle. \tag{4.98}$$

Rewriting equation 4.98 in terms of the HF reference $|0\rangle$ is equivalent to the commutator equation

$$[\tilde{\mathcal{H}}, \hat{R}]|0\rangle = (E_R - E_{\mathrm{CCSD}})\hat{R}|0\rangle = \Delta E_R \hat{R}|0\rangle, \tag{4.99}$$

involving the similarity transformed Hamiltonian $\tilde{\mathcal{H}}$ and the excitation energy ΔE_R. The scalars r_0, r_i^a and r_{ij}^{ab} have to be computed; this is done in an iterative way.

Due to the similarity transformed Hamiltonian being non-Hermitian, its left and right eigenvectors are not simply Hermitian conjugates. However, the distinction between left and right eigenstates becomes only important if one is interested in calculating properties

other than the energy, since equation 4.99 can be solved without any consideration of left eigenvectors [51]. It follows from the general properties of non-Hermitian eigenvalue problems that these two sets of solutions satisfy the property of biorthogonality.

The EOM framework can also be used to calculate excited states for other theories such as HF and RPA in the Tamm Dancoff approximation [52, 53]. Note that due to the commutator on the left-hand side of equation 4.99 only connected diagrams need to be considered.

Chapter 5

Numerical Methods

The goal of this thesis is to calculate the formation energies of the silicon self-interstitials at CCSD(T) level of theory, and the excited states of the two dimensional quantum dot with EE-EOM-CCSD theory.

As the first step, one has to define the structures in terms of the Born-Oppenheimer approximation and choose a basis set. In order to obtain the numerical values for ground state energies at CCSD(T) level of theory, one has to calculate the coulomb integrals needed to construct the reference and excited Slater determinants. In this thesis, this has been achieved using the Vienna ab initio simulation package (VASP) [54–56] for the silicon self-interstitials. For the quantum dot, a real space integration technique using semi analytic solutions to the Coulomb integral has been developed that will be discussed later. All CC calculations have been done using our high-performance open-source coupled cluster simulation code [57–60], coupled cluster for solids (CC4S).

In the upcoming sections, the numerical methods from VASP and CC4S will be presented.

5.1 Vienna Ab Initio Simulation Package

VASP is a ab initio simulation program for modeling materials at an atomic scale. It can compute approximate solutions to the many-body Schrödinger equation using either DFT or HF. In VASP a material is modeled in terms of a periodic supercell. The ion positions of the cell are specified, and the periodicity is implemented in terms of boundary conditions. The in $\vec{k}$ continuous Brillouin zone is sampled with a discrete mesh of Bloch vectors, introducing the finite size incompleteness error (FSIE). Converging this sampling is one of the essential tasks in many calculations, similar to the convergence

with basis set size. In VASP the key quantities, like the one-electron orbitals or the charge density, are expressed in a plane-wave basis set [26]. The interactions between the electrons and ions are modeled using norm-conserving or ultrasoft pseudopotentials, referred to as the projector-augmented-wave method [27]. It uses an array of highly efficient iterative matrix diagonalization techniques that speed up the self-consistency cycle [55].

5.1.1 Plane Wave Basis Set

A plane-wave basis set, in contrast to STO and GTO, is a delocalized basis set. Typically, the choice of the plane-wave basis set is based on an energy cutoff, the plane waves that fit below the energy cutoff criterion are then included in the calculation introducing the BSIE. Plane waves are popular in calculations involving three-dimensional periodic boundary conditions. In such systems, the one particle orbitals are Bloch orbitals

$$\langle \mathbf{r} + \mathbf{R} | \psi_{n\mathbf{k}} \rangle = \langle \mathbf{r} | \psi_{n\mathbf{k}} \rangle e^{i\mathbf{k}\mathbf{R}} \ , \tag{5.1}$$

where n is the band index and $\mathbf{k}$ is the k-point index. The Bloch orbitals can be expanded using the plane wave basis in reciprocal space as

$$\langle \mathbf{r} | \psi_{n\mathbf{k}} \rangle = \frac{1}{\sqrt{\Omega}} \sum_{\mathbf{G}} C_{n\mathbf{k}}^{\mathbf{G}} e^{i\mathbf{G}\mathbf{r}} \ . \tag{5.2}$$

Where Ω is the volume of the Wigner-Seitz cell. There are a few advantages to using plane waves, for example, the kinetic energy operator is diagonal in the reciprocal space, meaning that integrals over real space can be efficiently carried out using fast Fourier transforms. Also, they naturally fulfill the periodicity of the computational cell, as required by the Bloch theorem. Further, they are independent of the atomic composition of the computational cell. A single plane wave corresponds to a constant probability density

$$\Psi_{\mathbf{k}}(\vec{r}) = A e^{i\mathbf{k}\vec{r}} \tag{5.3}$$

$$\Psi_{\mathbf{k}}^{\star}(\vec{r}) \Psi_{\mathbf{k}}(\vec{r}) = A^2. \tag{5.4}$$

Therefore, it is easy to represent probability distributions that are not oscillating wildly with plane-wave basis sets, meaning wavefunctions with low gradients where the electrons are delocalized. The core electrons tend to be concentrated very close to the nuclei, resulting in localized probability distributions with high density gradients. For these electrons to be accurately described using plane waves, an impractically high energy cutoff for the basis set has to be chosen. In practice, this problem is solved using

an effective core potential, or pseudopotential [55], such that the plane waves are only used to describe the valence electron's charge density, which is usually delocalized.

5.1.2 The Projector-Augmented-Wave Method

In the PAW method [55], space is divided into two regions: the augmentation spheres, or core region, and the interstitial region between the spheres. The one electron Bloch orbitals $\psi_{n\mathbf{k}}$ are derived from the pseudo orbitals $\tilde{\psi}_{n\mathbf{k}}$ in terms of a linear transformation

$$|\psi_{n\mathbf{k}}\rangle = |\tilde{\psi}_{n\mathbf{k}}\rangle + \sum_i \left(|\phi_i\rangle - |\tilde{\phi}_i\rangle\right)\langle\tilde{p}_i|\tilde{\psi}_{n\mathbf{k}}\rangle \ , \tag{5.5}$$

where i is a short notation for the atomic site $\mathbf{R}_i$, with $|\phi_i\rangle$ containing the atomic orbitals uniquely characterized by the quantum numbers n, l and m. The pseudo Bloch orbitals $|\tilde{\psi}_{n\mathbf{k}}\rangle$ are variational quantities expanded using the plane waves in reciprocal space

$$\langle\mathbf{r}|\tilde{\psi}_{n\mathbf{k}}\rangle = \frac{1}{\sqrt{\Omega}}\sum_{\mathbf{G}} C^{\mathbf{G}}_{n\mathbf{k}\mathbf{G}} e^{i(\mathbf{G}+\mathbf{k})\mathbf{r}} \ . \tag{5.6}$$

The pseudo partial waves $|\tilde{\phi}_i\rangle$ are equivalent to the atomic orbitals ϕ_i outside a core radius r_c and are mapped continuously onto them inside the core radius. The core radius is typically chosen to be around one-half of the nearest neighbor's distance. The projector functions $|\tilde{p}_i\rangle$ are dual to the pseudo partial waves

$$\langle\tilde{p}_i|\tilde{\phi}_j\rangle = \delta_{ij}. \tag{5.7}$$

In the interstitial region, the pseudo orbitals $\tilde{\psi}_{n\mathbf{k}}$ are identical to the exact one electron Bloch orbital $\psi_{n\mathbf{k}}$ while in the core region, the pseudo orbitals are mapped onto the one electron orbitals through equation 5.5. Inside the spheres, the pseudo orbitals $\tilde{\psi}_{n\mathbf{k}}$ are only a computational tool and an inaccurate approximation to the true orbitals since the norm of the all-electron wavefunction is not reproduced. Yet they allow using a much smaller basis in the calculations, making them practically possible.

5.2 Coupled Cluster for Solids

CC4S [57–60] is a high-performance open-source coupled cluster simulation code. The main goal of CC4S is to study the electronic properties of solid-state systems, using coupled cluster theory with periodic boundary conditions. Solving the coupled cluster equations is computationally extremely demanding. Therefore, CC4S makes use

of state-of-the-art, high-performance libraries such as the Cyclops Tensor Framework (CTF), which is a parallel tensor contraction engine. Further, it uses the message-passing interface (MPI) and open multiprocessing (openMP) for parallelization.

CC4S takes as input a reference wavefunction and the Coulomb integrals. The reference wavefunction and Coulomb integrals can be prepared either using VASP or FHI-aims (Fritz Haber Institute ab initio materials simulations), with more interfaces in the making. With this information, CC4S can calculate the CCSD grounstate energy, the perturbative triples correction to it (CCSD(T)) and the EE-EOM-CCSD excited state energies. CC4S also includes a BSIE and FSIE correction algorithm tailored to CCSD theory.

5.2.1 Basis Set Correction

In all our CC calculations frozen natural orbitals (FNO) [61] were used, since they increase the convergence of CC calculations by an order of magnitude with no drawback. The FNOs are the eigenfunctions of the one-particle electron density matrix. They can be interpreted as a basis set transformation to virtual orbitals with a maximum electron density such that less basis set functions are needed to span the relevant part of the virtual orbital space and thus basis set convergence is increased substantially. However, the electron electron cusp [28] convergence problem still remains as discussed in section 4.3.0.1. The cusp represents the leading order term in the BSIE. In order to treat the BSIE in cc4s a pair-specific cusp correction scheme [59] is implemented which has been discussed thoroughly elsewhere [62–64]. This scheme is based on diagrammatically decomposed contributions to the electronic correlation energy that dominate the BSIE. This correction scheme is implemented on the level of CCSD theory, but it can be used to estimate the BSIE for CCSD(T) too.

5.2.2 Finite Size Correction

In every practical calculation a finite size system has to be simulated. This introduces the FSIE and it should be noted that many properties converge slowly with respect to the system size. This stems from the fact that wavefunction based theories capture long range correlation effects such as dispersion interaction explicitly. In cc4s a finite size correction interpolation technique is used similar to structure factor interpolation methods used in quantum Monte Carlo calculations. In CCSD theory the energy can be expressed as an integral over the electronic transition structure factor multiplied by the coulomb kernel in reciprocal space [60]. The FSIE partly originates from an inaccurate sampling of this integral. The value of the integral at and around the origin is known,

such that we can interpolate the region between the origin and our calculation with the FSIE and get a finite size correction. The technical details of this algorithm are described in [60].

Chapter 6

The Quantum Dot

In the following chapter the two dimensional quantum dot is presented. The quantum dot is modeled as a two dimensional harmonic oscillator, and approximated with a wide range of ab initio methods, including HF, MP2, CCSD and EOM-CCSD. A scheme to calculate the necessary Coulomb integrals utilizing semi-analytic solutions in realspace around the Coulomb kernels singularity is developed. Further, an analytic expression for the scaling of the BSIE error as a function of number of virtual orbitals is derived, allowing the extrapolation to the complete basis set limit energies. The ground and first three excited states energies are calculated in closed shell quantum dots with 2, 6 and 12 electrons in different regimes of correlation tuned through the harmonic oscillator strength ω. The ground state is calculated at the CCSD level of theory, while the excited states are calculated using EE-EOM-CCSD theory. The following discussion has been published in Ref. [65].

6.1 Introduction

A quantum dot (QD) is a semiconducting nanocrystal embedded in a host semiconductor with a larger band gap such that the excitons localized at the QD have a de Broglie wavelength comparable to the size of the crystal. The typical size of such a nanocrystal is 2nm–100nm and it is made out of roughly a million atoms. In this context, virtually all electrons are tightly bound to the nuclei of the material such that the number of free electrons in a QD ranges typically from 1 to 100. As described by the quantum mechanical theory of solids, the electrons do not get trapped in the real nuclei of the material but instead simply sense a potential well of the QD, thus forming discrete energy levels. These electrons behave as free electrons with a renormalized mass. For example, electrons in the semiconductor GaAs appear to carry a mass of only 7% of

the mass of free electrons. QDs are often referred to as artificial atoms because they exhibit similar properties as atoms such as level spacing, ionization energy and magnetic moments, albeit on different energy scales.

6.1.1 Practical Applications

Due to their tunable optical and electronic properties, QDs are widely used in many practical applications including solar cells, light-emitting diodes, laser technology as well as biological and biomedical applications [66–72]. The use of QDs as cosmetic hair dyes is the oldest known application, dating back more than 2000 years, when PbS QDs were synthesized using naturally occurring materials like $Ca(OH)_2$, PbO and water [73].

6.1.2 Experimental Developments and Theoretical Modeling

Over the past few decades, several ways to synthesize and investigate dynamical properties of QDs with extraordinary high precision have been developed [74]. Consequently, experimental and theoretical research on these nanoparticles has harnessed much attention and insight [71, 72, 75–98].

The simplest model used in theoretical studies of QDs, which has proven to be adequate, is the harmonic oscillator [99]. In this model, the interaction of the electrons with the surrounding semiconductor material is approximated through the material-specific effective mass of the electrons and a material-specific relative dielectric constant that screens the Coulomb interaction. In passing we note that a more realistic nanoscale model of QDs can be obtained by an empirical pseudopotential based approach [100, 101]. In contrast to other many-body systems, in QDs, the coupling strength of the two-body operator relative to the one-body operator can be freely varied over a wide range of values, thus giving rise to various regimes of interelectronic correlation.

6.1.3 Many-Body Methods Applied to the QD

The simple expression of the QD model Hamiltonian allows for a straightforward application of many-electron methods that have historically been developed for atoms and crystals. One-electron theories such as DFT in the Kohn-Sham framework of approximate exchange and correlation (XC) energy functionals [102–105] and the HF [80, 106–115] approximation often achieve a qualitatively correct agreement with experiment. In contrast to DFT calculations, FCI investigations of QDs yield exact results for a given basis set and have been applied to QDs in a number of studies [69, 114, 116–130].

Alternatively, QMC has been used for QDs thoroughly [129, 131–139]. Here the computational cost grows relatively modestly with the number of electrons and it provides highly accurate ground state energies. Moreover, there is the possibility to use the nodal structure of the ground state trial wavefunction to impose restrictions on the solutions. In this way, excited states can be calculated as well even if calculations on general excited states are not straightforward. CC theory, being numerically less expensive than FCI while having size consistency by construction, provides ground state and excited state energies with an accuracy that is comparable to quantum QMC calculations [140, 141]. MP2 and CCSD have been shown to be useful approaches to calculate atomic, molecular and solid-state properties [33, 142–146]. They have also been used to study QD Hamiltonians in a number of studies [140, 141, 147, 148, 148, 149]. Via the EOM formalism, CC theory can also be applied to excited states [51], and was already applied to atoms, molecules and recently even solids [33, 150–152] and quantum plasmons and excitons [153].

Here, we seek to apply EE-EOM-CCSD theory to study excited states in two dimensional QDs [154, 155]. To this end, we employ an implementation of EE-EOM-CCSD that was recently used to investigate defects in solids employing ab initio Hamiltonians [152].

6.2 The Harmonic Oscillator

Following the description in Ref. [99], a QD can be modeled as fermionic particles confined to two dimensions in a parabolic potential. The corresponding one-body Hamiltonian in such a potential is given in atomic units by

$$\hat{H}(x,y) = \frac{p_x^2 + p_y^2}{2} + \frac{1}{2}\omega^2\left(x^2 + y^2\right). \tag{6.1}$$

Here, ω is a measure of the confinement strength of the electron in the parabolic potential well. Consequently, the Schrödinger equation can be separated into x and y coordinates, resulting in the differential equation for the 1D harmonic oscillator

$$\left(-\frac{1}{2}\frac{\partial^2}{\partial x^2} + \frac{\omega^2 x^2}{2}\right)\psi(x) = E\psi(x), \tag{6.2}$$

admitting the well-known solutions

$$\psi_n(x) = \frac{1}{\sqrt{2^n n!}} \left(\frac{\omega}{\pi}\right)^{\frac{1}{4}} e^{-\frac{\omega x^2}{2}} H_n\left(\sqrt{\omega}x\right)$$
$$E_n = \omega\left(n + \frac{1}{2}\right)$$
$$H_n(x) = (-1)^n e^{x^2} \frac{\mathrm{d}^n}{\mathrm{d}x^n}\left(e^{-x^2}\right)$$

where $n \in \mathbb{N}$. The corresponding solutions to the non-interacting 2D problem are

$$\psi_{nm}(x,y) = \psi_n(x)\psi_m(y) \tag{6.3}$$
$$E_{nm} = E_n + E_m = \omega(n+m+1). \tag{6.4}$$

We note that the ground state is given by the solution with $m = 0$ and $n = 0$ and is non-degenerate. The first excited state is given by the solutions with $(n = 1, m = 0)$ and $(n = 0, m = 1)$ and has a degeneracy of 2. The second excited state is given by $(n = 2,\ m = 0)$, $(n = 0,\ m = 2)$ and $(n = 1,\ m = 1)$ and has a degeneracy of 3, and so forth.

The electronic structure of the 2D QD is strongly affected by electronic correlation effects caused by inter electronic interactions. To describe the true many-body nature of the 2D QD with N electrons, we have to include the two-body Coulomb interaction and consider the following two-body Hamiltonian

$$\hat{H} = \sum_{i=1}^{N} \hat{H}(x_i, y_i) + \frac{1}{2}\sum_{i\neq j}^{N} \frac{1}{\sqrt{(x_i - x_j)^2 + (y_i - y_j)^2}}, \tag{6.5}$$

where $\hat{H}(x_i, y_i)$ is the one-body operator defined by equation 6.1. Herein we employ the bare Coulomb interaction. We note, however, that many model Hamiltonians for QDs account for screening effects by including various approximations to the permittivity in the inter electronic interaction.

Given the fermionic character of the particles, the form and relative strength of the one-particle and two-particle operators of the above Hamiltonian, it is reasonable to assume that conventional quantum chemical many-electron wave function based methods yield reliable solutions for its ground and excited states. In this hierarchy of quantum chemical wavefunction based methods, the HF theory, employing a self consistent field approximation, is a well-established starting point.

6.3 Calculating the Coulomb Integrals

We calculate the ground state of the QD using closed shell CCSD theory and the first three excited states with EE-EOM-CCSD as described in chapter 4. In order to apply these methods one has to calculate the Coulomb integrals in the basis of the solutions to the 2D quantum harmonic oscillator. One has to compute the following integrals

$$\int_{-\infty}^{\infty}\int_{-\infty}^{\infty}\int_{-\infty}^{\infty}\int_{-\infty}^{\infty} \mathrm{d}x_1\mathrm{d}x_2\mathrm{d}y_1\mathrm{d}y_2 \frac{\psi^*_{nm}(x_1,y_1)\psi^*_{op}(x_2,y_2)\psi_{qr}(x_1,y_1)\psi_{st}(x_2,y_2)}{\sqrt{(x_1-x_2)^2+(y_1-y_2)^2}}, \tag{6.6}$$

where ψ_{nm} are the two dimensional orbitals introduced in equation 6.3. For Gaussian based basis sets and their derivatives, methods for analytical computation of such integrals exist, which are commonly based on recursive relations and can be implemented on a computer using code generation facilities [156–158]. Our numerical approach for calculating the Coulomb integrals is computationally less efficient but can be applied to arbitrary orbitals in realspace. This can potentially be useful for model Hamiltonians represented in a set of basis functions that are difficult to expand using Gaussian functions or their derivatives but can be well represented on a sufficiently dense spatial grid.

The main idea of our approach is to assume that the singular Coulomb kernel exhibits a more rapid spatial variation than the orbitals and that the employed real space grid is dense enough to approximate the orbitals by a constant inside any volume/area sampled by the grid.

To perform the integration in equation 6.6 we discretize the integration domain into hypercubes with an edge length of Δx centered at x_i, x_j, y_k, y_l.

$$\sum_{ijkl}\int_{x_i-\frac{\Delta x}{2}}^{x_i+\frac{\Delta x}{2}}\int_{x_j-\frac{\Delta x}{2}}^{x_j+\frac{\Delta x}{2}}\int_{y_k-\frac{\Delta x}{2}}^{y_k+\frac{\Delta x}{2}}\int_{y_l-\frac{\Delta x}{2}}^{y_l+\frac{\Delta x}{2}} \frac{\psi_{mnopqrst}(x_1,y_1,x_2,y_2)}{\sqrt{(x_1-x_2)^2+(y_1-y_2)^2}}\mathrm{d}x_1\mathrm{d}x_2\mathrm{d}y_1\mathrm{d}y_2. \tag{6.7}$$

With $i,j,k,l \in \mathbb{Z}$, $x_i = i\Delta x$, $x_j = j\Delta x$, $y_k = k\Delta x$, $y_l = l\Delta x$ and

$$\psi_{mnopqrst} = \psi^*_{mn}\psi^*_{op}\psi_{qr}\psi_{st}. \tag{6.8}$$

Employing simple quadrature, we approximate the wavefunction from 6.7 to be constant within each integration block.

$$\sum_{ijkl}\psi_{mnopqrst}(x_i,y_j,x_k,y_l)\iiint\frac{\mathrm{d}x_1\mathrm{d}x_2\mathrm{d}y_1\mathrm{d}y_2}{\sqrt{(x_1-x_2)^2+(y_1-y_2)^2}} \tag{6.9}$$

This leaves us with the integral over the Coulomb kernel, which cannot be treated in the same manner due to points with $x_i = x_j$ and $y_k = y_l$, where the Coulomb kernel becomes singular. We solve this problem using the Laplace transformation of the Coulomb kernel, leading to a simplified expression. We start with

$$\int_{x_i-\frac{\Delta x}{2}}^{x_i+\frac{\Delta x}{2}} \int_{x_j-\frac{\Delta x}{2}}^{x_j+\frac{\Delta x}{2}} \int_{y_k-\frac{\Delta x}{2}}^{y_k+\frac{\Delta x}{2}} \int_{y_l-\frac{\Delta x}{2}}^{y_l+\frac{\Delta x}{2}} \frac{\mathrm{d}x_1\mathrm{d}x_2\mathrm{d}y_1\mathrm{d}y_2}{\sqrt{(x_1-x_2)^2+(y_1-y_2)^2}}. \tag{6.10}$$

Applying the Laplace transformation

$$\frac{1}{|\vec{r_1}-\vec{r_2}|} = \frac{2}{\sqrt{\pi}} \int_0^\infty \mathrm{d}t e^{-t^2(|\vec{r_1}-\vec{r_2}|)^2} \tag{6.11}$$

yields

$$\frac{2}{\sqrt{\pi}} \int_0^\infty \mathrm{d}t \int_{-\frac{\Delta x}{2}}^{\frac{\Delta x}{2}} \int_{\Delta i\Delta x-\frac{\Delta x}{2}}^{\Delta i\Delta x+\frac{\Delta x}{2}} \mathrm{d}x_1\mathrm{d}x_2\ e^{-t^2(x_1-x_2)^2} \int_{-\frac{\Delta x}{2}}^{\frac{\Delta x}{2}} \int_{\Delta j\Delta x-\frac{\Delta x}{2}}^{\Delta j\Delta x+\frac{\Delta x}{2}} \mathrm{d}y_1\mathrm{d}y_2\ e^{-t^2(y_1-y_2)^2} \tag{6.12}$$

with $\Delta i = i - k$ and $\Delta j = j - l$. The integration over x_1 and x_2

$$\int_{-\frac{\Delta x}{2}}^{\frac{\Delta x}{2}} \int_{\Delta i\Delta x-\frac{\Delta x}{2}}^{\Delta i\Delta x+\frac{\Delta x}{2}} \mathrm{d}x_1\mathrm{d}x_2\ e^{-t^2(x_1-x_2)^2} \tag{6.13}$$

can be done analytically using the error function, analogously for y_1 and y_2. The result is

$$\begin{aligned} F(\Delta i,t) = \frac{1}{2t^2}(&e^{-\Delta x^2(\Delta i-1)^2t^2} - 2e^{-\Delta x^2\Delta i^2t^2} + e^{-\Delta x^2(\Delta i+1)^2t^2} + \Delta x\sqrt{\pi}t \\ &(-2\Delta i\mathrm{erf}(\Delta x\Delta it) + (\Delta i+1)\mathrm{erf}(\Delta x(\Delta i+1)t) - (\Delta i-1)\mathrm{erf}(\Delta x(-\Delta i+1)t))) \end{aligned} \tag{6.14}$$

And this leaves us with a 1D integral over the variable t for every Δi and Δj.

$$a(\Delta i,\Delta j) = \frac{2}{\sqrt{\pi}} \int_0^\infty \mathrm{d}t F(\Delta i,t)F(\Delta j,t) \tag{6.15}$$

As it can be seen in Figure 6.1 the integrand $F(\Delta i,t)F(\Delta j,t)$ is well behaved and can be integrated numerically without much computational cost. In some special cases for example $\Delta i = \Delta j = 0$ the analytic solution is available.

$$\int_{-\frac{\Delta x}{2}}^{\frac{\Delta x}{2}} \int_{-\frac{\Delta x}{2}}^{\frac{\Delta x}{2}} \int_{-\frac{\Delta x}{2}}^{\frac{\Delta x}{2}} \int_{-\frac{\Delta x}{2}}^{\frac{\Delta x}{2}} \frac{\mathrm{d}x_1\mathrm{d}x_2\mathrm{d}y_1\mathrm{d}y_2}{\sqrt{(x_1-x_2)^2+(y_1-y_2)^2}} = -\frac{4}{3}\left(\sqrt{2}-1-3\mathrm{asinh}(1)\right)\Delta x^3 \tag{6.16}$$

But for the general case $\Delta i \neq \Delta j$ we have to solve the integral numerically.

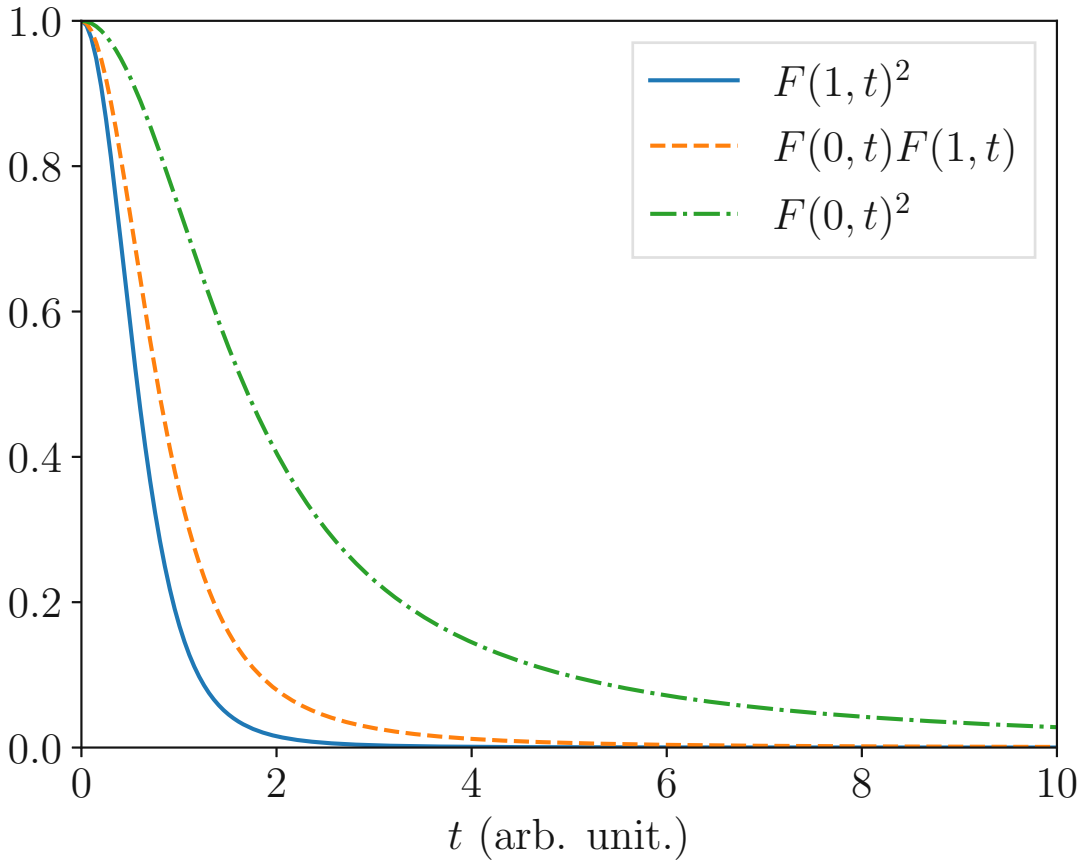

FIGURE 6.1: $F(1,t)^2, F(0,t)F(1,t), F(0,t)^2$ (equation 6.14) from left to right. See main text for more details.

The functional form of the integral is not dependent on the domain of integration. Therefore the integral will always be proportional to Δx^3 times a constant $a(\Delta i, \Delta j)$. Note that the Constants $a(\Delta i, \Delta j)$ are not dependent on Δx. Equation 6.7 can be rewritten as

$$\sum_{ijkl} \psi_{mnopqrst}(x_i, y_j, x_k, y_l) a(\Delta i, \Delta j) \Delta x^3. \tag{6.17}$$

We now evaluate the Coulomb integrals in real space numerically. Note that the constants $a(\Delta i, \Delta j)$ only need to be computed once and can be used for every Δx. Δi and Δj define the distance of the integration region from the singularity in steps of Δx. Approximating the Coulomb kernel by a constant in the region of integration becomes more accurate with increasing distance from the singularity. So a cutoff has to be chosen where the distance to the singularity is big enough such that we can use the constant approximation. With $\Delta i = 25$ and $\Delta j = 0$ equation 6.10 with the constant approximation gives $0.04\Delta x^3$, while evaluated with our scheme it gives $0.0400054\Delta x^3$. Thus we have chosen $\Delta i = 25$ as cutoff.

With this scheme, calculations of Coulomb integrals, and every other integral involving the Coulomb kernel, can be reduced to a tensor contraction with the constant universal matrix $a(\Delta i, \Delta j)$ by mapping the orbitals onto discretized realspace.

Note that this evaluation scheme for the Coulomb integrals can be generalized to three dimensional systems straightforwardly.

Now the Coulomb integral from equation (6.6) can be rewritten as a sum

$$\sum_{ijkl} \psi^*_{nm}(x_i, y_j)\psi^*_{op}(x_k, y_l)\psi_{qr}(x_i, y_j)\psi_{st}(x_k, y_l)a_{i-k,j-l}\Delta x^3. \tag{6.18}$$

where a_{ij} is a system independent matrix that does not depend on Δx. $\{i, j, k, l\}$ are here discretisation indices and are not to be confused with hole indices. Note that the factor Δx^3 implies that a_{ij} is dimensionless. Although this approach is computationally significantly less efficient than the recursive scheme, the computational bottle neck in the present study remains in the EE-EOM-CCSD calculations.

6.3.1 Convergence with Number of Gridpoints

We first discuss the numerical reliability of our approach. Let us note that our approach employs a single computational parameter, Δx, which defines the grid spacing used for the real space representation of all orbitals and the numerical integration. Table 6.1 shows the computed CCSD energies of the two-electron system with $\omega = 1.0$ for a range of Δx. Our findings show that 300×300 grid points suffice to achieve sub-mHa precision. For all further Coulomb integral calculations, we have therefore discretized the wavefunction into squares of edge length $\Delta x = 0.0342$ a.u., in a range where $|\psi(x, y)|^2 > 10^{-10}$. However, we note that a careful comparison between results summarized in our work and Refs. [140, 154] reveals that the published CCSD ground state energies do not always agree to within mHa. We attribute these discrepancies to different choices of basis sets in the CCSD and Hartree–Fock calculations, which can result in a different convergence behaviour of the energies to the complete basis set limit. Our basis set extrapolation approach will be discussed in the following sections.

6.4 Basis Set Convergence

Having assessed the reliability of our numerical approach, we now turn to the discussion of the ground state results obtained on the level of HF, MP2 and CCSD theories. We stress that it is necessary to converge all post-HF correlation energies with respect to

TABLE 6.1: Summary of the convergence of CCSD energies for the $N = 2$ electron system with $\omega = 1.0$ as a function of the number of grid points N_g used to represent the wavefunction. The CCSD energies have been computed for a finite basis set corresponding to 6 oscillator shells or 21 orbitals. All energies are in Hartree.

Δx (a.u.)	N_g	CCSD
0.1025	100×100	3.013673
0.0513	200×200	3.013621
0.0342	300×300	3.013613
0.0256	400×400	3.013610
0.0205	500×500	3.013612
0.0171	600×600	3.013613

the employed orbital basis set. For 3-dimensional ab initio systems and the uniform electron gas [159], it is known from second-order perturbation theory that the basis set error scales as $1/N_v$, where N_v refers to the number of virtual orbitals. The complete basis set limit is obtained by extrapolating $N_v \to \infty$.

For the studied system, the two dimensional QD, we expect a similar behavior for the correlation energies. In order to motivate the validity of this assumption, we have shown analytically that the asymptotic relation holds for the second-order perturbation theory correlation energy.

6.4.1 Asymptotic behavior of the Correlation Energy

The correlation energy in second-order perturbation theory is given by

$$E_{\text{corr}} = \sum_k \frac{|\langle 0| \frac{1}{r_{ij}} |k\rangle|^2}{E_k - E_0}. \tag{6.19}$$

Where $|0\rangle$ denotes the ground state, k is a excited state of the unperturbed Hamiltonian and E_0 and E_k are the corresponding energies. In theory, the summation goes over all excited states but in practice we have to truncate the summation at some cutoff k_{cut}. To replace the cutoff energy with the number of virtual orbitals in the above equation, we have to employ equation 6.3 and equation 6.4. We are only interested in the asymptotic behavior of the cutoff error, which is defined by

$$E_{\text{err}} = \lim_{N_v \to \infty} \sum_{k_{\text{cut}}}^{\infty} \frac{|\langle 0| \frac{1}{r_{ij}} |k\rangle|^2}{E_k - E_0}. \tag{6.20}$$

Furthermore, we can use the formula

$$\lim_{n\to\infty} e^{-\frac{x^2}{2}} H_n(x) \sim \frac{2^n}{\sqrt{\pi}}\Gamma\left(\frac{n+1}{2}\right)\cos\left(x\sqrt{2n}-\frac{n\pi}{2}\right) \tag{6.21}$$

to approximate our excited states with a simple cos function. Now the Coulomb integral can be calculated analytically, which leaves us with the result

$$\lim_{R\to\infty} \langle (00),(00)| \frac{1}{r_{ij}} |(RR),(RR)\rangle = \frac{4^R\Gamma\left(\frac{1+R}{2}\right)^4}{\pi^4(R!)^2} \tag{6.22}$$

where R denotes the shell of the orbital. Inserting this result into equation 6.20 and using the approximation for the gamma function

$$\lim_{x\to\infty} \Gamma(x+1) \sim \sqrt{2\pi x}\left(\frac{x}{e}\right)^x \tag{6.23}$$

gives us

$$E_{\text{err}} = \sum_R^{\infty} \frac{4(R-1)^2}{\pi^6 R^5}. \tag{6.24}$$

In the above equation, the sum can be replaced by an integration, yielding

$$E_{\text{err}} = \frac{4}{\pi^6}\left(-\frac{1}{2R^2}+\frac{2}{3R^3}-\frac{1}{4R^4}\right). \tag{6.25}$$

As the final step we have to convert the shell R to the number of orbitals N_{v}. By assuming filled shells we can write

$$R = \frac{1+\sqrt{8N_{\text{v}}+1}}{2} \tag{6.26}$$

which gives us the final result for the basis set error of second-order perturbation theory correlation energies computed using a truncated basis in the limit of $N_{\text{v}} \to \infty$:

$$\lim_{N_{\text{v}}\to\infty} E_{\text{err}} \sim \frac{1}{N_{\text{v}}}. \tag{6.27}$$

6.4.2 Basis Set Extrapolation

Numerical results for the correlation energies retrieved as a function of $1/N_{\text{v}}$ are depicted in Fig.6.2 and confirm the BSIE scaling for both MP2 and CCSD. From these numerical findings we conclude that the correlation energies can be linearly fitted using the following formula $E(N_{\text{v}}) = E_{\text{CBS}} + \frac{A}{N_{\text{v}}}$ with parameters (E_{CBS}, A).

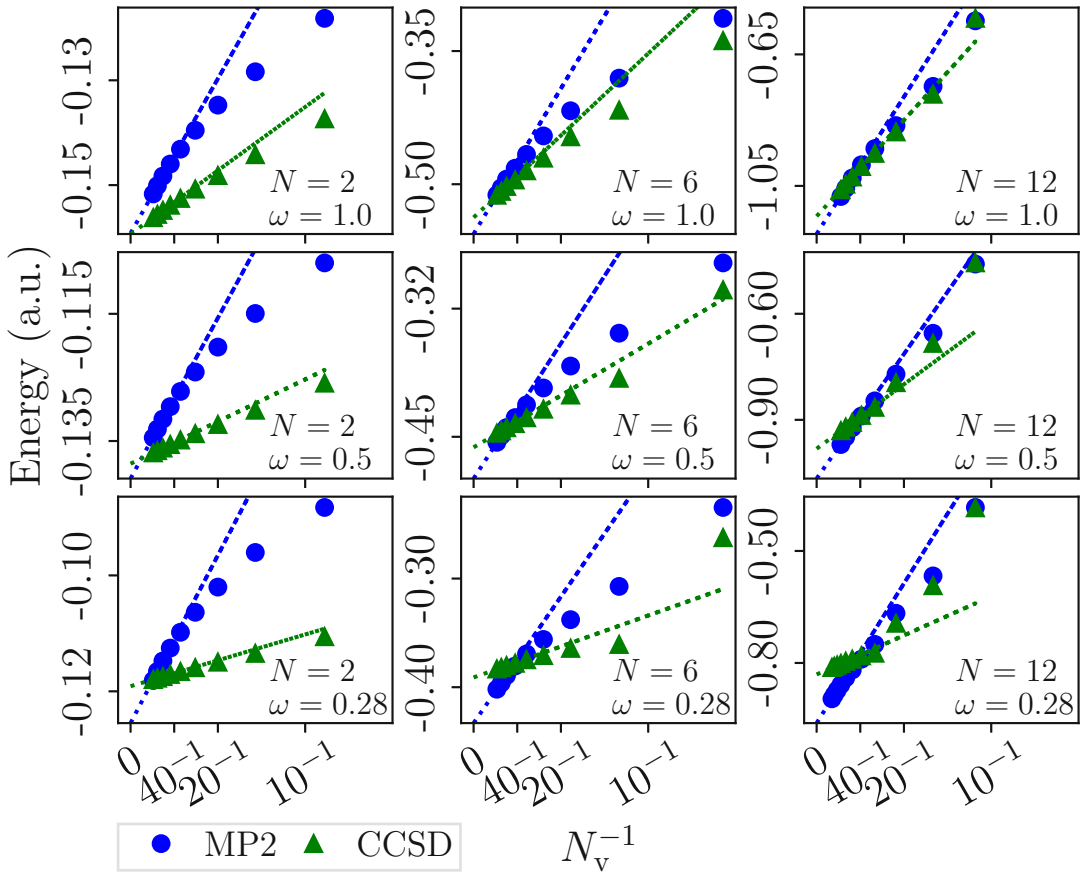

FIGURE 6.2: CCSD and MP2 correlation energies and their CBS extrapolations for $N \in \{2, 6, 12\}$ electron systems with $\omega \in \{1.0, 0.5, 0.28\}$ as a function of the inverse number of virtual orbitals. All energies are presented in Hartree and ω is given in atomic units.

Throughout this work E_{CBS} refers to extrapolated complete basis set limit energies that have been obtained by fitting the latter function using energies obtained with 65 and 77 orbitals.

It is worth noting that in the specific case of $\omega = 1.0$ for the 2 electron quantum dot the exact energy $E = 3.0$ is available from the literature [140, 160], also a variationally achieved energy as a function of ω that agrees to 5 decimal places with the analytic solution is available [154]. Comparing our CBS energy with the analytic solution $E = 3.0$ leaves a discrepancy that we attribute to the extrapolation scheme. The $1/N_{\mathrm{v}}$ extrapolation captures the leading order finite basis set errors. However, as evident from the convergence in table 6.2, other terms also contribute to the basis set error and sufficiently large N_{v} have to be used in order for the $1/N_{\mathrm{v}}$ extrapolation to obtain reliable results. Our analysis shows that including higher order terms in the extrapolation scheme (equation 6.25) brings us even closer to the exact energy. However, technically it's simpler and more robust to use only the leading term. Further, increasing the basis set

TABLE 6.2: Summary of CBS limit CCSD ground state energy for the 2 electron system with $\omega = 1.0$, with different functions used for the extrapolation. All energies are in Hartree.

Extrapolation function	E_{CBS}
$E_{\mathrm{CBS}} + \frac{a}{N_{\mathrm{v}}}$	3.00217
$E_{\mathrm{CBS}} + \frac{a}{N_{\mathrm{v}}} + \frac{b}{N_{\mathrm{v}}^{\frac{3}{2}}}$	3.00147
$E_{\mathrm{CBS}} + \frac{a}{N_{\mathrm{v}}} + \frac{b}{N_{\mathrm{v}}^{\frac{3}{2}}} + \frac{c}{N_{\mathrm{v}}^{2}}$	3.00083

TABLE 6.3: Summary of CBS limit CCSD ground state energy for the 2 electron system with $\omega = 1.0$, with different basis set sizes used for the extrapolation. All energies are in Hartree.

N_{v}	E_{CBS}
44 - 54	3.00259
54 - 65	3.00238
65 - 77	3.00217

size also brings us closer to the exact CBS limit, summarized in table 6.3. But at this point we cannot afford larger basis set sizes.

6.5 Results

We study QDs for a range of electron numbers and $\omega \in \{1.0, 0.5, 0.28\}$. ω characterizes the correlation strength in the system relative to the potential energy. Large ω correspond to weakly correlated systems whereas small ω correspond to stronger correlated systems [140].

Throughout this section all quantities are presented in atomic units (a.u.). In particular, all energy values are therefore given in Hartree.

6.5.1 Ground State Energies

Table 6.4 summarizes the HF, MP2 and CCSD correlation energies together with the CBS limit for $\omega \in \{1.0, 0.5, 0.28\}$ for the 2 electron system. Compared to the HF energy, the MP2 correlation energy changes only slightly with ω. However, on a relative scale the importance of the correlation energy contribution to the ground state energy increases from 5.3 % to 11.7 % (ratio of MP2/CCSD correlation energy and the ground state energy for $N = 2$, $\omega = 1.0$ a.u. and 0.28 a.u.). Low-order perturbation theories like MP2 become less reliable in the regime of strong correlation. CCSD, being a more accurate theory in the sense that it contains all contributions from MP3 theory and

TABLE 6.4: HF energy and correlation energy contributions on the level of MP2 and CCSD theory in Hartree for 2 electrons. N_v denotes the number of virtual orbitals, with its value at ∞ being the extrapolated value. Our results show that as ω increases, the HF ground state energies increases linearly with ω. HF is a good approximation in the limit of large ω where the inter electronic interaction is small compared to the one-body interaction.

ω (a.u.)	N_v	HF	MP2	CCSD
1.0	9	3.1626	-0.1182	-0.1374
	14	3.1618	-0.1284	-0.1442
	20	3.1618	-0.1347	-0.1482
	27	3.1618	-0.1395	-0.1508
	35	3.1618	-0.1431	-0.1526
	44	3.1618	-0.146	-0.1539
	54	3.1618	-0.1483	-0.1548
	65	3.1618	-0.1501	-0.1556
	77	3.1618	-0.1517	-0.1562
	∞	3.1618	-0.1602	-0.1596
0.5	9	1.7998	-0.107	-0.1259
	14	1.7997	-0.1149	-0.1302
	20	1.7997	-0.1202	-0.1324
	27	1.7997	-0.1242	-0.1339
	35	1.7997	-0.1272	-0.1348
	44	1.7997	-0.1296	-0.1356
	54	1.7997	-0.1315	-0.1361
	65	1.7997	-0.1331	-0.1365
	77	1.7997	-0.1345	-0.1369
	∞	1.7997	-0.1418	-0.1387
0.28	9	1.1417	-0.0962	-0.1129
	14	1.1417	-0.102	-0.1151
	20	1.1417	-0.1065	-0.1162
	27	1.1417	-0.1098	-0.1169
	35	1.1417	-0.1123	-0.1174
	44	1.1417	-0.1144	-0.1178
	54	1.1417	-0.1161	-0.1181
	65	1.1417	-0.1174	-0.1183
	77	1.1417	-0.1186	-0.1185
	∞	1.1417	-0.1249	-0.1194

TABLE 6.5: Summary of CBS limit CCSD energies for $N \in \{2, 6, 12\}$ electron systems with $\omega \in \{1.0, 0.5, 0.28\}$. All energies are in Hartree.

ω (a.u.)	Electrons	E_{CBS}
1.0	2	3.0022
	6	20.1839
	12	65.7644
0.5	2	1.6609
	6	11.8118
	12	39.2343
0.28	2	1.0222
	6	7.6292
	12	25.7190

more, is expected to yield more accurate results than MP2 for small ω. We can see that the relative CCSD and MP2 contributions to the ground state energy differ more as ω decreases.

The linear scaling of the correlation energies with ω and the basis set convergence shown in Fig.6.2 is found to be qualitatively independent of the number of electrons. All calculated CBS ground state energies are summarized in Table 6.5 for further reference. Our findings demonstrate that small electron numbers already serve as a good approximation to the behavior of ground state energies with the investigated parameters.

6.5.2 Excitation Energies

Having established a procedure to converge the ground state energies with the basis set, we now seek to discuss the excited state properties. To this end, we employ EE-EOM-CCSD theory and the same Hamiltonian employed for the ground state. We have calculated the first three excitation energies, where the first excited state in EE-EOM-CCSD theory corresponds to a triplet state while the second and third excited states are singlet states.

Analogously to the ground state, we need to converge the excitation energies carefully with the basis set. Figures 6.3, 6.4 and 6.5 give evidence that the EE-EOM-CCSD excitation energies converge in a similar manner to the complete basis set limit. However, the slope is significantly less steep, resulting in excitation energies with relatively small basis set incompleteness errors when employing $N_{\mathrm{v}} = 77$. Note that in the case of $N = 12$ and $\omega = 0.28$ we use $N_{\mathrm{v}} = 114$ for the extrapolation. We estimate the CBS limit of the excitation energies using an identical extrapolation procedure as used for

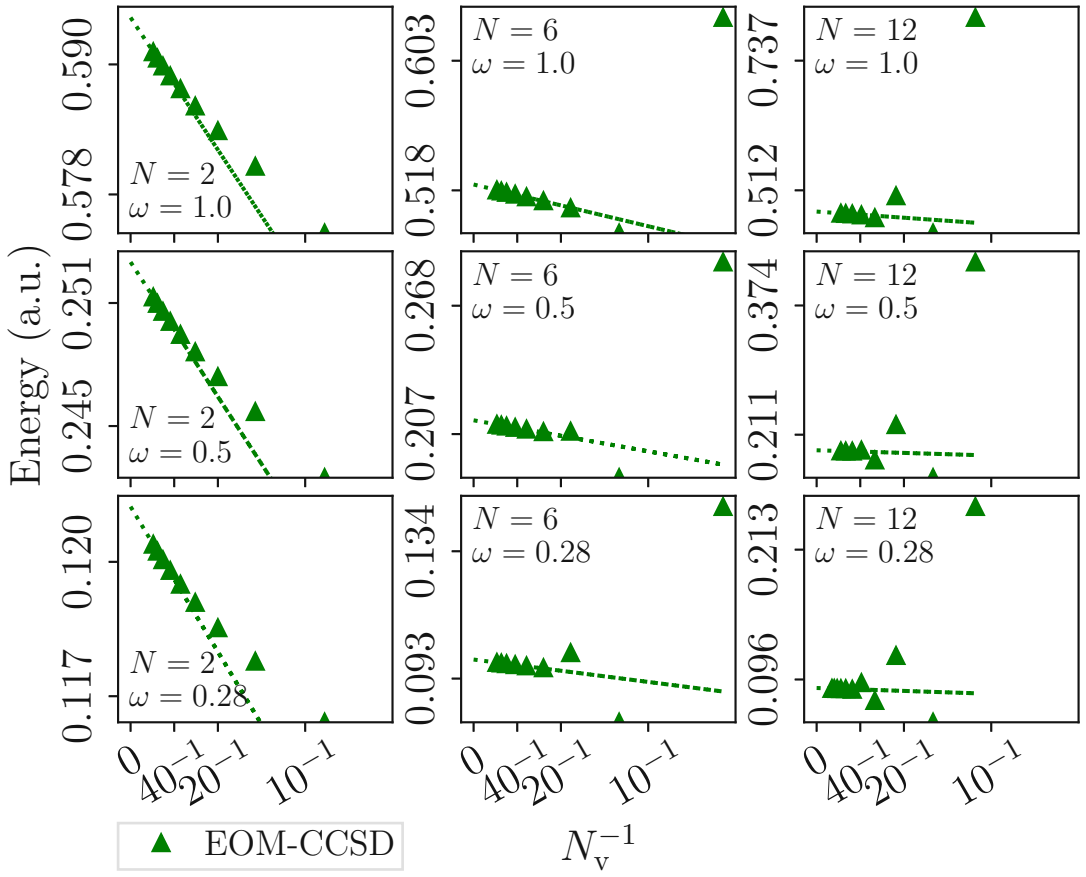

FIGURE 6.3: First EE-EOM-CCSD excitation energy for $N \in \{2, 6, 12\}$ electron systems with $\omega \in \{1.0, 0.5, 0.28\}$ retrieved as a function of the inverse number of virtual orbitals N_{v}^{-1}. All energies are in Hartree.

the ground state. In the case of excited states, as seen in figures 6.3 - 6.5, the slope of the extrapolation function is less steep, resulting in a more reliable result.

Figure 6.6 shows the first excitation energy (singlet-triplet gap) for $N = 2$ as a function of ω. EE-EOM-CCSD calculations predict an excitation energy that decreases with decreasing ω. Approximating the singlet-triplet gap on the level of UHF theory yields an inter system crossing at $\omega = 0.3926$ a.u.. However, UHF energies neglect correlation effects, which are expected to be larger in magnitude for the singlet state than for the triplet state. It has already been discussed that the singlet-triplet crossing predicted by UHF results from the neglect of the electron-electron correlation [110]. Indeed, we find that UMP2 and EOM-CC theory predict no singlet-triplet crossing. Details on how the UMP2 and UHF singlet-triplet gap was calculated can be found in appendix C.

Finally, Table 6.6 summarizes the CBS excitation energies from Fig. 6.3, 6.4 and 6.5. It shows that the linear scaling of the excitation energies with ω is qualitatively unchanged when comparing $N = 2$, $N = 6$ and $N = 12$ electron systems. Our findings show

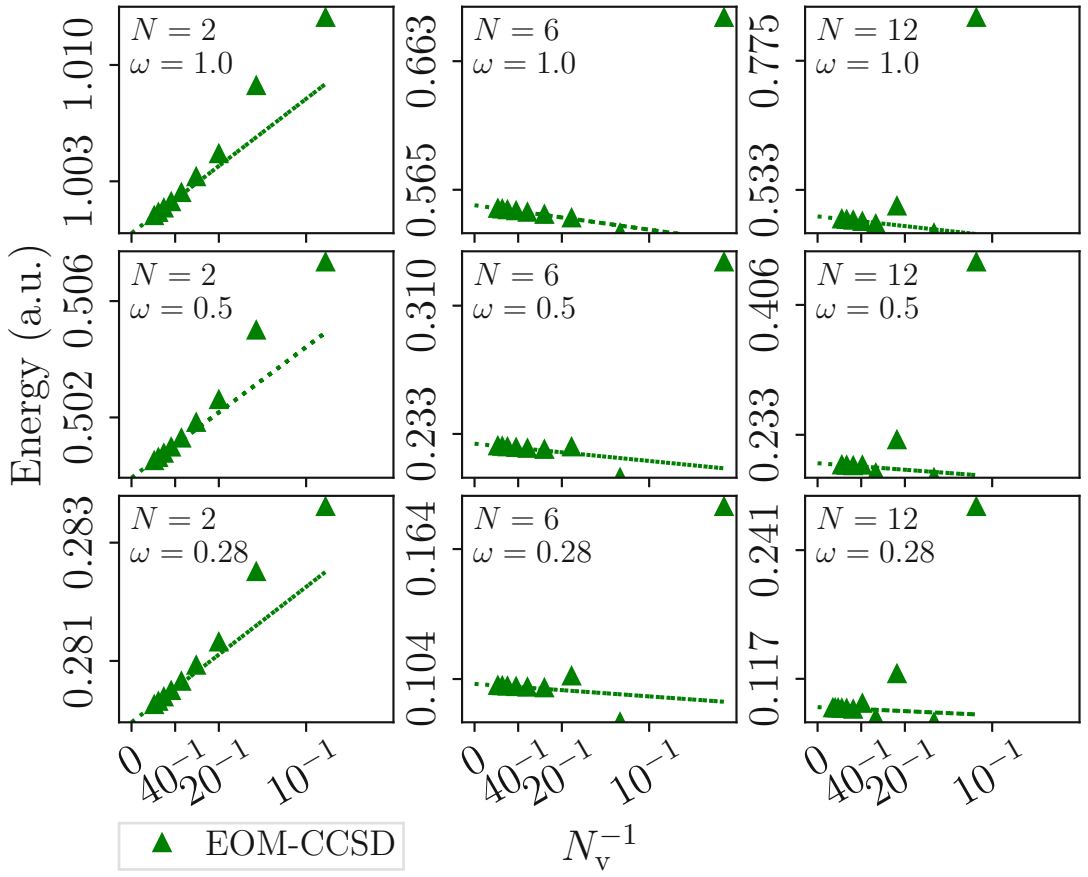

FIGURE 6.4: Second EE-EOM-CCSD excitation energy for $N \in \{2, 6, 12\}$ electron systems with $\omega \in \{1.0, 0.5, 0.28\}$ retrieved as a function of the inverse number of virtual orbitals N_v^{-1}. All energies are in Hartree.

that all excitation energies scale linearly with ω. For the 2 electron quantum dot the singlet-singlet excitations (in our work the second and third excitation) are variationally available [154]. We have compared our singlet-singlet excitation energies to values from Ref. [154] and they are in excellent agreement as summarized in Table 6.7. The remaining differences of the excitation energies can be attributed to the CBS extrapolation procedure and also to the numerical procedures regarding the Coulomb integrals and the wavefunction, as described in the previous section.

6.6 Conclusion and Summary

We have investigated a model Hamiltonian for two dimensional QDs using quantum chemical many-electron theories including HF, MP2 and CCSD. For the study of excited states we have employed the equation-of-motion formalism of CCSD theory (EOM-CCSD). We have outlined a numerical method to compute the Coulomb integrals for

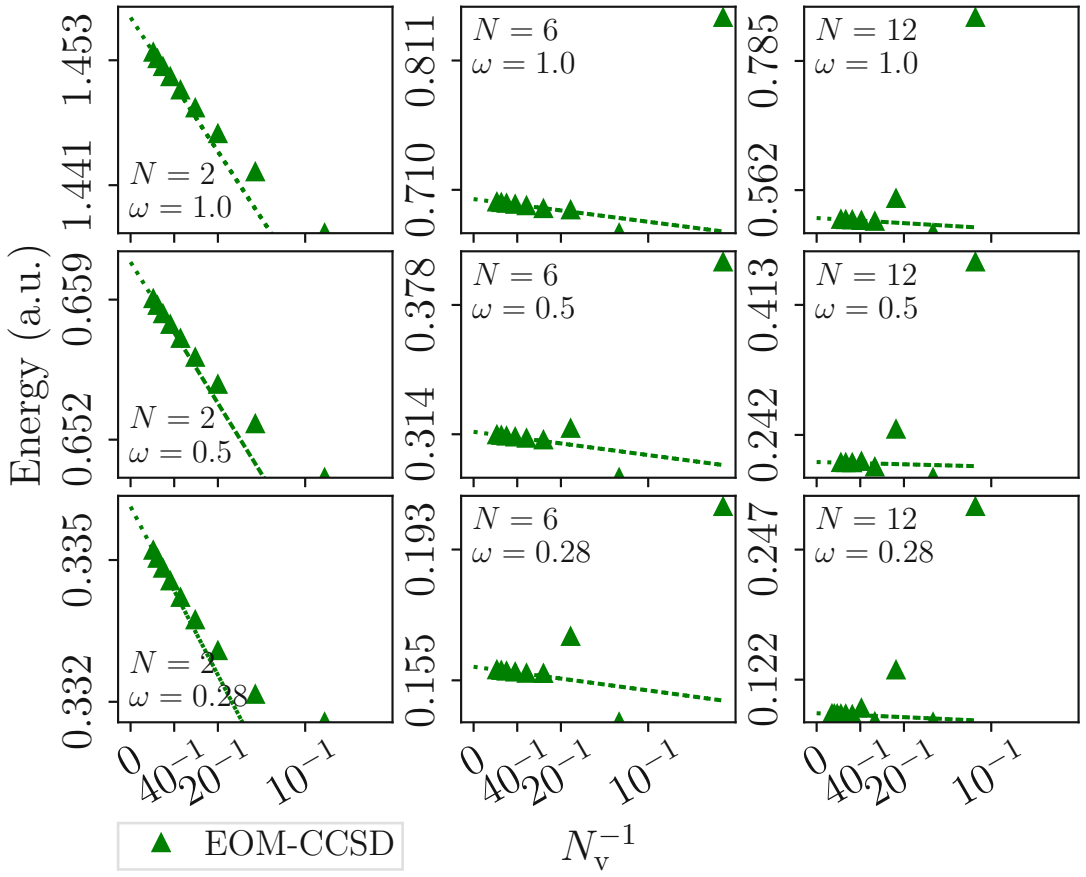

FIGURE 6.5: Third EE-EOM-CCSD excitation energy for $N \in \{2, 6, 12\}$ electron systems with $\omega \in \{1.0, 0.5, 0.28\}$ retrieved as a function of the inverse number of virtual orbitals N_v^{-1}. All energies are in Hartree.

arbitrary orbitals represented on a discrete numerical grid. Although this method is computationally less efficient than recursive schemes for orbitals that correspond to Gaussians or their derivatives, we note that it can become potentially useful for different model Hamiltonians that include a one-body part and corresponding eigenfunctions which are difficult to expand using Gaussians or their derivatives.

We have investigated the convergence of the computed correlation energies for ground and excited states with respect to the number of virtual orbitals numerically, finding a convergence behavior for two dimensional QDs which is identical to the basis set convergence of the second-order correlation energy in perturbation theory of the three dimensional electron gas. Furthermore, we have performed an analytic derivation for the two dimensional QD on the level of second-order perturbation theory that supports this convergence behavior. Based on this analysis, we have extrapolated all computed correlation energies for ground and excited states to the complete basis set limit assuming a $1/N_\mathrm{v}$ convergence of the remaining finite basis set errors and compared them partly to analytic and variationally achieved semi-analytic results.

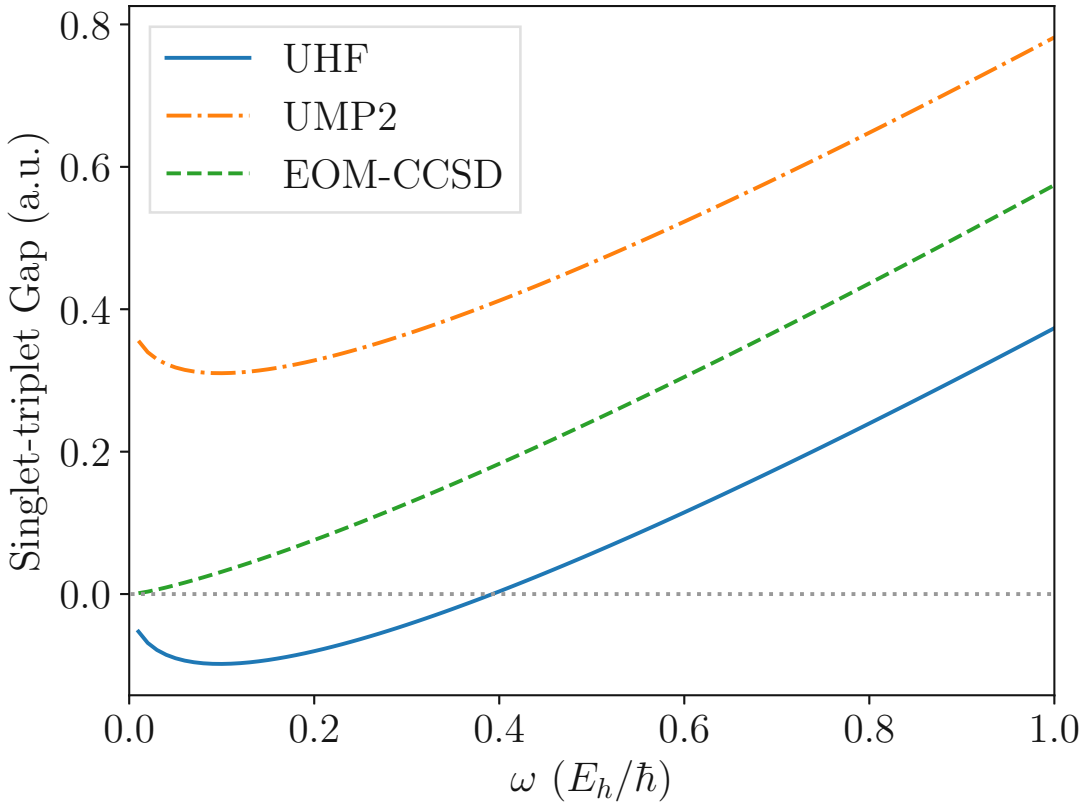

FIGURE 6.6: Singlet-triplet gap calculated with UHF, UMP2 and EE-EOM-CCSD as a function of ω in Hartree. All calculations are done with $N_v = 10$.

The computed ground state energies in a range of $\omega = 0.28$ a.u., which corresponds to a strongly correlated regime, to $\omega = 1.0$ a.u., has revealed that the HF energy scales linearly with respect to ω and that the relative contribution of the MP2 and CCSD correlation energies to the ground state energy increases with decreasing ω. Furthermore, we have observed that with decreasing ω the relative difference between the MP2 and CCSD correlation energy is increasing, outlining that CCSD captures higher order correlation effects than MP2.

Using the EE-EOM-CCSD formalism, we have calculated the first three excitation energies of the QD and partly compared them to values from the literature. Our findings show that the excitation energies scale linearly with ω and for $N = 12$ and $\omega = 0.28$ the second and third excitation become numerically degenerate.

Finally, our work also demonstrates that two dimensional QD model Hamiltonians serves not only as a suitable tool for experimental QDs but can also be used as efficient and well-controlled testing ground of approximate many-electron theories to study ground and excited state properties. Using a single parameter to tune the confinement via the harmonic potential, the Hamiltonian can be modified to switch between different regimes

TABLE 6.6: CBS limit excitation energies for $N \in \{2, 6, 12\}$ electron systems with $\omega \in \{1.0, 0.5, 0.28\}$. All quantities are expressed in atomic units.

ω (a.u.)	Electrons	First excitation	Second excitation	Third excitation
1.0	2	0.5943	0.9999	1.4571
	6	0.5218	0.5532	0.7028
	12	0.4752	0.4834	0.5138
0.5	2	0.2530	0.4999	0.6609
	6	0.2136	0.2271	0.3152
	12	0.1913	0.1951	0.2063
0.28	2	0.1212	0.2800	0.3361
	6	0.0991	0.1018	0.1589
	12	0.0883	0.0897	0.0897

TABLE 6.7: CBS limit ground state and excitation energies for the 2 electron system with $\omega \in \{1.0, 0.5\}$ compared to the variationally optimized energies from Ref. [154] on the right. All quantities are expressed in atomic units.

ω (a.u.)	Ground state	Second excitation	Third excitation
1.0	3.002/3.000	1.000/1.000	1.457/1.459
0.5	1.661/1.660	0.500/0.500	0.661/0.662

of correlation strengths and investigate the accuracy of finite-order perturbation theories. However, we find that EOM-CCSD performs qualitatively correctly for the investigated parameter ranges and that the remaining errors are expected to be only of quantitative interest. In future work we seek to investigate different levels of EOM theories and compare to other widely-used electronic structure theories that treat ground and excited state phenomena. Further, the improvement of the semi-analytic realspace evaluation of the Coulomb integrals, due to it's universal applicability, may be of interest in the future.

Chapter 7

Silicon Interstitials

In the following chapter we present a study of the self-interstitial point defect formation energies in silicon using a range of quantum chemical theories including the CC method within a periodic supercell approach. We study the formation energies of the so called X, T, H and C3V self-interstitials and the vacancy V. Our results are compared to findings obtained using different ab initio methods published in the literature and partly to experimental data. In order to achieve computational results that are converged with respect to system size and basis set, we employ the recently proposed finite size error corrections and basis set incompleteness error corrections. Our CCSD(T) calculations yield an order of stability of the X, H and T self-interstitials, which agrees both with quantum Monte Carlo results and with predictions obtained using the random-phase approximation as well as using screened hybrid functionals. Compared to quantum Monte Carlo results with backflow corrections, the CCSD(T) formation energies of X and H are only slightly larger by about 100 meV. However, in the case of the T self-interstitial, we find significant disagreement with all other theoretical predictions. Compared to quantum Monte Carlo calculations, CCSD(T) overestimates the formation energy of the T self-interstitial by 1.2 eV. Although this can partly be attributed to strong correlation effects, more accurate electronic structure theories are needed to understand these findings.

In the following sections a short presentation on the history, experimental developments and the importance of silicon is given, as well as a condensed matter physicist perspective on the silicon self-diffusion. The following discussion has been published in Ref. [161].

7.1 Introduction

With over half a century of producing nanometer-sized silicon devices, one would anticipate a comprehensive understanding of this material, particularly considering the current need for near-atomic precision in manufacturing today's nanometer-sized transistors.

Nevertheless, due to the miniaturization process, even the accidental formation of a single trapping center can have a significant impact on the electronic properties of the sample, making this phenomenon the most feared issue in the industry [162].

7.1.1 Experimental and Theoretical Developments

To better understand the influence of single isolated vacancies and interstitials, these have to be produced experimentally. This can be achieved with 1–3 MeV electron irradiation performed at cryogenic temperatures. The identification of these centers is possible through characterization techniques like electron paramagnetic spectroscopy (EPR), which is capable of targeting the atomic distortion triggered by the form of the localized electronic density [163, 164]. Infrared optical absorption and deep-level transient spectroscopy can also be used to identify center-induced states within the semiconductor gap [165–167]. The availability of experimental data motivated the development of simple theoretical models geared towards quantitatively reproducing the basic features of these defects. Furthermore, the rapid growth in computational resources made it possible to perform ab initio calculations to model and understand their properties thoroughly on an atomic level.

Point defects, such as vacancies, interstitials and anti-site defects, are the only thermodynamically stable defects at finite temperatures [168]. The presence of point defects often controls the kinetics of the material and can therefore fundamentally alter its electronic, optical and mechanical properties. This makes the understanding of point defects technologically important for a wide range of applications such as doping of semiconductors [169–172], production of quantum devices [173, 174], and controlling the transition temperature of shape memory alloys [175].

Of all materials, silicon is one of the most important for industrial use and plays a crucial role in a wide variety of devices, e.g., advanced electronic devices, power devices, solar cells, and microelectronic systems. In all these applications, Czochralski (CZ) and floating zone (FZ) silicon single crystals are used (except for some solar cells) [176]. The diffusion characteristics and thermodynamics of silicon self-interstitials and vacancies dominate the doping and annealing processes for electronics applications [170, 171]. However, the understanding of self-diffusion in silicon remains incomplete despite decades

of research [173, 177–197]. Questions regarding the role of the self-interstitials and the vacancy in the self-diffusion remain. One of the remaining questions, which needs to be addressed using quantum mechanical methods, is the formation energy of the silicon self-interstitials and vacancy.

7.1.2 Many-Body Methods for the Formation Energy

Again, the most widely used method in this regard is DFT. Exchange correlation functionals based on the local density approximation (LDA), general gradient approximation (GGA) and hybrid functionals predict formation energies in the range of 2 eV-4.5 eV [182]. Green's function based methods, such as the *GW* approximation, are expected to yield more accurate results and predict formation energies of about 4.5 eV [179]. A low-scaling implementation of the random-phase approximation reported formation energies on a similar scale [198]. QMC provides another computationally more expensive alternative to DFT and is among the most accurate electronic structure methods available. Several groups have calculated the formation energies using QMC [197, 199]. In this work, we focus only on the former [197], because it employs a Slater-Jastrow-backflow wavefunction, which changes the formation energies substantially.

The CC method is widely used in molecular quantum chemistry, where it achieves high accuracy in the prediction of reaction energies for a wide range of systems. While being an efficient method for calculating small to medium-sized molecules, single-reference CC methods have never been used to calculate the formation energies of silicon self-interstitials and the vacancy in diamond cubic crystal silicon. Only over the past few years have computationally efficient implementations of periodic CC methods become available to study such systems [58, 200–202]. Moreover, recent developments in embedding approaches also make it possible to study such local phenomena using CC methods [203–211]. The goal of this work is to calculate the formation energies of the silicon self-interstitials and vacancy at the level of CCSD(T) theory and compare them to experimental data [196, 212–215] and reference data from literature [179, 182, 197, 198].

7.2 Cell structure

In order to simulate a silicon self-interstitial one has to define a periodic simulation cell. The employed simulation cells of silicon self-interstitials are obtained by adding one Si atom to the diamond cubic crystal structure of bulk silicon and relaxing the atomic positions. The silicon self-interstitial structures are shown in figure 7.1.

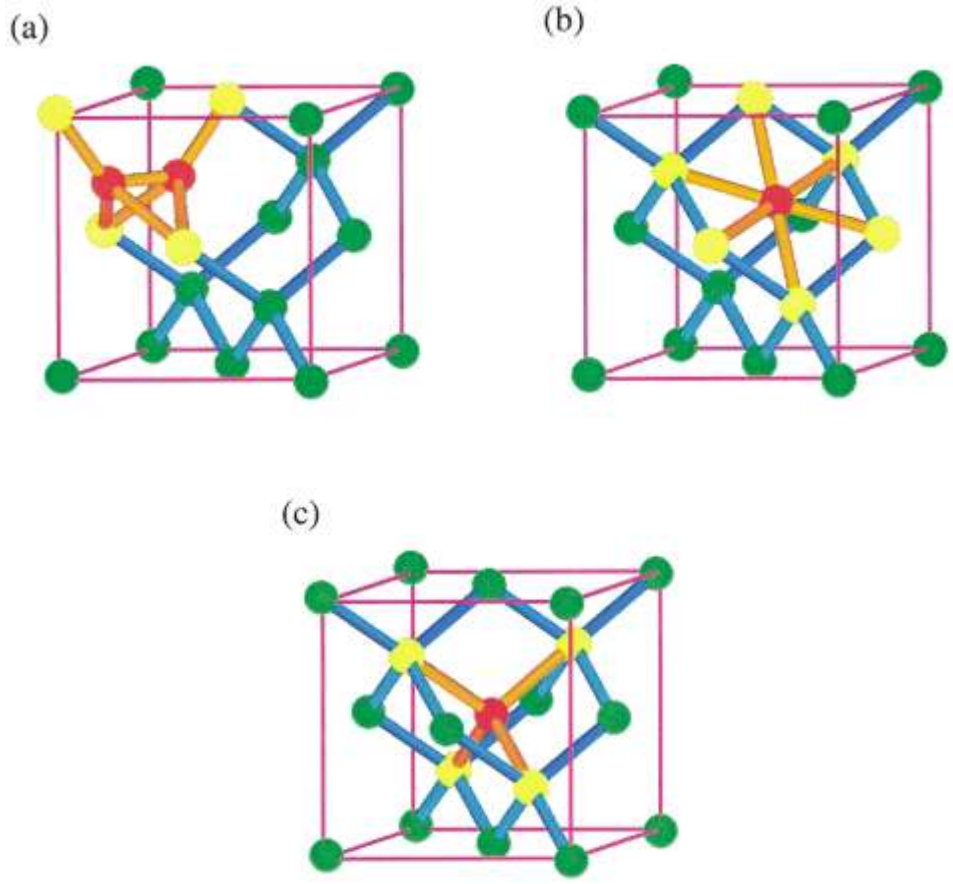

FIGURE 7.1: (a) The split-110 (X), (b) hexagonal (H), and (c) tetrahedral (T) interstitial defects. The atom(s) forming the defect are shown in red, while the nearest neighbors to the defect atoms are shown in yellow. The bonds between the defect and nearest neighbor atoms are shown in orange. The figures are taken from reference [183].

The energetically most stable silicon self-interstitial (X) is one in which two silicon atoms reside symmetrically shifted from the position previously occupied by one. The two atoms are oriented parallel to the [110] direction. The second most favorable self-interstitial (H) is where the additional Si atom is equidistant to six other atoms, forming a hexagonal ring. It is worth noting that this configuration is unstable in DFT-PBE, where the central atom of the ring is slightly moving away in a direction orthogonal to the ring (C3V) [179, 216]. The last self-interstitial considered in this work, with the highest energy, is where the additional Si atom is coordinated equidistantly to four nearest neighbors, forming a tetrahedron (T). For the T interstitial, the highest occupied state is threefold degenerate but only occupied by two electrons, which potentially introduces a multireference character. The vacancy is created by removing one Si atom from the bulk structure. Like the T interstitial, it has a threefold degenerate highest occupied state, occupied by two electrons. The vacancy is known to undergo a Jahn-Teller distortion to a D_{2d} symmetry [217].

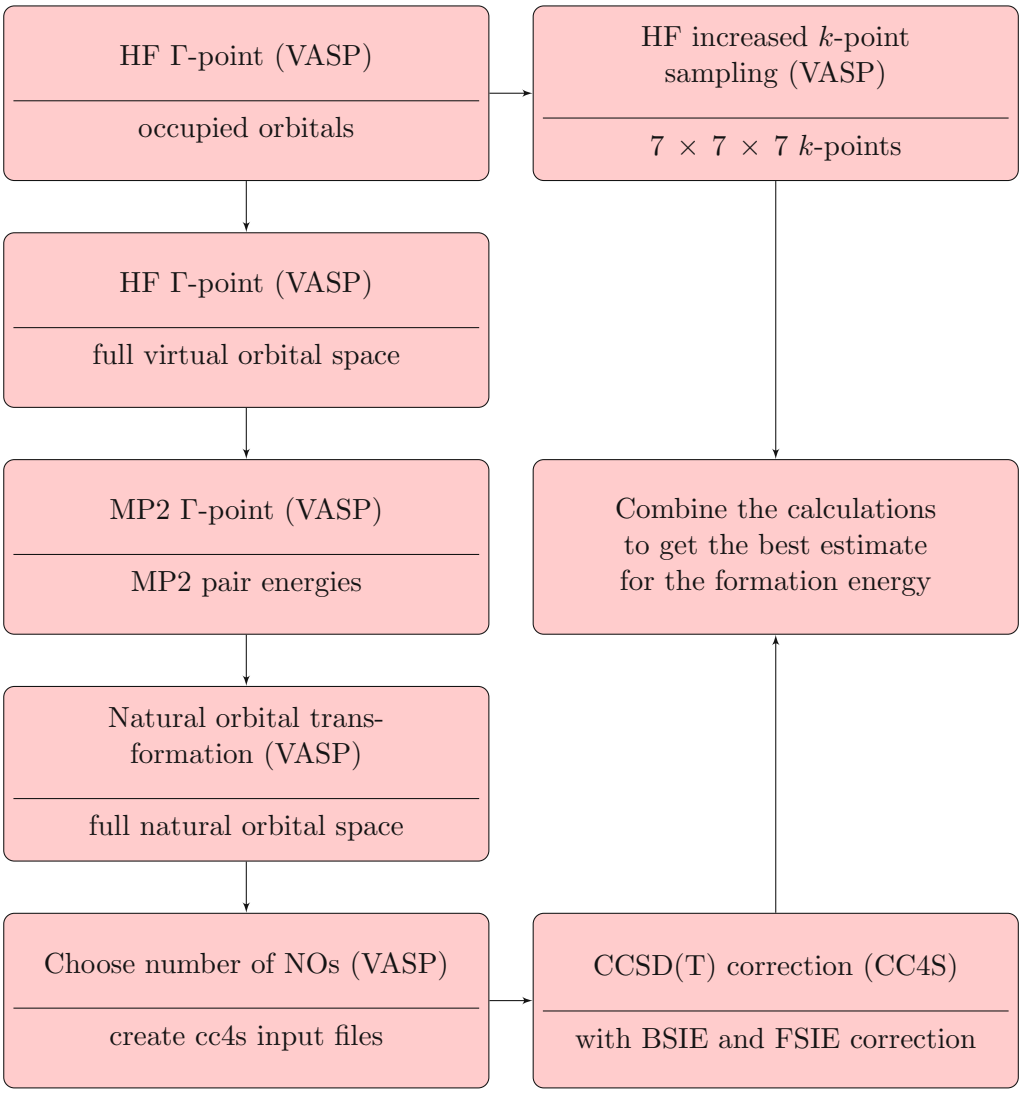

FIGURE 7.2: Schematic illustration of the workflow used to get the silicon self-interstitial formation energies.

All the ion positions of the used structures have been relaxed at the DFT level using the PBE exchange and correlation energy functional [16]. The shape and volume of the cells are kept fixed during the relaxation procedure.

7.3 Workflow

All coupled cluster calculations are performed using our high-performance open-source coupled cluster simulation code, cc4s. The preparation of the necessary reference wavefunction and the required intermediates was performed using the VASP [54–56].

The workflow is schematically depicted in figure 7.2.

For all calculations in VASP a plane-wave kinetic energy cut off of $E_{\text{cut}} = 400\,\text{eV}$ has been used. The employed smearing parameter is $\sigma = 10^{-4}\,\text{eV}$ and a convergence criterion of $\Delta E = 10^{-6}\,\text{eV}$ is used. All other numerical parameters were left unchanged from their default values. The HF calculations are performed using VASP and the structures described in section 7.2. The HF calculations are done using a Γ-centered $7 \times 7 \times 7$ k-point mesh. All post-HF calculations sample the first Brillouin zone using a single k-point only. Further, we need to compute all unoccupied HF orbitals since in CC theory we approximate the many-electron wavefunction using excited Slater determinants, constructed by occupied and unoccupied HF orbitals. In VASP this is achieved by setting the number of virtual orbitals to the maximum number of plane-waves in the basis set. The convergence of the CCSD electron correlation energy is very slow when using canonical HF orbitals. A much faster convergence to the complete basis set limit is achieved using natural orbitals. In VASP approximate natural orbitals can be calculated as described in Eq.(2) from Ref. [61]. After calculating all natural orbitals, a subset of them is chosen for the cc4s calculations. For the coupled-cluster theory calculations, we chose the number of unoccupied natural orbitals per occupied orbital to be 5, 10, 15, 20, 25 and 30. Additionally, for the basis set correction algorithm described in section 5.2.1 and in the references therein, the MP2 pair energies are needed. For this purpose, there are two algorithms available in VASP [218, 219]. In our case, we have used a 16-atom cell for the bulk with 32 occupied orbitals; therefore, the MP2 algorithm from Ref. [219] is more efficient. In the case of more than 50 occupied orbitals, a different algorithm based on LTMP2 might be faster and less memory consuming [218]. Note that the basis set correction algorithm uses a focal-point approach, and from now on, the basis set correction is also referred to as the focal-point correction (FPC). With these preparations done, VASP can provide all necessary files needed for the CCSD(T) calculation with the finite size and basis set error correction computed by cc4s. It is worth noting that the CCSD calculation in cc4s converges much faster when using the DIIS mixer instead of the default linear mixer. The described workflow with all necessary files can be found on zenodo [220].

After studying the BSIE, we chose our number of virtual orbitals per occupied orbital to be 10 and repeated all calculations with 10 randomly chosen k-point shifts in order to get a twist average estimate of the CCSD(T) correlation energies.

All calculations have been performed using 16 compute nodes, each equipped with 384 GB main memory.

Further, we have calculated the formation energies at the HSE level of theory with up to $5 \times 5 \times 5$ k-points (converged within 10-–20 meV.), as shown in Table 7.2 below.

7.4 Results

We now discuss the formation energies of the silicon self-interstitial structures described in section 7.2 at the CCSD(T) level of theory. We use 16 atom cells for the pristine bulk crystal with periodic boundary conditions, the interstitial cells have 17 atoms, while the vacancy has 15 atoms. The HF energies, CCSD, CCSD(T), finite size and basis set energy corrections can be found in appendix D in table D.1.

The formation energy is calculated by subtracting the energy of the interstitial cell with the energy of the bulk cell scaled to the same number of atoms:

$$E_{\mathrm{F}} = E_{\mathrm{int}} - \frac{N_{\mathrm{int}}}{N_{\mathrm{bulk}}} E_{\mathrm{bulk}}. \tag{7.1}$$

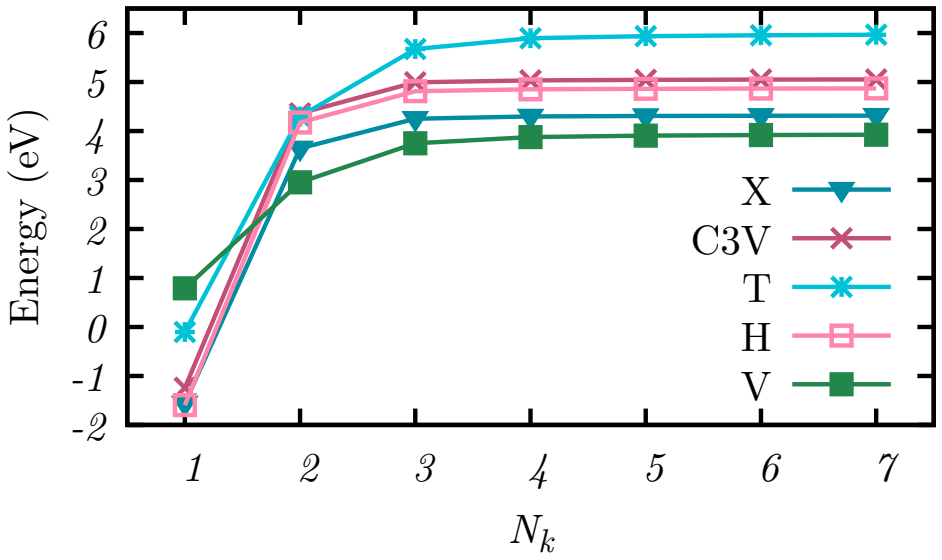

FIGURE 7.3: The formation energy as a function of the number of k-points used in the Hartree-Fock calculation for all self-interstitials. A Γ-centered cubic k-point mesh was used with N_k x N_k x N_k gridpoints.

7.4.1 HF Formation Energy Finite Size Convergence

We first discuss the convergence of the HF energy contribution to the formation energies. Figure 7.3 shows the convergence of the HF formation energies with respect to the size of the k-point mesh used in the HF calculation. We used a Γ-centered cubic k-point mesh with up to 7×7×7 grid points. Using only one k-point gives qualitatively and quantitatively wrong formation energies. With a k-point mesh size of 5×5×5, the

formation energies are already well converged and increasing the k-point grid size further to 7×7×7 increases the formation energies of X, H and C3V by less than 8.5 meV, while T and V increase by 29 meV and 19 meV.

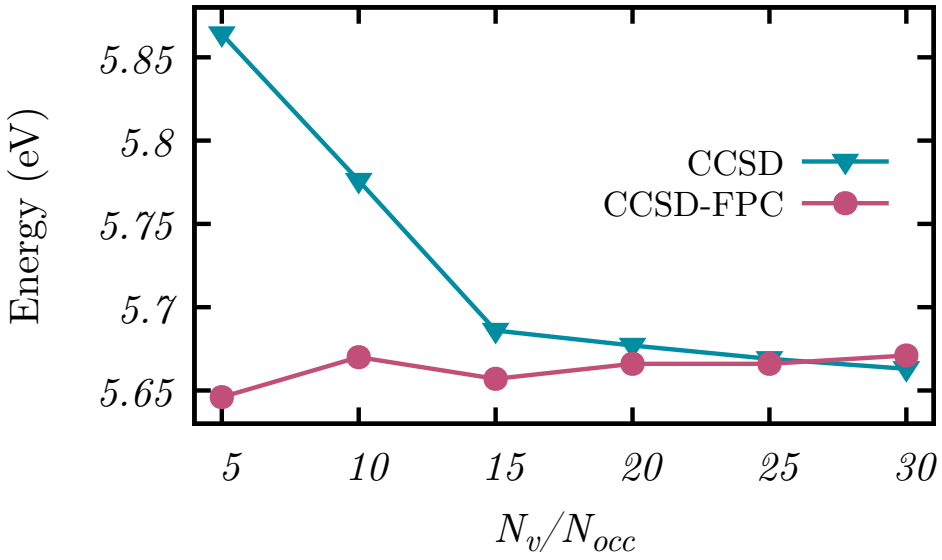

FIGURE 7.4: CCSD formation energy of the X interstitial as a function of the number of orbitals per occupied orbital with and without the basis set correction scheme (FPC). A Γ-centered cubic mesh was used.

7.4.2 Basis Set Convergence

We now discuss the convergence of the correlation energy contributions to the formation energies with respect to the number of virtual orbitals. Let us note that the HF formation energy Contributions are independent of the virtual orbital basis set size. The MP2 calculations employ the complete virtual orbital basis set defined by the kinetic energy cutoff of the plane wave basis set. Furthermore the MP2 correlation energies are automatically extrapolated to the complete basis set limit using a procedure explained in Ref. [218]. For the post-MP2 correlation energy calculations, we employ approximate natural orbitals as virtual orbitals and seek to converge the correlation energies explicitly by increasing the number of virtual orbitals. We find that this approach allows for an effective cancellation between basis set incompleteness errors of correlation energies for different systems when taking their differences. Furthermore, we add a basis set incompleteness error correction described in Ref. [59] to accelerate the convergence of the CCSD correlation energy. The effect of the basis set correction on the formation energy is highlighted in figure 7.4, which depicts the formation energy retrieved as a function of the number of virtual orbitals per occupied orbital for the X interstitial.

Our results indicate that between 10 and 20 virtual orbitals per occupied orbital suffice to achieve converged formation energies with and without the basis set correction, respectively. The remaining basis set incompleteness error is caused by fluctuations on the scale of about 10 meV, which is smaller than the expected accuracy of the employed theories. Figure 7.5 shows the convergence of the CCSD(T) formation energies of all

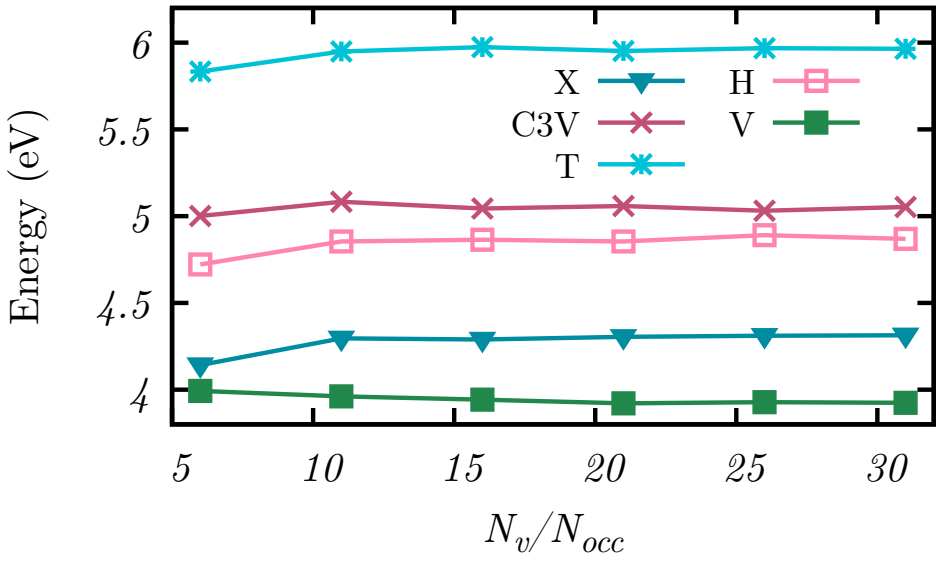

FIGURE 7.5: CCSD(T) formation energies as a function of the number of virtual orbitals per occupied orbital for all self-interstitials include finite size and basis set corrections.

self-interstitials with respect to the number of natural orbitals, including the finite size and basis set corrections. Note that the basis set correction behaves similarly for all self-interstitials. From figure 7.5, we see that $N_\mathrm{v}/N_\mathrm{occ} = 10$ is already accurate enough to assume convergence within chemical accuracy (≈ 43 meV).

7.4.3 CCSD(T) Formation Energy Finite Size Correction

7.4.3.1 Twist Averaging

With $N_\mathrm{v}/N_\mathrm{occ} = 10$, we repeat all calculations at 10 random k-points in order to obtain a twist-averaged estimate of the correlation energy contribution to the formation energies. This approach reduces finite size errors in CC calculations that originate from single-particle effects [58]. The energy corrections for the twist averaging can be found in the appendix D, in tables D.2-D.7. Using 10 random k-points our standard deviation from the average CCSD(T) energy is in decreasing order for $E_\mathrm{F}(\mathrm{T}) = 227$ meV, $E_\mathrm{F}(\mathrm{V}) =$

TABLE 7.1: CCSD and CCSD(T) formation energies of the silicon self-interstitials and the vacancy with and without the basis set and finite size correction as a function of the unoccupied to occupied orbital ratio N_v/N_{occ} at the Γ-point. FPC and FS denote that the basis set/finite size corrections are included.

HF/MP2	N_v/N_{occ}	CCSD	CCSD(T)	CCSD-FS	CCSD-FPC	CCSD-FS-FPC	CCSD(T)-FS-FPC
C3V	5	6.659	5.981	6.149	6.334	5.824	5.001
8.502	10	6.484	5.753	6.012	6.343	5.871	5.083
4.408	15	6.374	5.614	5.907	6.305	5.837	5.044
	20	6.347	5.577	5.880	6.317	5.850	5.059
	25	6.330	5.556	5.864	6.288	5.822	5.031
	30	6.315	5.537	5.849	6.308	5.843	5.053
X	5	5.864	5.094	5.285	5.646	5.067	4.142
7.930	10	5.776	4.982	5.254	5.670	5.148	4.296
3.780	15	5.686	4.866	5.169	5.657	5.141	4.289
	20	5.677	4.853	5.162	5.666	5.150	4.305
	25	5.669	4.842	5.155	5.666	5.152	4.311
	30	5.663	4.831	5.150	5.671	5.158	4.313
T	5	7.857	7.051	7.238	7.435	6.816	5.833
9.954	10	7.628	6.764	7.055	7.455	6.882	5.949
5.355	15	7.531	6.641	6.964	7.469	6.902	5.974
	20	7.511	6.611	6.944	7.447	6.880	5.952
	25	7.489	6.584	6.923	7.458	6.892	5.968
	30	7.476	6.565	6.910	7.456	6.890	5.964
H	5	6.358	5.717	5.877	5.986	5.504	4.722
8.162	10	6.231	5.538	5.783	6.053	5.605	4.854
4.212	15	6.132	5.413	5.689	6.058	5.615	4.864
	20	6.103	5.376	5.661	6.046	5.604	4.854
	25	6.090	5.360	5.649	6.075	5.635	4.890
	30	6.075	5.341	5.634	6.056	5.616	4.869
V	5	5.291	4.866	4.820	4.999	4.528	3.993
5.554	10	5.034	4.546	4.573	4.952	4.492	3.961
4.305	15	4.960	4.443	4.500	4.942	4.483	3.942
	20	4.942	4.413	4.484	4.925	4.467	3.921
	25	4.926	4.394	4.470	4.928	4.472	3.928
	30	4.919	4.380	4.462	4.928	4.472	3.924

101 meV, $E_F(X) = 80$ meV, $E_F(C3V) = 73$ meV and $E_F(H) = 51$ meV. After twist averaging, the formation energy of V, T and X increases by 818 meV, 367 meV and 239 meV. While the formation energy of the C3V and H interstitial decreases by 85 meV and 44 meV, indicating that it is important to account for this contribution.

The Γ-point formation energies are shown in Table 7.1, while the twist-averaged formation energies are shown in Table 7.2 for X, H, and T and in Tables D.7 and D.3 in the appendix D for V and C3V. Further, we calculate the formation energies at the DFT level of theory, utilizing the Heyd-Scuseria-Ernzerhof (HSE) exchange correlation functional again in Table 7.2. The HF energies, CCSD, CCSD(T), and finite-size and basis set energy corrections can be found in Table D.1 in the appendix D.

TABLE 7.2: Computed and converged HF, CCSD, CCSD(T) and HSE formation energies including all reported corrections in this work compared to QMC [197], RPA [198], PBE [198], LDA [179, 182] and G_0W_0 [179] from the literature and also experimental data [196, 212–215]. All results have been obtained for the 16/17 atom cells except RPA(216), which employed 216/217 atom cells.

Cell	HF	CCSD	CCSD(T)	QMC	QMC (nobf)	G_0W_0	RPA	RPA (216)	HSE	PBE	LDA	Exp.
X	7.930	5.295	4.535	4.4	4.9	4.46	4.27	4.17	4.46	3.56	3.29	
T	9.954	7.127	6.316	5.1	5.2		4.53	4.44	4.92	3.66	3.56	
H	8.162	5.559	4.810	4.7	4.9	4.4	4.45	4.37	4.82	3.74	3.4	4.2 - 4.7

7.4.3.2 FSIE Correction

Next, we briefly discuss the effect of the FSIE correction based on the structure factor interpolation, which accounts for two-electron finite size errors. Table 7.1 summarizes the computed CCSD formation energies with and without the corresponding finite size correction denoted as CCSD-FS and CCSD, respectively. It is not surprising that this correction is significant and on the scale of about 0.5 eV. However, based on previous results reported in Ref. [58] we expect that the employed finite size correction will suffice for the 16/17 atom cells to achieve chemical accuracy in the convergence of the computed formation energies with respect to the employed system size. Furthermore, it can be concluded from the comparison between CCSD-FS and CCSD in table 7.1, that the computed finite size correction is already well converged using $N_\mathrm{v}/N_\mathrm{occ} = 10$. Note that the finite size correction can currently only be applied to the CCSD calculation. The (T) contribution to the formation energies is significantly smaller than the CCSD correlation energy contribution, which makes it plausible to neglect the finite size correction to the (T) contribution.

7.5 Comparison to Other Methods and Discussion

Table 7.1 also includes results for the vacancy formation energy. We note that these calculations employ a 15-atom cell only. Due to the small supercell size, the system does not undergo a Jahn-Teller distortion [217], which can be observed for larger cells and which significantly changes the formation energy. Therefore, we note that these results are only meaningful as benchmarks for other theories employing identical geometries and can not be compared to experiment. Our best estimates of the formation energies at the level of HF, CCSD and CCSD(T) theory including all corrections discussed above are compared to values from the literature and experiment in table 7.2. We see that the formation energies calculated with LDA and PBE are small (3–4 eV) and close to each other for all self-interstitials, with a difference of $80 - 160$ meV. Yet the order of stability is not the same; for LDA the most stable self-interstitial is X then H and T.

For PBE T has a lower energy than H. Incorporating a portion of the exact exchange correlation energy in the HSE functional increases the formation energies, and their difference to 360 meV and 100 meV, with the order of stability of X, H and T. RPA predicts the same order of stability with a difference between X and H of 180 meV, while the difference between H and T is 80 meV. Increasing the cell size to 216 atoms changes the differences significantly to 130 meV and 600 meV, still with the same order of stability. G_0W_0 for 16 atom cells predicts that H is more stable than X while their difference is only 60 meV. In QMC, using 16 atom cells without a backflow correction, X and H are nearly degenerate, while the difference to T is 300 meV. Including the backflow correction gives the order of stability as X, H and T with clear differences of 300 meV and 400 meV. We now turn to the wavefunction methods employed in this work. The formation energies calculated with HF are much larger than the ones calculated with the other theories presented. While the order of stability is in agreement with the corrected QMC calculations, their difference is 232 meV and 1792 meV. Expanding the correlation space further to CCSD and CCSD(T) theory, including the basis set and finite size correction, lowers the formation energies by 2.8–2.6 eV and another 811–749 meV. Their relative difference also changes to 264 meV and 1568 meV for CCSD theory and 275 meV and 1506 meV for CCSD(T) theory. Our estimated CCSD(T) formation energies are in good agreement with extrapolated QMC calculations [197] employing a Slater-Jastrow-backflow correction for the X and H interstitial. However, we have a discrepancy of 1.2 eV for the T interstitial. This could stem from the fact that in DFT the energetically highest occupied orbitals are threefold degenerate while being occupied by two electrons. It may be an indication that a multireference treatment is needed. Our CCSD(T) formation energy for the H interstitial is within reasonable agreement with experiment, being 110 meV above the experimental upper bound.

7.6 Conclusion and Summary

We have calculated the formation energies of the silicon self-interstitials and the vacancy in a periodic supercell at the CCSD(T) level of theory. We have used correction schemes tailored to CC theory to reduce the BSIE and the FSIE. Our results have been compared to data from the literature and experiment, including LDA, PBE, HSE, RPA, G_0W_0 and QMC.

In general, DFT using the LDA and PBE functionals fails to differentiate the structures, resulting in small energy differences between the self-interstitials while also underestimating the formation energies. Additionally, HF overestimates the formation energies. The HSE functional offers a compromise, and its formation energies are in

good agreement with the much more expensive and accurate QMC calculations. The QMC formation energies of the two most stable self-interstitials, X and H, are nearly degenerate. This degeneracy is lifted by employing the Slater-Jastrow-backflow trial wavefunction [197].

Our CCSD(T) formation energies are in good agreement with QMC calculations employing a Slater-Jastrow-backflow wavefunction for the X and H interstitials. The CCSD(T) formation energy for the H interstitial is within reasonable agreement with experimental data, being 110 meV above the upper bound. However, the CCSD(T) formation energy of the T interstitial is 1.2 eV higher than in the QMC calculations. Since in DFT the highest occupied orbital of the T interstitial is threefold degenerate but only occupied by two electrons, we suppose a multireference approach may be necessary. We stress that none of the discussed methods is expected to work for strongly correlated systems. DFT based approaches underestimate the formation energy of strongly correlated defects due to the introduction of partly filled orbitals that reduce the self-interaction error. QMC techniques require multideterminant trial wavefunctions for strongly correlated systems to reduce the error from the fixed-node approximations, and RPA is expected to inherit part of the DFT errors for the treatment of strongly correlated systems. Therefore, we have to conclude that more sophisticated theories will be needed in future studies to fully resolve the observed discrepancy for the formation energy of the T interstitial.

Although we demonstrated that basis set convergence can be achieved efficiently at the level of CCSD(T) theory using recently presented methods, the treatment of finite size errors is still challenging and relatively large defect concentrations had to be employed. However, we note that recently developed embedding methods will allow to investigate much lower defect concentrations in a computationally efficient manner [221].

Chapter 8

Conclusion and Summary

Zero-dimensional systems and the modeling of their physical properties are a very broad field of research on their own. In order to achieve an accurate description of their electronic structure, it is often necessary to go beyond DFT. The main goal of this thesis is to model specifically the excited states of the two dimensional parabolic quantum dot and the self-interstitial point defects in silicon. This has been done by applying one of the most accurate ab initio many-body methods available, coupled cluster theory. Specifically for the silicon interstitials, we use CC theory utilizing a plane wave basis set within the PAW framework. In this work, we aim at both applying CC theory to model the QD and the silicon interstitials as well as evaluating the performance and applicability of CC theory itself as well as providing benchmark results.

In the first part of the thesis, an introduction is given (chapter 1), followed by an incremental history of the key concepts of quantum mechanics, including the atomic many-body problem, wavefunction symmetry and relativistic considerations regarding the Schrödinger equation in chapter 2. In chapter 3 the attention is shifted towards the many-body problem in solids, presenting the crystal structure and Bloch's theorem, leading to the Born-Oppenheimer approximation and the many-body electronic structure Hamiltonian. In chapter 4 the most popular ab initio many-body methods used to approximate solutions to the many-body electronic structure Hamiltonian are presented and discussed, with an emphasis on density functional theory, coupled cluster theory and quantum Monte Carlo theory, followed by a discussion of the calculations of excited states. In chapter 5 the programs VASP and cc4s, which have been extensively used in this thesis, are presented, including details on their algorithms.

In the second part of the thesis, the two dimensional parabolic quantum dot and the self-interstitial point defects in silicon are presented. In chapter 6 the QD is presented,

including its practical applications and a thorough historic perspective on the experimental and theoretical developments regarding the QD. The harmonic oscillator, which is used to model the QD, is presented, followed by the presentation of a semi-analytic scheme to calculate the necessary Coulomb integrals. A basis set extrapolation based on the asymptotic behavior of the MP2 correlation energy is presented and discussed, leading to the CCSD ground state energy and the EE-EOM-CCSD excited state energies of the QD in different regimes of correlation with different numbers of electrons. The results are discussed and compared to values from the literature, with which we are in good agreement, showing that the QD model Hamiltonian is not only a suitable tool to describe experimental QDs but can also be used as an efficient and well-controlled testing ground for many-body methods. In chapter 7 the self-interstitial point defects in silicon are presented, highlighting the importance of silicon self-diffusion, including a history of the experimental and theoretical developments regarding silicon self-diffusion and silicon self-interstitial formation energies. The cell structures used for the periodic supercell calculation are presented, followed by a description of the workflow used to get the best estimates for the BSIE and FSIE corrected CCSD(T) formation energies. Our results are compared to a wide array of other many-body methods from the literature, including QMC, DFT and experimental data. The results are in good agreement with backflow-corrected QMC calculations; however, there is a significant deviation between the CCSD(T) and QMC formation energies of 1.2eV, for the tetrahedral interstitial, which is discussed and attributed to a possible multi-reference character, but ultimately remains unresolved.

This thesis has demonstrated that periodic CC calculations can be applied to calculate the properties of solids and zero-dimensional structures embedded in solids at the level of CCSD(T) theory, which will help to extend the scope and further the improvement of computationally more efficient yet less accurate methods by providing a more accurate benchmark result.

Appendix A

Slater-Condon Rules

In wavefunction based theories, one needs to calculate the matrix elements of the Hamiltonian projected onto arbitrary excited Slater determinants

$$\mathcal{H}_{IJ} = \langle \Phi_I | \hat{\mathcal{H}} | \Phi_J \rangle. \tag{A.1}$$

The Slater-Condon rules allow the calculation of these matrix elements for any pair of orthonormal Slater determinants Φ_I and Φ_J. Assuming the usuall HF reference determinant Φ, one can describe the matrix elements of the hamiltonian projected onto all other determinants simply by their difference in spin-orbitals.

The Hamiltonian can be split into one-body and two-body parts

$$\begin{aligned} \hat{\mathcal{H}} =& \hat{H}_1 + \hat{H}_2 \ , \\ \hat{H}_1 =& \sum_{i}^{\text{occ.}} \hat{h}(i) \ , \\ \hat{H}_2 =& \sum_{i \neq j}^{\text{occ.}} \frac{1}{r_{ij}} \ . \end{aligned} \tag{A.2}$$

The Slater-Condon rules for the one-body part $\hat{H}_1$ are

$$\begin{aligned} \langle \Phi | \hat{H}_1 | \Phi \rangle =& \sum_{i}^{\text{occ.}} \langle \psi_i | \hat{h} | \psi_i \rangle \ , \\ \langle \Phi_i^a | \hat{H}_1 | \Phi \rangle =& \langle \psi_a | \hat{h} | \psi_i \rangle \ , \\ \langle \Phi_{ij}^{ab} | \hat{H}_1 | \Phi \rangle =& 0 \qquad \text{(A.3)} \\ \langle \Phi_{ijk}^{abc} | \hat{H}_1 | \Phi \rangle =& 0 \qquad \text{(A.4)} \\ & \vdots \end{aligned}$$

The matrix elements of the two-body part $\hat{H}_2$ are

$$\begin{aligned}
\langle\Phi|\hat{H}_2|\Phi\rangle &= \frac{1}{2}\sum_{ij}^{\text{occ.}} \left[\langle\psi_i\psi_j|\frac{1}{r_{12}}|\psi_i\psi_j\rangle - \langle\psi_i\psi_j|\frac{1}{r_{12}}|\psi_j\psi_i\rangle\right] , \\
\langle\Phi_i^a|\hat{H}_2|\Phi\rangle &= \sum_{j}^{\text{occ.}} \left[\langle\psi_a\psi_j|\frac{1}{r_{12}}|\psi_i\psi_j\rangle - \langle\psi_a\psi_j|\frac{1}{r_{12}}|\psi_j\psi_i\rangle\right] , \\
\langle\Phi_{ij}^{ab}|\hat{H}_2|\Phi\rangle &= \langle\psi_a\psi_b|\frac{1}{r_{12}}|\psi_i\psi_j\rangle - \langle\psi_a\psi_b|\frac{1}{r_{12}}|\psi_j\psi_i\rangle , \\
\langle\Phi_{ijk}^{abc}|\hat{H}_2|\Phi\rangle &= 0 , \qquad \text{(A.5)} \\
\langle\Phi_{ijkl}^{abcd}|\hat{H}_2|\Phi\rangle &= 0 , \qquad \text{(A.6)} \\
&\vdots
\end{aligned}$$

Appendix B

Rayleigh–Schrödinger Perturbation Theory

In Rayleigh-Schrödinger perturbation theory we are looking for the solutions of the time-independent Schrödinger equation

$$\hat{\mathcal{H}}\Psi_n = E_n\Psi_n \ , \tag{B.1}$$

The main idea is to split the Hamiltonian into two parts

$$\hat{\mathcal{H}} = \hat{\mathcal{H}}_0 + \lambda\hat{\mathcal{V}} \ , \tag{B.2}$$

where $\hat{\mathcal{H}}_0$ is the uperturbed Hamiltonian and $\hat{\mathcal{V}}$ is the perturbation. λ is a scalar parameter that later will be set to one. The ground-state wavefunction Ψ and energy E are now expanded as a Taylor series of λ

$$\Psi(\lambda) = \Psi^{(0)} + \lambda\Psi^{(1)} + \lambda^2\Psi^{(2)} + \dots \ , \tag{B.3}$$

$$E(\lambda) = E^{(0)} + \lambda E^{(1)} + \lambda^2 E^{(2)} + \dots \ , \tag{B.4}$$

with

$$\begin{aligned} \Psi^{(k)} &= \frac{1}{k!}\left(\frac{\partial^k\Psi}{\partial\lambda^k}\right)_{\lambda=0} \ , \\ E^{(k)} &= \frac{1}{k!}\left(\frac{\partial^k E}{\partial\lambda^k}\right)_{\lambda=0} \ . \end{aligned} \tag{B.5}$$

If we use the Taylor expansion of the wavefunction and energy in the time idependent Schrödinger equation and equate the coefficients of same powers of λ we arrive at a

hierarchy of equations

$$\left[\hat{\mathcal{H}}_0 - E^{(0)}\right]|\Psi^{(0)}\rangle = 0 \tag{B.6}$$
$$\left[\hat{\mathcal{H}}_0 - E^{(0)}\right]|\Psi^{(1)}\rangle + \left[\hat{\mathcal{V}} - E^{(1)}\right]|\Psi^{(0)}\rangle = 0 \tag{B.7}$$
$$\left[\hat{\mathcal{H}}_0 - E^{(0)}\right]|\Psi^{(2)}\rangle + \left[\hat{\mathcal{V}} - E^{(1)}\right]|\Psi^{(1)}\rangle - E^{(2)}|\Psi^{(0)}\rangle = 0 \tag{B.8}$$
$$\vdots$$

Multiplying each equation from the left with $\langle\Psi^{(0)}|$ and using the orthogonality $\langle\Psi^{(0)}|\Psi^{(k)}\rangle = \delta_{k0}$, yields the following equations for the energies

$$E^{(0)} = \langle\Psi^{(0)}|\hat{\mathcal{H}}|\Psi^{(0)}\rangle \tag{B.9}$$
$$E^{(1)} = \langle\Psi^{(0)}|\hat{\mathcal{V}}|\Psi^{(0)}\rangle \tag{B.10}$$
$$E^{(2)} = \langle\Psi^{(0)}|\hat{\mathcal{V}}|\Psi^{(1)}\rangle \tag{B.11}$$
$$\vdots$$

In order on to determine the second order correction to the energy $E^{(2)}$, one has to determine the first order correction to the wavefunction $\Psi^{(1)}$. Assuming we have an orthonormal set of solutions $\Psi_n^{(0)}$ for the zeroth order Hamiltonian $\hat{\mathcal{H}}_0$, one can represent the first order wavefunction in terms of $\Psi_n^{(0)}$

$$\Psi^{(1)} = \sum_m C_m^{(1)}\Psi_m^{(0)} \ , \tag{B.12}$$

The coefficients $C_l^{(1)}$ can be obtained by inserting equation B.12 into equation B.7 and multiplying with $\langle\Psi_l^{(0)}|$ from the left,

$$\sum_m C_m^{(1)}\langle\Psi_l^{(0)}|\hat{\mathcal{H}}_0 - E^{(0)}|\Psi_m^{(0)}\rangle + \sum_m C_m^{(1)}\langle\Psi_l^{(0)}|\hat{\mathcal{V}} - E^{(1)}|\Psi^{(0)}\rangle = 0 \ , \tag{B.13}$$

and therefore

$$C_l^{(1)} = \frac{\langle\Psi_l^{(0)}|\hat{\mathcal{V}}|\Psi^{(0)}\rangle}{E^{(0)} - E_l^{(0)}} \ . \tag{B.14}$$

Appendix C

Singlet Triplet Gap Calculation

In order to calculate the singlet and triplet ground state energy of the 2 electron QD with HF and MP2 theory the following Slater determinants have been used:

$$|\Psi_{\text{singlet}}\rangle = |(00,\uparrow)(00,\downarrow)\rangle$$
$$|\Psi_{\text{triplet}}\rangle = |(00,\uparrow)(01,\uparrow)\rangle\,.$$

The HF ground state energy for the 2 electron QD is given by

$$E_{\text{HF}} = \langle\Psi_{\text{gs}}|\,\hat{H}\,|\Psi_{\text{gs}}\rangle + \langle\Psi_{\text{gs}}|\,\hat{V}\,|\Psi_{\text{gs}}\rangle$$

where $\hat{H}$ is the single-body part of the Hamiltonian and $\hat{V}$ is the Coulomb repulsion between the electrons. Inserting the ansatz for the wavefunctions of singlet and triplet states and applying the Slater-Condon rules gives

$$E_{\text{s}} = \omega + \langle 0000|0000\rangle$$
$$E_{\text{t}} = 2\omega + \langle 0001|0001\rangle - \langle 0000|0101\rangle\,.$$

The MP2 ground state energy is

$$E_{\text{MP2}} = E^{(0)} + E^{(1)} + E^{(2)}$$
$$E^{(0)} = \langle\Psi_{\text{gs}}|\,\hat{H}\,|\Psi_{\text{gs}}\rangle$$
$$E^{(1)} = \langle\Psi_{\text{gs}}|\,\hat{V}\,|\Psi_{\text{gs}}\rangle$$
$$E^{(2)} = \sum_{k\neq\Psi_{\text{gs}}} \frac{|\,\langle k|\,\hat{V}\,|\Psi_{\text{gs}}\rangle\,|^2}{E_{\text{k}} - E_{\text{gs}}}.$$

Applying the Slater-Condon rules and using the same singlet and triplet wavefunctions as for HF yields a additional contribution to the HF energy

$$E_{\mathrm{MP2,s}} = E_{\mathrm{s}} + \sum_{\mathrm{abcd}} \frac{|\langle 0000|abcd\rangle - \langle 00ab|00cd\rangle|^2}{\omega(-a-b-c-d)}$$

$$E_{\mathrm{MP2,t}} = E_{\mathrm{t}} + \sum_{\mathrm{abcd}} \frac{|\langle 0001|abcd\rangle - \langle 00ab|01cd\rangle|^2}{\omega(1-a-b-c-d)}$$

Appendix D

Silicon Interstitials: Raw Data

D.1 Γ-point Calculations and Basis Set Convergence

Table D.1 shows the CCSD and CCSD(T) energy corrections to the HF ground state energies, as well as the basis set and the finite size correction. The HF energy was calculated using a Γ-centered 7×7×7 k-point mesh. All the other corrections were calculated at the Γ-point.

TABLE D.1: HF formation energies of all calculated structures, as well as the CCSD, CCSD(T), finite size and basis set corrections. All energies are in eV.

HF	N_v/N_{occ}	CCSD	CCSD(T)	FS	BS
Bulk	5	-43.4765	-2.3715	-3.7478	-9.7135
-151.920	10	-49.9044	-3.4427	-3.8412	-4.0339
	15	-51.6199	-3.7680	-3.8593	-2.4171
	20	-52.3780	-3.9174	-3.8633	-1.6891
	25	-52.8151	-4.0039	-3.8653	-1.2599
	30	-53.0515	-4.0461	-3.8654	-1.0200
C3V	5	-48.0369	-3.1975	-4.4917	-10.6451
-152.9134	10	-55.0409	-4.3890	-4.5530	-4.4268
	15	-56.9736	-4.7637	-4.5677	-2.6377
	20	-57.8062	-4.9321	-4.5715	-1.8250
	25	-58.2881	-5.0274	-4.5724	-1.3807
	30	-58.5542	-5.0770	-4.5723	-1.0903
X	5	-48.2597	-3.2894	-4.5609	-10.5387
-153.4851	10	-55.1774	-4.4519	-4.6033	-4.3915
	15	-57.0905	-4.8230	-4.6169	-2.5965
	20	-57.9043	-4.9867	-4.6201	-1.8062
	25	-58.3773	-5.0805	-4.6210	-1.3409
	30	-58.6339	-5.1316	-4.6207	-1.0757
T	5	-48.2917	-3.3253	-4.6008	-10.7425
-151.4606	10	-55.3498	-4.5223	-4.6540	-4.4593
	15	-57.2692	-4.8940	-4.6676	-2.6304
	20	-58.0948	-5.0627	-4.6716	-1.8590
	25	-58.5816	-5.1593	-4.6727	-1.3693
	30	-58.8459	-5.2094	-4.6727	-1.1039
H	5	-47.9977	-3.1610	-4.4635	-10.6933
-153.2528	10	-54.9550	-4.3508	-4.5291	-4.4641
	15	-56.8764	-4.7222	-4.5437	-2.6421
	20	-57.7108	-4.8892	-4.5467	-1.8522
	25	-58.1881	-4.9839	-4.5476	-1.3534
	30	-58.4548	-5.0331	-4.5472	-1.1027
V	5	-41.0219	-2.6484	-3.9846	-9.3988
-136.8709	10	-47.3057	-3.7151	-4.0613	-3.8637
	15	-48.9880	-4.0494	-4.0775	-2.2835
	20	-49.7164	-4.2020	-4.0798	-1.6001
	25	-50.1419	-4.2861	-4.0802	-1.1794
	30	-50.3710	-4.3320	-4.0803	-0.9470

D.2 Random k-point Calculations

Tables D.2-D.7 show the CCSD and CCSD(T) energy corrections to the HF ground state energies, as well as the basis set and the finite size correction for 10 random k-points using 10 virtual orbitals per occupied orbital.

TABLE D.2: Twist averaged results for the bulk. All energies are in eV.

HF	CCSD	CCSD(T)	FS	BS
Bulk	-49.8167	-3.7600	-4.2053	-4.0146
-151.920	-49.7882	-3.6116	-4.0349	-4.0027
	-49.7887	-3.6936	-4.1435	-4.0076
	-49.7851	-3.6124	-4.0151	-4.0076
	-49.7881	-3.6590	-4.1462	-4.0077
	-49.8101	-3.7460	-4.1749	-4.0190
	-49.7918	-3.6290	-4.0086	-4.0090
	-49.8083	-3.7545	-4.2244	-4.0303
	-49.8207	-3.7633	-4.1717	-4.0173
	-49.7976	-3.7073	-4.1158	-4.0102
Average	-49.7995	-3.6937	-4.1240	-4.0126
Formation	Energy	0		

TABLE D.3: Twist averaged results for the C3V interstitial. All energies are in eV.

HF	CCSD	CCSD(T)	FS	BS
C3V	-55.0793	-4.6865	-4.8126	-4.3949
-152.9134	-55.0242	-4.5504	-4.6772	-4.3986
	-55.1168	-4.6773	-4.8237	-4.3960
	-55.0566	-4.5760	-4.6621	-4.3849
	-55.0991	-4.6385	-4.8578	-4.3967
	-55.1570	-4.7165	-4.7976	-4.3899
	-55.0867	-4.6046	-4.6337	-4.3900
	-55.1814	-4.7321	-4.9133	-4.3893
	-55.1799	-4.7372	-4.7677	-4.3942
	-55.1135	-4.6757	-4.7427	-4.3928
Average	-55.1094	-4.65948	-4.76885	-4.39272
Formation	Energy	4.998		

TABLE D.4: Twist averaged results for the X interstitial. All energies are in eV.

HF	CCSD	CCSD(T)	FS	BS
X	-55.0427	-4.6651	-4.8119	-4.3681
-153.4851	-55.1184	-4.5860	-4.7078	-4.3438
	-55.0224	-4.6324	-4.7803	-4.3883
	-55.0596	-4.5699	-4.6657	-4.3641
	-55.0501	-4.6117	-4.8226	-4.3873
	-55.0537	-4.6725	-4.8059	-4.3848
	-55.0422	-4.5854	-4.6454	-4.3788
	-55.0168	-4.6710	-4.9005	-4.4082
	-55.0689	-4.6791	-4.7565	-4.3684
	-55.0544	-4.6451	-4.7333	-4.3727
Average	-55.0530	-4.63182	-4.76299	-4.37646
Formation	Energy	4.535		

TABLE D.5: Twist averaged results for the T interstitial. All energies are in eV.

HF	CCSD	CCSD(T)	FS	BS
T	-55.2699	-4.7589	-4.8835	-4.3863
-151.4606	-55.2986	-4.6747	-4.7801	-4.3943
	-55.3547	-4.7756	-4.8900	-4.3931
	-55.2511	-4.6547	-4.7454	-4.4002
	-55.1553	-4.6366	-4.8288	-4.3856
	-55.2156	-4.7206	-4.8375	-4.3851
	-55.0346	-4.5578	-4.6527	-4.4022
	-55.0616	-4.6681	-4.8444	-4.4209
	-55.1094	-4.6811	-4.7886	-4.3854
	-55.1468	-4.6625	-4.7681	-4.3789
Average	-55.1897	-4.67906	-4.80191	-4.39320
Formation	Energy	6.316		

TABLE D.6: Twist averaged results for the H interstitial .All energies are in eV.

HF	CCSD	CCSD(T)	FS	BS
H	-55.0364	-4.6706	-4.7986	-4.3909
-153.2528	-54.9589	-4.5200	-4.6609	-4.3890
	-55.0356	-4.6364	-4.7915	-4.3832
	-54.9648	-4.5345	-4.6405	-4.3797
	-55.0054	-4.5977	-4.8300	-4.3916
	-55.0608	-4.6697	-4.7742	-4.3860
	-54.9979	-4.5684	-4.6153	-4.3882
	-55.0974	-4.6879	-4.8865	-4.3808
	-55.0909	-4.6923	-4.7437	-4.3858
	-55.0385	-4.6379	-4.7173	-4.3803
Average	-55.0287	-4.62153	-4.74585	-4.38555
Formation	Energy	4.810		

TABLE D.7: Twist averaged results for the vacancy. All energies are in eV.

HF	CCSD	CCSD(T)	FS	BS
V	-46.8932	-3.7864	-4.1677	-3.8147
-136.8709	-46.9264	-3.7007	-4.0489	-3.8173
	-46.9694	-3.7560	-4.1327	-3.7825
	-46.8965	-3.6820	-4.0553	-3.8076
	-46.8375	-3.6923	-4.0976	-3.8153
	-46.8939	-3.7783	-4.1499	-3.8024
	-46.8376	-3.6612	-4.0657	-3.8129
	-46.7661	-3.7462	-4.1541	-3.8628
	-46.8131	-3.7611	-4.1651	-3.8299
	-46.8483	-3.7296	-4.1263	-3.8017
Average	-46.8682	-3.72940	-4.11633	-3.81470
Formation	Energy	4.779		

Bibliography

[1] E. Schrödinger, Phys. Rev. **28**, 1049 (1926).

[2] W. Pauli, Zeitschrift für Physik **31**, 765 (1925).

[3] P. A. M. Dirac and R. H. Fowler, Proceedings of the Royal Society of London. Series A, Containing Papers of a Mathematical and Physical Character **117**, 610 (1928).

[4] W. Demtröder, *Experimentalphysik 3 - Atome, Moleküle und Festkörper* (Springer-Verlag, Berlin Heidelberg New York, 2016).

[5] A. Borrelli, "Spin statistics theorem," in *Compendium of Quantum Physics*, edited by D. Greenberger, K. Hentschel, and F. Weinert (Springer Berlin Heidelberg, Berlin, Heidelberg, 2009) pp. 733–736.

[6] M. Born and R. Oppenheimer, Annalen der Physik **389**, 457 (1927).

[7] S. McArdle, S. Endo, A. Aspuru-Guzik, S. C. Benjamin, and X. Yuan, Rev. Mod. Phys. **92**, 015003 (2020).

[8] W. Kohn, Rev. Mod. Phys. **71**, 1253 (1999).

[9] P. Hohenberg and W. Kohn, Phys. Rev. **136**, B864 (1964).

[10] E. Runge and E. K. U. Gross, Phys. Rev. Lett. **52**, 997 (1984).

[11] W. Kohn and L. J. Sham, Phys. Rev. **140**, A1133 (1965).

[12] J. P. Perdew and K. Schmidt, AIP Conference Proceedings **577**, 1 (2001).

[13] V. E. Van Doren and P. Van Alsenoy, C.and Geerlings, *Density functional theory and its application to materials* (American Institute of Physics Melville, N.Y., Melville, N.Y., 2001).

[14] D. M. Ceperley and B. J. Alder, Phys. Rev. Lett. **45**, 566 (1980).

[15] J. Alonso and N. Cordero, in *Recent Developments and Applications of Modern Density Functional Theory*, Theoretical and Computational Chemistry, Vol. 4, edited by J. Seminario (Elsevier, 1996) pp. 239–294.

[16] J. P. Perdew, K. Burke, and M. Ernzerhof, Phys. Rev. Lett. **77**, 3865 (1996).

[17] T. Van Voorhis and G. E. Scuseria, The Journal of Chemical Physics **109**, 400 (1998).

[18] A. D. Becke, The Journal of Chemical Physics **98**, 5648 (1993).

[19] U. von Barth and L. Hedin, Journal of Physics C: Solid State Physics **5**, 1629 (1972).

[20] O. Gunnarsson and B. I. Lundqvist, Phys. Rev. B **13**, 4274 (1976).

[21] S. Grimme and F. Neese, The Journal of Chemical Physics **127**, 154116 (2007).

[22] D. R. Hartree, Mathematical Proceedings of the Cambridge Philosophical Society **24**, 89–110 (1928).

[23] V. Fock, Zeitschrift für Physik **61**, 126 (1930).

[24] J. C. Slater, Phys. Rev. **35**, 210 (1930).

[25] A. Szabó and N. Ostlund, *Modern Quantum Chemistry: Introduction to Advanced Electronic Structure Theory* (Dover Publications, New York, 1996).

[26] B. Nagy and F. Jensen, "Basis sets in quantum chemistry," in *Reviews in Computational Chemistry* (John Wiley and Sons, Ltd, 2017) Chap. 3, pp. 93–149.

[27] G. Kresse and D. Joubert, Phys. Rev. B **59**, 1758 (1999).

[28] T. Kato, Communications on Pure and Applied Mathematics **10**, 151 (1957).

[29] D. P. Tew, W. Klopper, and T. Helgaker, Journal of Computational Chemistry **28**, 1307 (2007).

[30] C. Hättig, W. Klopper, A. Köhn, and D. P. Tew, Chemical Reviews **112**, 4 (2012).

[31] E. Schrödinger, Annalen der Physik **385**, 437 (1926).

[32] C. Møller and M. S. Plesset, Phys. Rev. **46**, 618 (1934).

[33] R. J. Bartlett and M. Musiał, Rev. Mod. Phys. **79**, 291 (2007).

[34] P. Pulay, Chemical Physics Letters **73**, 393 (1980).

[35] S. Hirata, I. Grabowski, M. Tobita, and R. J. Bartlett, Chemical Physics Letters **345**, 475 (2001).

[36] K. Raghavachari, The Journal of Chemical Physics **82**, 4607 (1985), https://pubs.aip.org/aip/jcp/article-pdf/82/10/4607/11258402/4607_1_online.pdf .

[37] K. Raghavachari, G. W. Trucks, J. A. Pople, and M. Head-Gordon, Chemical Physics Letters **157**, 479 (1989).

[38] M. Urban, J. Noga, S. J. Cole, and R. J. Bartlett, The Journal of Chemical Physics **83**, 4041 (1985), https://pubs.aip.org/aip/jcp/article-pdf/83/8/4041/10986834/4041_1_online.pdf .

[39] G. E. Scuseria and T. J. Lee, The Journal of Chemical Physics **93**, 5851 (1990), https://pubs.aip.org/aip/jcp/article-pdf/93/8/5851/11208116/5851_1_online.pdf .

[40] A. G. Donchev, A. G. Taube, E. Decolvenaere, C. Hargus, R. T. McGibbon, K.-H. Law, B. A. Gregersen, J.-L. Li, K. Palmo, K. Siva, M. Bergdorf, J. L. Klepeis, and D. E. Shaw, Scientific Data **8**, 55 (2021).

[41] J. Řezáč and P. Hobza, Journal of Chemical Theory and Computation **9**, 2151 (2013), pMID: 26583708, https://doi.org/10.1021/ct400057w .

[42] M. Caffarel and R. Assaraf, "A pedagogical introduction to quantum monte-carlo," in *Mathematical Models and Methods for Ab Initio Quantum Chemistry* (Springer Berlin Heidelberg, Berlin, Heidelberg, 2000) pp. 45–73.

[43] M. Caffarel, "Quantum monte carlo," (2022).

[44] S. M. Rothstein, E. Ospadov, and C. Bruzzese, in *Mathematical Physics in Theoretical Chemistry*, Developments in Physical and Theoretical Chemistry, edited by S. Blinder and J. House (Elsevier, 2019) pp. 189–217.

[45] E. Y. Loh, J. E. Gubernatis, R. T. Scalettar, S. R. White, D. J. Scalapino, and R. L. Sugar, Phys. Rev. B **41**, 9301 (1990).

[46] M. Petersilka, U. J. Gossmann, and E. K. U. Gross, Phys. Rev. Lett. **76**, 1212 (1996).

[47] L. Hedin, Phys. Rev. **139**, A796 (1965).

[48] D. Golze, M. Dvorak, and P. Rinke, Frontiers in Chemistry **7** (2019), 10.3389/fchem.2019.00377.

[49] E. E. Salpeter and H. A. Bethe, Phys. Rev. **84**, 1232 (1951).

[50] S. R. White, Phys. Rev. Lett. **69**, 2863 (1992).

[51] J. F. Stanton and R. J. Bartlett, The Journal of Chemical Physics **98**, 7029 (1993).

[52] D. Rowe, Nuclear Physics **80**, 209 (1966).

[53] D. J. ROWE, Rev. Mod. Phys. **40**, 153 (1968).

[54] G. Kresse and J. Hafner, Phys. Rev. B **47**, 558 (1993).

[55] G. Kresse and J. Furthmüller, Phys. Rev. B **54**, 11169 (1996).

[56] G. Kresse and J. Furthmüller, Computational Materials Science **6**, 15 (1996).

[57] F. Hummel, T. Tsatsoulis, and A. Grüneis, The Journal of Chemical Physics **146**, 124105 (2017), https://pubs.aip.org/aip/jcp/article-pdf/doi/10.1063/1.4977994/15525179/124105_1_online.pdf .

[58] T. Gruber, K. Liao, T. Tsatsoulis, F. Hummel, and A. Grüneis, Phys. Rev. X **8**, 021043 (2018).

[59] A. Irmler, A. Gallo, and A. Grüneis, The Journal of Chemical Physics **154**, 234103 (2021).

[60] K. Liao and A. Grüneis, The Journal of Chemical Physics **145**, 141102 (2016).

[61] A. Grüneis, G. H. Booth, M. Marsman, J. Spencer, A. Alavi, and G. Kresse, Journal of Chemical Theory and Computation **7**, 2780 (2011), pMID: 26605469.

[62] A. Grüneis, Phys. Rev. Lett. **115**, 066402 (2015).

[63] A. Grüneis, J. J. Shepherd, A. Alavi, D. P. Tew, and G. H. Booth, The Journal of Chemical Physics **139**, 084112 (2013).

[64] D. Usvyat, The Journal of Chemical Physics **139**, 194101 (2013).

[65] F. Salihbegović, A. Gallo, and A. Grüneis, Phys. Rev. B **105**, 115111 (2022).

[66] D. Bimberg and U. W. Pohl, Materials Today **14**, 388 (2011).

[67] C.-Y. Han, H.-S. Kim, and H. Yang, Materials **13**, 897 (2020).

[68] S. Kargozar, S. J. Hoseini, P. B. Milan, S. Hooshmand, H.-W. Kim, and M. Mozafari, Biotechnology Journal **15**, 2000117 (2020).

[69] Y. Sajeev and N. Moiseyev, Physical Review B **78**, 075316 (2008).

[70] N. Ganguli, S. Acharya, and I. Dasgupta, Physical Review B **89**, 245423 (2014).

[71] G. Bester, S. Nair, and A. Zunger, Phys. Rev. B **67**, 161306 (2003).

[72] R. Singh and G. Bester, Phys. Rev. Lett. **103**, 063601 (2009).

[73] P. Walter, E. Welcomme, P. Hallégot, N. J. Zaluzec, C. Deeb, J. Castaing, P. Veyssière, R. Bréniaux, J.-L. Lévêque, and G. Tsoucaris, Nano Letters **6**, 2215 (2006).

[74] R. C. Ashoori, **379**, 413 (1996).

[75] A. Henglein, Chemical Reviews **89**, 1861 (1989).

[76] M. Sundaram, S. A. Chalmers, P. F. Hopkins, and A. C. Gossard, Science **254**, 1326 (1991).

[77] R. Cingolani and K. Ploog, Advances in Physics **40**, 535 (1991).

[78] A. P. Alivisatos, Science **271**, 933 (1996).

[79] N. F. Johnson, Journal of Physics Condensed Matter **7**, 965 (1995).

[80] C. Sloggett and O. P. Sushkov, Surface Science Wagga Symposium on Surfaces and Interfaces - 2006, **601**, 5788 (2007).

[81] S. Akbar and I.-H. Lee, Physical Review B **63**, 165301 (2001).

[82] F. Bolton, Physical Review Letters **73**, 158 (1994).

[83] P. A. Maksym and T. Chakraborty, Physical Review Letters **65**, 108 (1990).

[84] B. Partoens, A. Matulis, and F. M. Peeters, Physical Review B **59**, 1617 (1999).

[85] F. Holka, P. Neogrády, V. Kellö, M. Urban, and G. H. F. Diercksen, Molecular Physics **103**, 2747 (2005).

[86] N. M. Parzuchowski, T. D. Morris, and S. K. Bogner, Physical Review C **95**, 044304 (2017).

[87] L. P. Kouwenhoven, T. H. Oosterkamp, M. W. S. Danoesastro, M. Eto, D. G. Austing, T. Honda, and S. Tarucha, Science **278**, 1788 (1997).

[88] H. Yakobi, E. Eliav, and U. Kaldor, Journal of Chemical Physics **134**, 054503 (2011).

[89] C. Metzner and G. H. Döhler, Physical Review B **60**, 11005 (1999).

[90] M. Korkusinski and P. Hawrylak, Physical Review B **87**, 115310 (2013).

[91] B. Larade and A. M. Bratkovsky, Physical Review B **68**, 235305 (2003).

[92] V. Janiš and J. Yan, Physical Review B **103**, 235163 (2021).

[93] P. Xue, Physical Review A **81**, 052331 (2010).

[94] G.-P. Guo, H. Zhang, T. Tu, and G.-C. Guo, Physical Review A **75**, 050301 (2007).

[95] A. N. Al-Ahmadi, (2006), 10.1021/acsenergylett.6b00569.

[96] V. Moldoveanu and B. Tanatar, Physical Review B **77**, 195302 (2008).

[97] L. A. Agapito, N. Kioussis, and E. Kaxiras, Physical Review B **82**, 201411 (2010).

[98] S. Schröter, P.-A. Hervieux, G. Manfredi, J. Eiglsperger, and J. Madroñero, Physical Review B **87**, 155413 (2013).

[99] S. M. Reimann and M. Manninen, Rev. Mod. Phys. **74**, 1283 (2002).

[100] L.-W. Wang and A. Zunger, Phys. Rev. B **59**, 15806 (1999).

[101] G. Bester, Journal of Physics: Condensed Matter **21**, 023202 (2008).

[102] P. Matagne and J.-P. Leburton, Phys. Rev. B **65**, 155311 (2002).

[103] D. V. Melnikov, P. Matagne, J.-P. Leburton, D. G. Austing, G. Yu, S. Tarucha, J. Fettig, and N. Sobh, Phys. Rev. B **72**, 085331 (2005).

[104] M. Koskinen, M. Manninen, and S. M. Reimann, Phys. Rev. Lett. **79**, 1389 (1997).

[105] M. Macucci, K. Hess, and G. J. Iafrate, Phys. Rev. B **55**, R4879 (1997).

[106] M. Fujito, A. Natori, and H. Yasunaga, Phys. Rev. B **53**, 9952 (1996).

[107] S. Bednarek, B. Szafran, and J. Adamowski, Phys. Rev. B **59**, 13036 (1999).

[108] C. Yannouleas and U. Landman, Phys. Rev. Lett. **82**, 5325 (1999).

[109] U. De Giovannini, F. Cavaliere, R. Cenni, M. Sassetti, and B. Kramer, Phys. Rev. B **77**, 035325 (2008).

[110] B. Szafran, J. Adamowski, and S. Bednarek, Physica E: Low-dimensional Systems and Nanostructures **5**, 185 (1999).

[111] A. Emperador, E. Lipparini, and L. Serra, Physical Review B **73**, 235341 (2006).

[112] B. Reusch and H. Grabert, Physical Review B **68**, 045309 (2003).

[113] A. Puente, L. Serra, and V. Gudmundsson, Physical Review B **64**, 235324 (2001).

[114] R. M. Abolfath and P. Hawrylak, Journal of Chemical Physics **125**, 034707 (2006).

[115] Y. Nandan and M. S. Mehata, Scientific Reports **9**, 2 (2019).

[116] N. A. Bruce and P. A. Maksym, Phys. Rev. B **61**, 4718 (2000).

[117] B. Szafran, S. Bednarek, and J. Adamowski, Phys. Rev. B **67**, 115323 (2003).

[118] S. M. Reimann, M. Koskinen, and M. Manninen, Phys. Rev. B **62**, 8108 (2000).

[119] S. A. Mikhailov, Phys. Rev. B **65**, 115312 (2002).

[120] S. A. Mikhailov, Phys. Rev. B **66**, 153313 (2002).

[121] M. Rontani, C. Cavazzoni, D. Bellucci, and G. Goldoni, The Journal of Chemical Physics **124**, 124102 (2006).

[122] V. Popsueva, R. Nepstad, T. Birkeland, M. Førre, J. P. Hansen, E. Lindroth, and E. Waltersson, Phys. Rev. B **76**, 035303 (2007).

[123] E. Waltersson, E. Lindroth, I. Pilskog, and J. P. Hansen, Phys. Rev. B **79**, 115318 (2009).

[124] S. Kvaal, Phys. Rev. B **80**, 045321 (2009).

[125] L. Sælen, E. Waltersson, J. P. Hansen, and E. Lindroth, Phys. Rev. B **81**, 033303 (2010).

[126] S. A. Blundell and K. Joshi, Physical Review B **81**, 115323 (2010).

[127] T. Ezaki, N. Mori, and C. Hamaguchi, Physical Review B **56**, 6428 (1997).

[128] G. W. Bryant, Physical Review Letters **59**, 1140 (1987).

[129] A. Harju, V. A. Sverdlov, R. M. Nieminen, and V. Halonen, Physical Review B **59**, 5622 (1999).

[130] A. Brataas, U. Hanke, and K. A. Chao, Physical Review B **54**, 10736 (1996).

[131] H. Saarikoski and A. Harju, Phys. Rev. Lett. **94**, 246803 (2005).

[132] R. Egger, W. Häusler, C. H. Mak, and H. Grabert, Phys. Rev. Lett. **82**, 3320 (1999).

[133] R. Egger, W. Häusler, C. H. Mak, and H. Grabert, Phys. Rev. Lett. **83**, 462 (1999).

[134] F. Pederiva, C. J. Umrigar, and E. Lipparini, Phys. Rev. B **62**, 8120 (2000).

[135] A. J. Williamson, J. C. Grossman, R. Q. Hood, A. Puzder, and G. Galli, Phys. Rev. Lett. **89**, 196803 (2002).

[136] A. Ghosal, A. Guclu, C. Umrigar, D. Ullmo, and H. Baranger, Nature Physics **2** (2006), 10.1038/nphys293.

[137] S. Weiss and R. Egger, Phys. Rev. B **72**, 245301 (2005).

[138] L. Zeng, W. Geist, W. Y. Ruan, C. J. Umrigar, and M. Y. Chou, Phys. Rev. B **79**, 235334 (2009).

[139] I. Kylänpää and E. Räsänen, Physical Review B **96**, 205445 (2017).

[140] M. Pedersen Lohne, G. Hagen, M. Hjorth-Jensen, S. Kvaal, and F. Pederiva, Phys. Rev. B **84**, 115302 (2011).

[141] E. Waltersson, C. J. Wesslén, and E. Lindroth, Phys. Rev. B **87**, 035112 (2013).

[142] T. Gruber, K. Liao, T. Tsatsoulis, F. Hummel, and A. Grüneis, Physical Review X **8** (2018), 10.1103/PhysRevX.8.021043.

[143] T. Schäfer, B. Ramberger, and G. Kresse, The Journal of Chemical Physics **148** (2018), 10.1063/1.5016100.

[144] T. Schäfer, N. Daelman, and N. López, The Journal of Physical Chemistry Letters , 6277 (2021).

[145] A. Grüneis, M. Marsman, and G. Kresse, The Journal of Chemical Physics **133**, 074107 (2010).

[146] I. Heidari, N. Vaval, S. Pal, and D. G. Kanhere, Chemical Physics Letters **555**, 263 (2013).

[147] C. Sloggett and O. P. Sushkov, Phys. Rev. B **71**, 235326 (2005).

[148] E. Waltersson and E. Lindroth, Phys. Rev. B **76**, 045314 (2007).

[149] I. Heidari, S. Pal, B. S. Pujari, and D. G. Kanhere, The Journal of Chemical Physics **127**, 114708 (2007).

[150] A. I. Krylov, Annual Review of Physical Chemistry **59**, 433 (2008).

[151] X. Wang and T. C. Berkelbach, Journal of Chemical Theory and Computation **16**, 3095 (2020).

[152] A. Gallo, F. Hummel, A. Irmler, and A. Grüneis, The Journal of Chemical Physics **154**, 064106 (2021).

[153] B. T. G. Lau and T. C. Berkelbach, The Journal of Chemical Physics **152**, 224704 (2020).

[154] T. M. Henderson, K. Runge, and R. J. Bartlett, Physical Review B **67**, 045320 (2003).

[155] M. Florian, C. Gies, F. Jahnke, H. A. M. Leymann, and J. Wiersig, Physical Review B **87**, 165306 (2013).

[156] S. F. Boys, Proceedings of the Royal Society A: Mathematical, Physical and Engineering Sciences **200**, 542 (1950).

[157] S. Obara and A. Saika, The Journal of Chemical Physics **84**, 3963 (1986).

[158] R. Ahlrichs, Phys. Chem. Chem. Phys. **8**, 3072–3077 (2006).

[159] J. J. Shepherd, A. Grüneis, G. H. Booth, G. Kresse, and A. Alavi, Phys. Rev. B **86**, 035111 (2012).

[160] M. Taut, Journal of Physics: Condensed Matter **12**, 3689 (2000).

[161] F. Salihbegovic, A. Gallo, and A. Grüneis, Phys. Rev. B **108**, 115125 (2023).

[162] K. Graff, *Metal impurities in silicon-device fabrication*, Springer Series in Materials Science, Vol. 24 (Springer Science & Business Media, 2013).

[163] E. Weber, Kristall und Technik **16**, 209 (1981).

[164] S. T. Pantelides, *Deep centers in semiconductors : a state-of-the-art approach*, 2nd ed. (Gordon and Breach Science Publishers Yverdon, Switzerland, Yverdon, Switzerland, 1992).

[165] G. D. Watkins, Materials Science in Semiconductor Processing **3**, 227 (2000).

[166] O. Breitenstein and J. Heydenreich, Scanning **7**, 273 (1985).

[167] N. Fukata and M. Suezawa, Journal of Applied Physics **86**, 1848 (1999).

[168] R. J. Tilley, in *Encyclopedia of Inorganic and Bioinorganic Chemistry* (John Wiley and Sons, Ltd, 2018) pp. 1–23.

[169] P. M. Fahey, P. B. Griffin, and J. D. Plummer, Rev. Mod. Phys. **61**, 289 (1989).

[170] D. J. Eaglesham, P. A. Stolk, H. Gossmann, and J. M. Poate, Applied Physics Letters **65**, 2305 (1994).

[171] D. A. Richie, J. Kim, S. A. Barr, K. R. A. Hazzard, R. Hennig, and J. W. Wilkins, Phys. Rev. Lett. **92**, 045501 (2004).

[172] R. Vaidyanathan, M. Y. L. Jung, and E. G. Seebauer, PHYSICAL REVIEW B **75** (2007), 10.1103/PhysRevB.75.195209.

[173] D. Riedel, F. Fuchs, H. Kraus, S. Väth, A. Sperlich, V. Dyakonov, A. A. Soltamova, P. G. Baranov, V. A. Ilyin, and G. V. Astakhov, Phys. Rev. Lett. **109**, 226402 (2012).

[174] A. M. Tyryshkin, S. Tojo, J. J. L. Morton, H. Riemann, N. V. Abrosimov, P. Becker, H.-J. Pohl, T. Schenkel, M. L. W. Thewalt, K. M. Itoh, and S. A. Lyon, Nature Materials **11**, 143 (2011).

[175] K. Otsuka and X. Ren, Intermetallics **7**, 511 (1999).

[176] W. Gao and A. Tkatchenko, Phys. Rev. Lett. **111**, 045501 (2013).

[177] F. Bruneval, Phys. Rev. Lett. **108**, 256403 (2012).

[178] R. Ramprasad, H. Zhu, P. Rinke, and M. Scheffler, Phys. Rev. Lett. **108**, 066404 (2012).

[179] P. Rinke, A. Janotti, M. Scheffler, and C. G. Van de Walle, Phys. Rev. Lett. **102**, 026402 (2009).

[180] C. G. Van de Walle and A. Janotti, physica status solidi (b) **248**, 19 (2011).

[181] C. G. Van de Walle and J. Neugebauer, Journal of Applied Physics **95**, 3851 (2004).

[182] E. R. Batista, J. Heyd, R. G. Hennig, B. P. Uberuaga, R. L. Martin, G. E. Scuseria, C. J. Umrigar, and J. W. Wilkins, Phys. Rev. B **74**, 121102 (2006).

[183] W.-K. Leung, R. J. Needs, G. Rajagopal, S. Itoh, and S. Ihara, Phys. Rev. Lett. **83**, 2351 (1999).

[184] P. E. Blöchl, E. Smargiassi, R. Car, D. B. Laks, W. Andreoni, and S. T. Pantelides, Phys. Rev. Lett. **70**, 2435 (1993).

[185] Y. Bar-Yam and J. D. Joannopoulos, Phys. Rev. B **30**, 1844 (1984).

[186] R. Vaidyanathan, M. Y. L. Jung, and E. G. Seebauer, Phys. Rev. B **75**, 195209 (2007).

[187] V. Ranki and K. Saarinen, Phys. Rev. Lett. **93**, 255502 (2004).

[188] H. Bracht, J. F. Pedersen, N. Zangenberg, A. N. Larsen, E. E. Haller, G. Lulli, and M. Posselt, Phys. Rev. Lett. **91**, 245502 (2003).

[189] A. Ural, P. B. Griffin, and J. D. Plummer, Phys. Rev. Lett. **83**, 3454 (1999).

[190] H. Bracht, E. E. Haller, and R. Clark-Phelps, Phys. Rev. Lett. **81**, 393 (1998).

[191] H. Bracht, N. A. Stolwijk, and H. Mehrer, Phys. Rev. B **52**, 16542 (1995).

[192] H. Bracht, H. H. Silvestri, I. D. Sharp, and E. E. Haller, Phys. Rev. B **75**, 035211 (2007).

[193] Y. Shimizu, M. Uematsu, and K. M. Itoh, Phys. Rev. Lett. **98**, 095901 (2007).

[194] P. M. Fahey, P. B. Griffin, and J. D. Plummer, Rev. Mod. Phys. **61**, 289 (1989).

[195] S. Dannefaer, P. Mascher, and D. Kerr, Phys. Rev. Lett. **56**, 2195 (1986).

[196] A. Ural, P. B. Griffin, and J. D. Plummer, Journal of Applied Physics **85**, 6440 (1999).

[197] W. D. Parker, J. W. Wilkins, and R. G. Hennig, physica status solidi (b) **248**, 267 (2011).

[198] M. Kaltak, J. c. v. Klimeš, and G. Kresse, Phys. Rev. B **90**, 054115 (2014).

[199] W. K. Leung, R. Needs, G. Rajagopal, S. Itoh, and S. Ihara, VLSI Design **13** (2001), 10.1155/2001/83797.

[200] G. H. Booth, A. Grüneis, G. Kresse, and A. Alavi, Nature **493**, 365 (2013).

[201] T. Gruber and A. Grüneis, Phys. Rev. B **98**, 134108 (2018).

[202] J. McClain, Q. Sun, G. K.-L. Chan, and T. C. Berkelbach, J. Chem. Theory Comput. **13**, 1209 (2017), pMID: 28218843.

[203] M. Schütz, L. Maschio, A. J. Karttunen, and D. Usvyat, The Journal of Physical Chemistry Letters **8**, 1290 (2017).

[204] D. Usvyat, L. Maschio, and M. Schütz, WIREs Computational Molecular Science **8**, 1 (2018).

[205] M. Nusspickel and G. H. Booth, Phys. Rev. X **12**, 011046 (2022).

[206] J. Chen, N. A. Bogdanov, D. Usvyat, W. Fang, A. Michaelides, and A. Alavi, The Journal of Chemical Physics **153**, 204704 (2020).

[207] J. Sauer, Accounts of Chemical Research **52**, 3502 (2019).

[208] H. H. Lin, L. Maschio, D. Kats, D. Usvyat, and T. Heine, Journal of Chemical Theory and Computation **16**, 7100 (2020).

[209] J. D. Goodpaster, T. A. Barnes, F. R. Manby, and T. F. Miller, The Journal of Chemical Physics **140**, 18A507 (2014).

[210] T. Schäfer, F. Libisch, G. Kresse, and A. Grüneis, The Journal of Chemical Physics **154**, 011101 (2021).

[211] B. T. G. Lau, G. Knizia, and T. C. Berkelbach, The Journal of Physical Chemistry Letters **12**, 1104 (2021), pMID: 33475362.

[212] P. M. Fahey, P. B. Griffin, and J. D. Plummer, Rev. Mod. Phys. **61**, 289 (1989).

[213] H. Bracht, N. A. Stolwijk, and H. Mehrer, Phys. Rev. B **52**, 16542 (1995).

[214] H. Bracht, E. E. Haller, and R. Clark-Phelps, Phys. Rev. Lett. **81**, 393 (1998).

[215] A. Ural, P. B. Griffin, and J. D. Plummer, Phys. Rev. Lett. **83**, 3454 (1999).

[216] O. K. Al-Mushadani and R. J. Needs, Phys. Rev. B **68**, 235205 (2003).

[217] F. Corsetti and A. A. Mostofi, Phys. Rev. B **84**, 035209 (2011).

[218] T. Schäfer, B. Ramberger, and G. Kresse, The Journal of Chemical Physics **146**, 104101 (2017).

[219] M. Marsman, A. Grüneis, J. Paier, and G. Kresse, The Journal of Chemical Physics **130** (2009), 10.1063/1.3126249, 184103.

[220] Salihbegovic, "salihbegovic/silicon-ccsd-t-: Workflow si-interstitials ccsd(t)," (2023).

[221] T. Schäfer, F. Libisch, G. Kresse, and A. Grüneis, The Journal of Chemical Physics **154**, 011101 (2021).

Publications

- Faruk Salihbegović , Alejandro Gallo , and Andreas Grüneis

  "Coupled cluster theory for the ground and excited states of two-dimensional quantum dots"

  Phys. Rev. B 105, 115111 (2022)

- Faruk Salihbegović , Alejandro Gallo , and Andreas Grüneis

  "Formation energies of silicon self-interstitials using periodic coupled cluster theory"

  Phys. Rev. B 108, 115125 (2023)

Conferences and Posters

- ISTPC 2022

  June 19 - July 2, 2022 Aussois, France

- Psi-k 2022

  August 22 – August 25, 2022 Lausanne, Switzerland

- ICQC 2023

  June 26 – July 1, 2023 Bratislava, Slovakia